THE UNIVERSITY OF CHICAGO

OBSERVATION OF ENVIRONMENT-MEDIATED MECHANISMS OF EFFECTIVE ENERGY TRANSFER IN PHOTOSYNTHETIC LIGHT HARVESTING

A DISSERTATION SUBMITTED TO

THE FACULTY OF THE DIVISION OF THE PHYSICAL SCIENCES

IN CANDIDACY FOR THE DEGREE OF

DOCTOR OF PHILOSOPHY

DEPARTMENT OF CHEMISTRY

BY

SIDDHARTHA SOHONI

CHICAGO, ILLINOIS

JUNE 2024

To my grandparents, Ajoba, Appa Aba, Revati Aji and Shubhaji,

for their endless love and priceless teachings

That's my Middle West – … the thrilling returning trains of my youth, and the street lamps and sleigh bells in the frosty dark and the shadows of holly wreaths thrown by lighted windows on the snow.

I see now that this has been a story of the West, after all.

-F. Scott Fitzgerald in *The Great Gatsby*

Contents

List of Figures

Abstract

Upon light absorption by photosynthetic pigments in light-harvesting antenna proteins, Coulombically bound electron-hole pairs called excitons are created. Excitons hop from the site of creation to the reaction center in the light-harvesting antenna network. The process of exciton hopping along the antenna pigment network is near-unity efficient. This thesis reports the observation of photosynthetic design strategies that enable the high transfer efficiency of excitons in photosynthesis. In Chapter 2, I demonstrate adaptation of the spatial patterns of the arrangements of proteins on the photosynthetic membrane towards maximum efficiency in different light fluences. I show that reaction center clustering is favored in high light fluences to maximize exciton trapping. In Chapters 3 and 4, I have described mechanisms for effective energy capture through chromophore-protein interactions in the cyanobacterial light-harvesting antenna, phycobilisome. In Chapter 4, I show that single-residue level hydrogen-bonding interactions with phycobilisome chromophores prevent excited-state relaxation that hampers energy transfer. In Chapter 4, I also observe that environmental vibrations are tuned to enhance directional downhill energy transfer through the antenna. In Chapter 3, I observe that the energetic landscape of the antenna is tuned through quaternary-level chromophore-protein interactions to create directional energy flow. In Chapter 5, I observe chiral regulation of energy transfer in the LH2 antenna of purple bacteria. I observe that right-handed exciton states in the antenna transfer energy faster than left-handed states. The findings in these chapters describe how coupling to the environment is tuned in photosynthesis to regulate energy release to the environment and to create unidirectional exciton flow.

Acknowledgments

First, I thank my advisor, Professor Gregory S. Engel, for teaching me so many skills over the past six years, and for treating me with kindness, dignity, and respect throughout this time. I had a great time working with him. I thank my thesis committee members, Professors Sarah King and Norbert Scherer for their valuable time and for accepting to be on my thesis committee. I thank Dr. Karen Watters for teaching me the scientific thought process and writing. Next, I thank the wonderful colleagues I had the pleasure of working with early on in my PhD. I would like to thank Dr. Lawson Lloyd first for training me in the lab and for solving many experimental problems with me that would have otherwise made work presented here not possible. I also could not have been able to perform experiments without inputs from Drs. Ryan Wood, Polina Navotnaya, Sara Sohail, Richard Mazuski, Marco Allodi, Sara Massey and Po-Chieh Ting and my friend Sami Abdulhadi. I thank Drs. Will Hollingsworth, Elizabeth Bain and Jacob Higgins for great office times. I had the good fortune of getting valuable advice from Profs. Justin Caram, Peter Dahlberg and Dugan Hayes at various conferences and over phone calls. I thank my amazing colleagues who I overlapped with in the second half of my PhD. I am excited about each of their scientific endeavors. I would like to thank Caitlin Bellora, Coco Li, Indranil Ghosh, Qijie Shen and Eric Wu for many shared research projects and memories. I would like to thank Rachel Leech, Olivia Wedig, Emma McNesby, Katelyn Feuling, Claire Jones, Keerthi Mani, Andrew Huang and Molly Roesch for many fruitful science chats and fun times. I thank undergraduate students of the Engel group, Nick Cleland, Anna Dardia, Malachi Elue, James Hayman, Karen Ji, Sarah Martin, Hugh Cairney, Felice Chan, Cooper Costello, Ainsley Iwanicki, Sarah Kress and Daniela Santillán-Enríquez for working with me on various projects. I would also like to thank high-school rotators

Charles Chen and Michael Talapin for their inputs in various experiments. I thank Professors Aaron Dinner, Benoît Roux, Steven Sibener and Andrei Tokmakoff for their scientific inputs, encouragement, and support. I thank my first-year teaching colleagues Dr. Julia Murphy, Nasim Mirzajani, Ruiyu Li, Chatipat Lorpaiboon, Shiqi Chen and all other cohort friends for their constant support and encouragement. I thank collaborators Dr. Nikita Onizhuk, Professor Giulia Galli, Dr. Geoffrey Nash, Dr. Taokun Luo, Professor Wenbin Lin, Dr. Andrew Hitchcock, Dr. Craig MacGregor-Chatwin, Dr. David Swainsbury, Professor C. Neil Hunter, Dr. Aritrajit Gupta, Professor Dmitri Talapin, Dr. Andrew Christofferson and Dr. Anjay Manian. The work in this thesis would not have been possible without their theoretical and materials support. I thank Ms. Brenda Thomas, Dr. Melinda Moore, Dr. Vera Dragisich and Dr. Meishan Zhao for helping me navigate through the department and JFI. I thank Mr. Luigi Mazzenga, Dr. Elena Solomaha, Dr. Justin Jureller for making experiments presented in this thesis possible. I also thank the GCIS facilities and housekeeping teams for keeping our lab and office functioning through delicate experiments. I thank the University's Office of International Affairs for a seamless and fast experience with visa-related work. Similarly, I would like to thank UChicagoGrad for providing a lounge with snacks and other resources. I thank Gordon Research Conferences for providing a collaborative scientific environment at their conferences and for encouraging graduate student participation. I thank the Department of Chemistry for its ceaseless support and investment in me. I thank them for the Benjamin Ball Freud scholarship to fund me for an academic year, and for the Gerhard and Liselotte Closs memorial fund for allowing me to invite guest speakers to the department. I encourage the reader to donate to the Closs memorial fund to continue the tradition of chemistry graduate students inviting seminar speakers. I thank my friends and my family. I will always try to live up to their expectations.

Chapter 1

Introduction

Matter is quantum mechanical in nature:[1] nuclei, electrons, and collective motions that constitute matter occupy discrete energy levels. When light interacts with matter, a transition occurs in the material from its initial energy state to a new, higher energy discrete state in which either nuclei or electrons have redistributed[1] spatially.

Visible and near-infrared (NIR) wavelengths constitute the largest fraction of the terrestrial solar spectrum.[2] Visible and NIR light typically interacts with electrons in matter to drive transitions between ground- and excited electronic energy levels.[1] Absorption and harvesting of visible sunlight by matter on Earth drives life. This process is the first step of photosynthesis[3] and has also gained interest in the past few decades due the advent of photovoltaics.[2] Visible and NIR light-absorption drives a redistribution of electron density along the constituent molecules of the material. The new electron density is a higher energy configuration that is oftentimes more charge-separated than the resting configuration of the molecules at room temperature.[4]

The change in electron density upon photoexcitation of a material occurs along a fixed direction along the molecule. This direction is decided by the resting electron density and the nuclear configuration of the molecules. The dipole moment of the molecule also changes with respect to the molecule's ground-state (resting) configuration upon photoexcitation due to the reorganization of electron density. These two quantities, direction, and change of dipole moment, are packaged together in a vector called the transition dipole moment (TDM) in the quantum

mechanical treatment of the absorption process.[4] For a molecule to have a chance of absorbing impinged light, it is required that its transition dipole moment not be perpendicular to the polarization of the incident light wave. Here, the polarization of the light wave refers to the direction in which its electric field oscillates perpendicular to the direction of propagation.[1]

Upon photoexcitation, electrons redistribute along the molecule almost instantaneously.[5] Electronic redistribution causes the relatively massive nuclei to move towards a new energy minimum within the excited electronic state.[6] The relaxation of nuclei releases heat into the bath connected to the photoexcited molecules.[7] Eventually, the excited-electronic state relaxes back to its ground state due to infrequent interactions with the vacuum.[1] The relaxation processes following photoexcitation of molecules are of fundamental importance because they govern plants' and our ability to harness sunlight effectively.[8] Humanity's studies of these processes have also led to significant advances in the understanding of the quantum mechanical nature of matter around us.[9] This thesis describes the observation of selective coupling of the energy transfer process to the bath to drive effective energy capture in photosynthesis using spectroscopy. For a few decades now, third-order time-resolved electronic spectroscopy has been the cutting-edge technique of choice for the study of light-induced electronic dynamics.

Pump-probe electronic spectroscopy is the most fundamental and basic third-order spectroscopy used to study processes following visible photoexcitation.[10] In pump-probe spectroscopy, a first laser pulse, called the pump pulse, interacts with the molecules of interest, the sample. Following a time delay, a second pulse, called the probe pulse, interacts with the sample and is then directed to a visible light detector to have its intensity measured. The intensity of the probe pulse is recorded in the presence and absence of the pump pulse. An optical grating spectrally resolves the probe pulse on the detector. By itself, the intensity of the probe pulse

changes upon passing through the sample because some of it gets absorbed by the sample. In the presence of the pump pulse however, a portion of the sample gets bleached, so a larger fraction of the probe pulse can now pass through the sample, and a higher intensity is now detected on the detector. The difference between the pump-on and pump-off probe intensities constitutes the pump-probe signal. The time delay between pump and probe pulses is varied to observe the relaxation process of the excited molecules. When the time delay between the pump and the probe is larger than a few ns-μs,[11] most molecules have relaxed back to the electronic ground state after the pump interaction, no change in the probe intensity is recorded at the detector, and a complete relaxation of the excited molecules is thereby indicated. Apart from bleaching, the probe pulse can also stimulate emission from the excited population and increase in intensity in the pump-on condition as opposed to the pump-off condition. Finally, the excited-state of the sample can have a new absorption profile, that can reduce the transmission of the probe in the pump-on condition. This process is called photoinduced absorption.

As a thought experiment, we consider static two-level molecules aligned in a particular direction as our sample. For our pump pulse, we use a light source whose polarization is along the transition dipole moment of the static molecules. For the probe pulse, we use a polarization that is perpendicular to the polarization of the pump pulse. If such an experiment were to be performed, we would not observe a change in the probe intensity in the pump on and off conditions, because the molecules would not interact with the probe pulse in the absence of the pump pulse in the first place. Interactions between incident light and molecules are therefore governed by the magnitude of the projection of the light polarization on the molecular transition dipole moments to a very large extent.

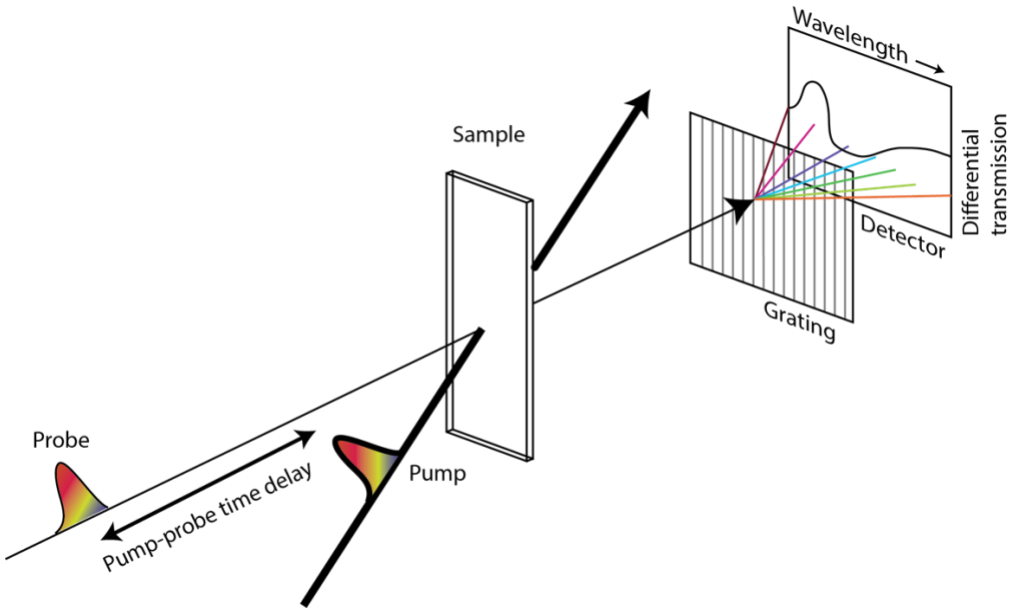

Fig 1.1: A schematic pump-probe experiment setup. The pump pulse excites the sample first. Following pump excitation, the probe interacts with the sample to detect changes caused by the pump. These changes are spectrally resolved by a grating and detected by a detector

An optical grating like the one depicted in *Fig 1.1* is almost always placed before the detector in the probe path. Incident broadband probe light gets diffracted off the grating and gets separated into the different constituent wavelengths. A change in intensity detected for a particular wavelength at the detector informs us of the difference between the two electronic energy levels in the material.

In the theory of pump-probe spectroscopy, two light-matter interactions are required to create an excited-state population.[12] The first light-matter interaction creates a coherence between the ground- and excited-state, and the second interaction then creates an excited-state population.[12] This population is probed with one interaction by the probe pulse that creates a new coherence. This coherence emits a signal that copropagates with the probe to change its intensity at the detector.[12] Pump-probe spectroscopy is a third-order spectroscopy because of the three light-matter interactions mentioned above. A mathematical and accurate description of pump-probe

spectroscopy uses third-order perturbation theory from quantum mechanics.[1, 13] The bookkeeping of all perturbation terms arising from pump-probe spectroscopy are easily condensed into Feynman pathways on the density matrix of the initial state of the sample.[12] In Feynman pathways, light-matter interactions depicted by arrows operate on the density matrix to change its state reflecting a laser interaction with the molecular transition dipole moment. Information of the linear momentum of the laser pulses, molecular coherences and populations, and absorption and detection wavelengths of particular signals are preserved in the Feynman pathway formalism.[13]

An example Feynman pathway for a stimulated emission signal in pump-probe spectroscopy is presented in *Fig 1.1*.

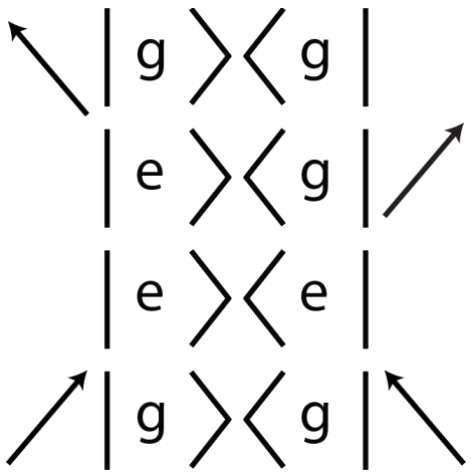

Fig 1.2: Pump-probe Feynman pathway for a stimulated emission signal

In the Feynman pathway depicted in *Fig 1.2*, |g> corresponds to the ground electronic state, and |e> corresponds to the excited electronic state. The two pump interactions act on the bra and ket sides of the density matrix to create an excited state population. The third arrow from bottom up depicts the probe interaction. It stimulates the emission process and creates a coherence

between the ground and excited states. The final arrow depicts the emission of the signal from the |e><g| coherence. The emitted signal travels with the probe to change its intensity and is detected on the detector after diffracting off the optical grating. The grating Fourier-transforms the signal and allows us to obtain the energy difference between the ground and excited states of the sample by wavelength-resolving the signal.

In the experiment depicted in *Fig 1.1*, we use broadband pump and probe pulses to excite and detect as many spectral transitions as we can. The optical grating allows us to detect the wavelengths of the emitted signals. However, electronic states within molecules relax and exchange energy with each other over the pump-probe delay time. For example, emission is typically redshifted with respect to the main molecular absorption feature because of the nuclear relaxation of the electronic excited state. Therefore, a differential transmission of the probe detected at a particular wavelength may not have been created by the same wavelength light in the pump. To track the flow of energy with information about the exciting and detecting energies, we must spectrally resolve the pump interactions with the sample also. The simplest way to do so is to use a narrowband pump pulse and tune its frequency along the spectral range of interest. This method is widely used in the exploration of excited electronic dynamics.[14] However, it suffers from two limitations. First, both pump interactions with the sample remain instantaneous in this procedure, so that we cannot independently control the polarization of the two light pulses. We remain restricted to observing those processes in which both pump interactions with the sample are identical. Second, using a narrowband frequency profile spreads the pulse out in time in accordance with the Fourier limit, and prevents us from observing the earliest fs-ps of the excited state dynamics.[1]

We can consider two, two-level molecules in proximity that impact each other's electrostatic Hamiltonians with perpendicular transition dipole moments as our sample to understand this limitation. In this situation, a pump-probe experiment only allows us to selectively excite one of the chromophores in coupled dimer because the pump polarization remains fixed between the two pump-matter interactions. To observe the excited state dynamics of the coupled system, independent control of the polarization of the two pump interactions is required.

To have independent control on the polarization of the two pump interactions without losing temporal resolution, we use two-dimensional electronic spectroscopy in the BOXCARS (CARS stands for Coherent anti-Stokes Raman) geometry in experiments presented in this thesis.[15, 16] Two-dimensional electronic spectroscopy (2DES) uses two pump pulses separated by a variable time delay called coherence time, as opposed to a single pump pulse in pump-probe spectroscopy.[14, 17] The time-delay between the two pump pulses is varied from 0 to 90 fs in our setup, and the emitted signal intensity is collected as a function of this time delay along with the 'pump-probe' time delay. The obtained signal as a function of coherence time is then Fourier transformed to provide us the excitation frequency resolution. Therefore, by spectrally resolving the pump pulse in the time domain and the probe pulse in the frequency domain, we can track dynamics of excited states with complete information of exciting and detecting energies. Another advantage of separating the pump interactions is that it allows us to independently control the polarization of the two pump interactions. The formalism of Feynman pathways in equally applicable to 2DES.

In the BOXCARS geometry, the two pump pulses and the probe pulse propagate along three corners of a box before getting spatially focused to the same spot at the sample position. The emitted signal does not travel with the probe in the BOXCARS geometry, but travels along the

fourth corner of the box. This phenomenon arises from the addition of the momenta of the first three pulses, also known as phase-matching.[13] A local-oscillator pulse is made to travel along the signal direction to serve as a proxy of the probe and to allow us to detect differential changes in light intensity. This pulse is required in BOXCARS 2DES as opposed to in pump-probe spectroscopy because in pump-probe spectroscopy is self-phase-matched. In the BOXCARS 2DES setup, we can control not only the polarization of all pulses, but also select signals of specific polarizations by tuning the polarization of the local oscillator pulse. A simplified schematic of this setup is shown in *Fig 1.3*.

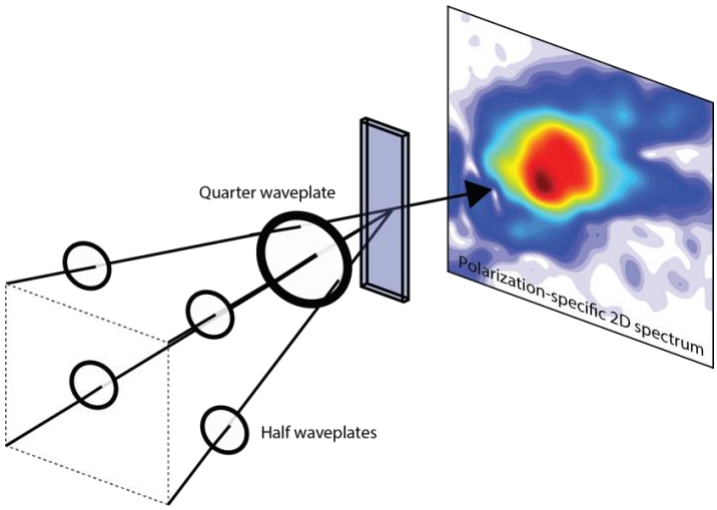

Fig 1.3: Schematic of polarization-controlled BOXCARS 2DES. A combination of half- and quarter waveplates in the beam paths allows independent control of polarizations of pumps, probe and signal.

So far, we have only considered scenarios in which the transition dipole moments of our samples are linear. However, in helical condensed-matter bands[15] and chiral aggregates of chromophores,[18] light-matter interactions can drive helical motion of electrons upon photoexcitation. Excited-state dynamics in such systems can also be studied in our setup.[15] In this thesis, I have used this ability to observe chirality-controlled electronic energy transfer.

The ability of polarization-controlled 2DES to extract specific signals pertaining to excited state energy transfer has been exploited in many previous works.[13, 15, 19-24] For example, an earlier work from our group showed that this technique can be used to observe uphill energy transfer between chromophores of the LH2 complex of purple bacteria.[24] Similarly, another work demonstrated exciton scattering timescales between left- and right-handed helical valleys in monolayer molybdenum disulphide.[15] In this thesis, I have utilized "cross-peak-specific"[25, 26] two-dimensional electronic spectroscopy to selectively observe the capture of the photoexcited energy by the phycobilisome light-harvesting antenna of cyanobacteria. In many photosynthetic proteins, the dynamics of electronic excited states of interest are obfuscated by spectral congestion which occurs due to the presence of hundreds of light-absorbing pigments.[27, 28] By choosing the polarizations of pump and probe pulses, I demonstrate selective observation of dynamics that were hitherto inaccessible to pump-probe spectroscopies.[28-31] I observe that biological tuning of the energetic landscape of the antenna drives highly efficient light harvesting in this protein supercomplex. The detailed experimental setup is shown in *Fig 1.4* and is adapted from ref[32].

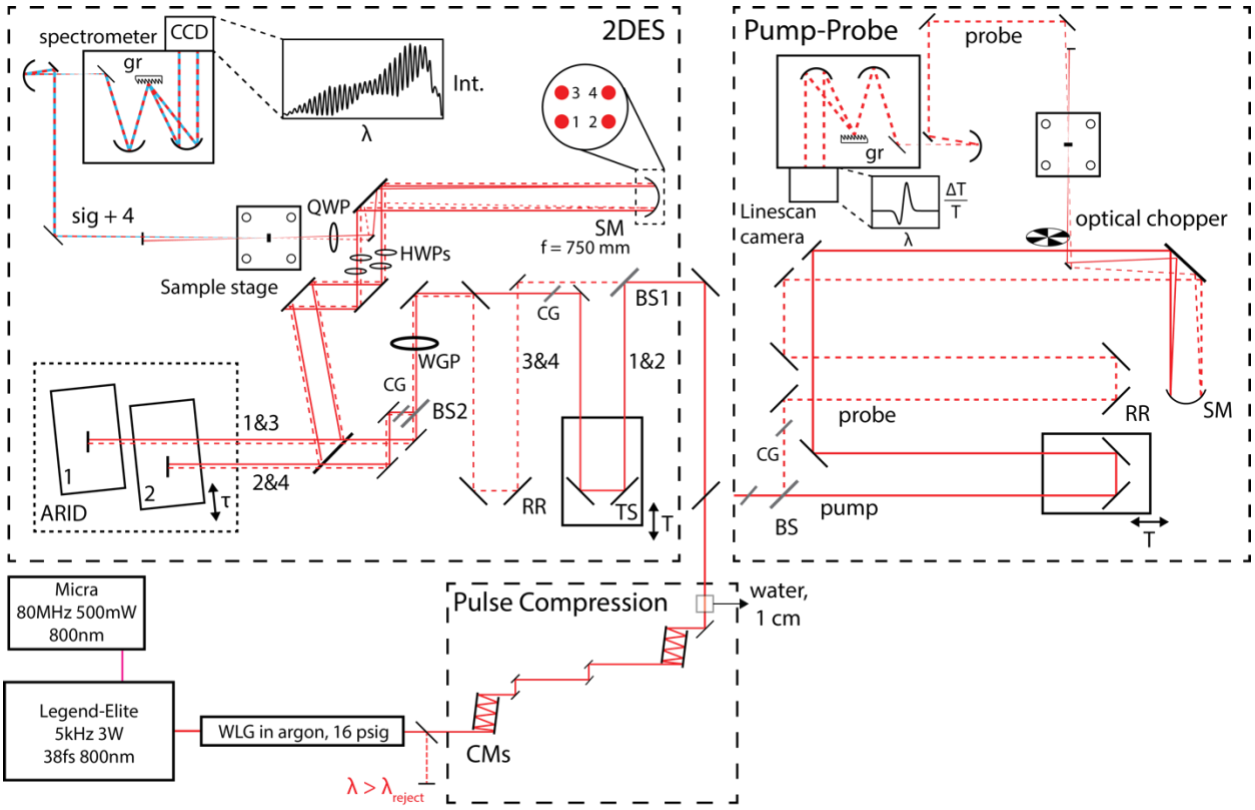

Fig. 1.4: Detailed optical layout[32] of the pump-probe and 2DES spectrometers used for experiments presented in this thesis. Self-phase modulation of an 800 nm, 5 kHz,35 fs pulsed fundamental in high-pressure Argon creates a white-light continuum. The continuum is spectrally shaped, filtered, and compressed with spectral filters, DCM 9 and DCM 10 chirped mirror pairs from Laser Quantum, and a 1 cm cuvette of water. The light is then directed to the pump-probe and 2DES spectrometers.

Similarly, in Chapter 5, I utilize the ability to control pump pulse polarization to selectively access chiral electronic excited states in the LH2 antenna of purple bacteria. In these experiments, I uncover that right- and left- handed chiral excited states interact differently with the nuclei of the chromophores and the surrounding protein bath, resulting in different energy transfer rates for these two states. These observations demonstrate that the optical degree of freedom can be utilized in principle for logic operations due to their distinct dynamics.

From Chapters 3, 4 and 5, I learn that isotropically observed dynamics often fails to reveal processes in excited state dynamics that depend on transition dipole moment geometries as much

as on the energetics of the system. The observations made in this thesis could guide our design of future materials for tailored control of excited electronic states. The methods I developed upon for this thesis could be used to probe a multitude of physiologically and technologically important light-harvesting materials.

From Chapters 2, 3, and 4, I learn that the photosynthetic light-harvesting is an active process that requires energy usage for efficient operation. Unlike other cellular processes though, the energy required for this process is not provided metabolically through ATP hydrolysis.[33] Instead, a part of the excitonic energy is released in every exciton-hopping step during the light-harvesting process, creating a unidirectional network of antenna pigments that performs this function with near-unity efficiency.

Bibliography

(1) Townsend, J. S. *A Modern Approach to Quantum Mechanics*; University Science Books, 2013.
(2) Scholes, G. D.; Fleming, G. R.; Olaya-Castro, A.; van Grondelle, R. Lessons from Nature about Solar Light Harvesting. *Nature Chemistry* **2011**, *3* (10), 763-774.
(3) Blankenship, R. E. Antenna Complexes and Energy Transfer Processes. In *Molecular Mechanisms of Photosynthesis*, Wiley, 2002; pp 61-94.
(4) Attila Szabo, N. S. O. *Modern Quantum Chemistry: Introduction to Advanced Electronic Structure Theory*; Dover, 1996.
(5) Condon, E. U. The Franck-Condon principle and related topics. *American journal of physics* **1947**, *15* (5), 365-374.
(6) Born, M.; Oppenheimer, R. On the Quantum Theory of Molecules. In *Quantum Chemistry*, pp 1-24.
(7) Kasha, M. Characterization of electronic transitions in complex molecules. *Discussions of the Faraday society* **1950**, *9*, 14-19.
(8) *Light-Harvesting Antennas in Photosynthesis*; Springer, 2003.
(9) Rydberg, J. R. XXXIV. On the structure of the line-spectra of the chemical elements. *The London, Edinburgh, and Dublin philosophical magazine and journal of science* **1890**, *29* (179), 331-337.
(10) Dantus, M.; Rosker, M. J.; Zewail, A. H. Real-time femtosecond probing of ‘‘transition states’’ in chemical reactions. *The Journal of Chemical Physics* **1987**, *87* (4), 2395-2397.
(11) van Amerongen, H.; van Grondelle, R.; Valkunas, L. *Photosynthetic Excitons*; World Scientific, 2000. DOI: doi:10.1142/3609.
(12) Mukamel, S. *Principles of nonlinear optical spectroscopy*; 1995.
(13) Hamm, P.; Zanni, M. *Concepts and Methods of 2D Infrared Spectroscopy*; Cambridge University Press, 2011. DOI: DOI: 10.1017/CBO9780511675935.
(14) Biswas, S.; Kim, J.; Zhang, X.; Scholes, G. D. Coherent Two-Dimensional and Broadband Electronic Spectroscopies. *Chemical Reviews* **2022**, *122* (3), 4257-4321.
(15) Lloyd, L. T.; Wood, R. E.; Mujid, F.; Sohoni, S.; Ji, K. L.; Ting, P.-C.; Higgins, J. S.; Park, J.; Engel, G. S. Sub-10 fs Intervalley Exciton Coupling in Monolayer MoS2 Revealed by Helicity-Resolved Two-Dimensional Electronic Spectroscopy. *ACS Nano* **2021**, *15* (6), 10253-10263.
(16) Zheng, H.; Caram, J. R.; Dahlberg, P. D.; Rolczynski, B. S.; Viswanathan, S.; Dolzhnikov, D. S.; Khadivi, A.; Talapin, D. V.; Engel, G. S. Dispersion-free continuum two-dimensional electronic spectrometer. *Appl. Opt.* **2014**, *53* (9), 1909-1917.
(17) Fresch, E.; Camargo, F. V. A.; Shen, Q.; Bellora, C. C.; Pullerits, T.; Engel, G. S.; Cerullo, G.; Collini, E. Two-dimensional electronic spectroscopy. *Nature Reviews Methods Primers* **2023**, *3* (1), 84.
(18) Fidler, A. F.; Singh, V. P.; Long, P. D.; Dahlberg, P. D.; Engel, G. S. Dynamic localization of electronic excitation in photosynthetic complexes revealed with chiral two-dimensional spectroscopy. *Nature Communications* **2014**, *5* (1), 3286.
(19) Farrell, K. M.; Yang, N.; Zanni, M. T. A polarization scheme that resolves cross-peaks with transient absorption and eliminates diagonal peaks in 2D spectroscopy. *Proceedings of the National Academy of Sciences* **2022**, *119* (6), e2117398119.

(20) Ginsberg, N. S.; Davis, J. A.; Ballottari, M.; Cheng, Y.-C.; Bassi, R.; Fleming, G. R. Solving structure in the CP29 light harvesting complex with polarization-phased 2D electronic spectroscopy. *Proceedings of the National Academy of Sciences* **2011**, *108* (10), 3848-3853.
(21) Thyrhaug, E.; Tempelaar, R.; Alcocer, M. J. P.; Žídek, K.; Bína, D.; Knoester, J.; Jansen, T. L. C.; Zigmantas, D. Identification and characterization of diverse coherences in the Fenna–Matthews–Olson complex. *Nature Chemistry* **2018**, *10* (7), 780-786.
(22) Schlau-Cohen, G. S.; Ishizaki, A.; Calhoun, T. R.; Ginsberg, N. S.; Ballottari, M.; Bassi, R.; Fleming, G. R. Elucidation of the timescales and origins of quantum electronic coherence in LHCII. *Nature Chemistry* **2012**, *4* (5), 389-395.
(23) Massey, S. C.; Ting, P.-C.; Yeh, S.-H.; Dahlberg, P. D.; Sohail, S. H.; Allodi, M. A.; Martin, E. C.; Kais, S.; Hunter, C. N.; Engel, G. S. Orientational Dynamics of Transition Dipoles and Exciton Relaxation in LH2 from Ultrafast Two-Dimensional Anisotropy. *The Journal of Physical Chemistry Letters* **2019**, *10* (2), 270-277.
(24) Fidler, A. F.; Singh, V. P.; Long, P. D.; Dahlberg, P. D.; Engel, G. S. Probing Energy Transfer Events in the Light Harvesting Complex 2 (LH2) of *Rhodobacter sphaeroides* with Two-dimensional Spectroscopy. *The Journal of Chemical Physics* **2013**, *139* (15).
(25) Zanni, M. T.; Ge, N.-H.; Kim, Y. S.; Hochstrasser, R. M. Two-dimensional IR Spectroscopy can be Designed to Eliminate the Diagonal peaks and Expose only the Crosspeaks Needed for Structure Determination. *Proceedings of the National Academy of Sciences* **2001**, *98* (20), 11265-11270.
(26) Read, E. L.; Engel, G. S.; Calhoun, T. R.; Mančal, T.; Ahn, T. K.; Blankenship, R. E.; Fleming, G. R. Cross-peak-specific two-dimensional electronic spectroscopy. *Proceedings of the National Academy of Sciences* **2007**, *104* (36), 14203-14208.
(27) Anna, J. M.; Ostroumov, E. E.; Maghlaoui, K.; Barber, J.; Scholes, G. D. Two-Dimensional Electronic Spectroscopy Reveals Ultrafast Downhill Energy Transfer in Photosystem I Trimers of the Cyanobacterium *Thermosynechococcus elongatus*. *The Journal of Physical Chemistry Letters* **2012**, *3* (24), 3677-3684.
(28) van Stokkum, I. H. M.; Gwizdala, M.; Tian, L.; Snellenburg, J. J.; van Grondelle, R.; van Amerongen, H.; Berera, R. A Functional Compartmental Model of the *Synechocystis* PCC 6803 Phycobilisome. *Photosynthesis Research* **2018**, *135* (1), 87-102.
(29) Tian, L.; Gwizdala, M.; van Stokkum, Ivo H. M.; Koehorst, Rob B. M.; Kirilovsky, D.; van Amerongen, H. Picosecond Kinetics of Light Harvesting and Photoprotective Quenching in Wild-Type and Mutant Phycobilisomes Isolated from the Cyanobacterium *Synechocystis* PCC 6803. *Biophysical Journal* **2012**, *102* (7), 1692-1700.
(30) Tian, L.; van Stokkum, I. H. M.; Koehorst, R. B. M.; Jongerius, A.; Kirilovsky, D.; van Amerongen, H. Site, Rate, and Mechanism of Photoprotective Quenching in Cyanobacteria. *Journal of the American Chemical Society* **2011**, *133* (45), 18304-18311.
(31) Fălămaș, A.; Porav, S. A.; Tosa, V. Investigations of the Energy Transfer in the Phycobilisome Antenna of *Arthrospira platensis* Using Femtosecond Spectroscopy. *Applied Sciences* **2020**, *10* (11), 4045.
(32) Lloyd, L. T. Resolving Exciton Dynamics and Couplings in Atomically Thin Semiconductors with Multidimensional Spectroscopy. Ph.D., The University of Chicago, United States -- Illinois, 2022.
(33) Bruce, A. *Molecular biology of the cell*; Second edition. New York : Garland Pub., [1989] ©1989, 1989.

Chapter 2

Spatial Patterns of Light-harvesting Antenna Complex Arrangements Tune the Transfer-to-trap Efficiency of Excitons in Purple Bacteria

Reproduced with permission from Onizhuk, Sohoni*, Galli, Engel, J. Phys. Chem. Lett., 2021*

In photosynthesis, the efficiency with which a photogenerated exciton reaches the reaction center is dictated by chromophore energies and the arrangement of chromophores in the supercomplex. In this chapter, I explore the interplay between the arrangement of light-harvesting antennae and the efficiency of exciton transport in purple bacterial photosynthesis. Using a Miller–Abrahams-based exciton hopping model, we compare different arrangements of light-harvesting proteins on the intracytoplasmic membrane. We find that arrangements with aggregated LH1s have a higher efficiency than arrangements with randomly distributed LH1s in a wide range of physiological light fluences. This effect is robust to the introduction of defects on the intracytoplasmic membrane. Our result explains the absence of species with aggregated LH1 arrangements in low-light niches and the large increase seen in the expression of LH1 dimer complexes in high fluences. We suggest that the effect seen in our study is an adaptive strategy toward solar light fluence across different purple bacterial species.

Photosynthesis employs a spatio-energetic funnel to maximize the transfer-to-trap efficiency of excitons.[1, 2] Chromophores are arranged to absorb from higher to lower energies as they get closer to the reaction center. For example, in cyanobacterial photosynthesis, high energy excitons created in the phycobilisome move energetically downhill to photosystem I. Within

photosystem I, the lowest energy red chlorophylls spatially surround the RC.[1, 3] Another striking example of a spatio-energetic funnel is found in purple bacteria. On purple bacterial intracytoplasmic membranes (ICMs), LH2 proteins absorbing 850 and 800 nm light surround LH1 proteins absorbing light at a longer wavelength (lower energy), 875 nm. Photosynthetic reaction centers (RC) are embedded in the LH1 proteins, thus creating a well-defined two-step energetic funnel, or downhill hopping gradient for excitons to move from LH2 to LH1 and then on to the RC.[4, 5] The funnel facilitates a highly efficient transfer-to-trap process in purple bacteria. The efficiency with which a photogenerated exciton gets quenched at the RC (transfer-to-trap efficiency) has been reported to be in the range of 80-95% for purple bacteria.[1, 6-8]

Over the past few decades, chromophore-environment interactions that tune the energies of photosynthetic chromophores have been extensively studied.[3, 9-13] On the other hand, the role of the membrane organization in tuning transfer-to-trap efficiency and excitonic pathways has been comparatively less explored. In purple bacteria, quinone diffusion, variable internal conversion in RCs and maximal surrounding of RCs by LH2, among other parameters, have been suggested as drivers of the different arrangements of light harvesting complexes observed in nature.[8, 14-16,] Atomic force microscopy (AFM) studies on purple bacterial ICMs have shown that in *Rb. sphaeroides*, LH1 proteins form dimers and aggregate to make LH1 islands of eight complexes typically arranged in two rows of four (2x4), whereas in *Rps. acidophila, Rsp. photometricum* and other species, the distribution of LH1s is random.[5, 8, 17, 18] Light-conditions are known to affect LH1:LH2 complex ratios, and LH1:LH2 ratios between 1:2 and 1:14, the result of light-dependent LH2 expression, have been reported on purple bacterial ICMs.[19-21] AFM studies have also uncovered a plethora of defects on the lattice structure of the membrane, including LH1s with

broken or missing RCs and incorrectly "wrapped" LH2s and LH1s.[17, 18, 22] Non-photosynthetic proteins present on the membrane can also disrupt excitonic pathways.

In this chapter, I examine the effect of different membrane protein arrangements on the robustness and transfer-to-trap efficiency of photosynthesis by modelling exciton dynamics with kinetic Monte-Carlo simulations based on the Miller-Abrahams model. We verify our model by recovering trends in exciton lifetimes on purple bacterial ICMs with varied LH1:LH2 ratios and light fluences. We find that different arrangements of LH1 and LH2 on the membrane show differences of up to 2% in transfer-to-trap efficiency at low and medium solar light-fluences. We posit that this difference could manifest in a potential ecological advantage over many generations of proliferation and that the formation of LH1 islands could be an adaptation to light fluences across purple bacterial species.

The chapter is organized as follows: We begin with describing our adapted computational model of the ICM. We then state the results of our simulations. Finally, we discuss their implications and explain the observed phenomena.

To model exciton dynamics on the purple bacterial ICMs, we use kinetic Monte-Carlo exciton hopping simulations incorporating the Miller-Abrahams model of weighting exciton hopping steps on a purple bacterial ICM lattice. This model is naturally dissipative and downhill hopping of excitons is favored over uphill hopping.[23] Specifically, downhill hops between a donor, i and an acceptor j proceed with a fixed rate constant k_h, but uphill hops are weighted by the Boltzmann factor of the energy difference ΔE_{ij} between the two chromophores i and j:

$$k_{ij} = \frac{k_h}{6} e^{-\left(\frac{\Delta E_{ij} + |\Delta E_{ij}|}{2k_B T}\right)} \quad (Equation\ 2.1).$$

Here, k_{ij} is the hopping rate between i and j, k_B is the Boltzmann constant and T is the temperature. We assume that the rates of LH1 and LH2 fluorescence and transfer of excitons to the RC are constant. The Miller-Abrahams model has been used previously to describe spin-hopping on lattices, exciton hopping in nanoparticle arrays and charge hopping in organic photovoltaics.[24-26] Due to its preferential downhill hopping feature which mirrors the energetic funnel in photosynthesis, Miller-Abrahams weighting of hopping steps is particularly suitable for exciton simulations on purple bacterial ICMs. Other models including FRET can incorporate downhill funneling, static disorder[27] and distance dependence in simulations. However, when many like complexes are involved and the inter-complex distance is fixed due to a lattice structure, the Miller-Abrahams model can be used to recover salient features of incoherent hopping if the relevant hopping constants are known experimentally.

The purple bacterial ICM is modelled by a 24×24 periodic two-dimensional hexagonal lattice with periodic boundary conditions; each lattice site is occupied by either an LH1 or LH2 protein.[16, 17] We use a hexagonal lattice as a simple approximation to structures reported in multiple AFM studies showing prominent hexagonal close packing of proteins.[8, 16] Each site is assigned an energy randomly picked from a Gaussian energy distribution with widths obtained from the measured fluorescence linewidths of LH1 and LH2 (10930.5 ± 119.5 cm^{-1} for LH1 and 11547 ± 72 cm^{-1} for LH2).[28-30] For the 1:2 ratio lattice, the exciton is created at a random position on the lattice, with a 14% chance of being created on LH1 and otherwise on LH2, in accordance with the absorption cross-section at 800 nm.[19] For all other ratios, we have interpolated the exciton branching ratios obtained by Timpmann and co-workers[19] for our model. The inter-complex hopping rate from lattice site i to j is determined by Equation 2.1. Temperature is set to 298 K for all simulations. The hop constant k_h in Equation 2.1 is set to the experimentally measured value

of 0.37 ps^{-1}.[5] The rate of fluorescence is assumed constant for each type of protein and is consistent with experimentally measured fluorescence lifetimes of the corresponding complexes: $k_F^{LH1} = 0.005$ ps^{-1} [31] and $k_F^{LH2} = 0.0025$ ps^{-1}.[32] The only free parameter left is the transfer rate from LH1 to the RC, which is obtained as $k_{RC}^{LH1} = 0.015625$ ps^{-1} by fitting the exciton lifetime in the membrane with an LH1:LH2 ratio of 1:2 to 60 ps.[19] Hops beyond nearest neighbors are neglected owing to the strong distance dependence of incoherent hopping. *Figure 2.1* shows the ICM membrane with the Miller-Abrahams model.

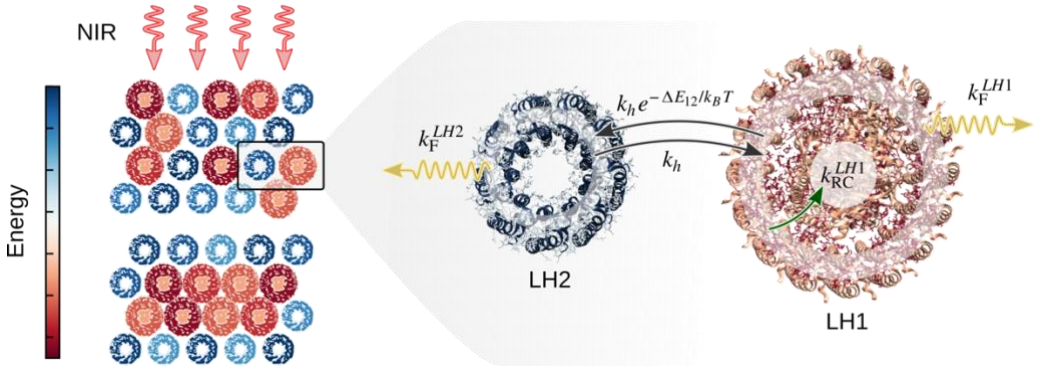

Fig 2.1: Lattice model for the purple-bacterial intracytoplasmic membrane: LH1 (red) and LH2 (blue) proteins occupy each site on a hexagonal lattice. Inset: exciton hopping between proteins is Boltzmann weighted for energetically uphill hops as per the Miller-Abrahams model.

To compute exciton lifetime as a function of LH2 expression, we use LH1:LH2 ratios of 1:2, 1:3, 1:4, 1:5 and 1:6 with random arrangements of LH1 and LH2 on the membrane. We also consider defects in the light harvesting network. In the real system, this "defect" is likely some other membrane protein that is neither LH2 nor LH1. We model a defect site on the membrane as a lattice site with effectively infinite energy, *i.e.*, a void to which an exciton cannot hop. We keep

the LH1:LH2 ratio constant at 1:2 and vary the fraction of defective sites on the membrane. LH1, LH2 and defect placements are random.

To examine the effect of LH1 arrangements on transfer-to-trap efficiency at all physical fluences, in our simulations we account for the difference between the photon absorption rate and the rate of exciton dissociation at the RC (RC turnover rate) using a dynamic RC closing method.[4,] Across much of the physiological solar fluence range the photon absorption rate of the membrane is greater than the RC turnover rate, creating a bottleneck for exciton quenching.

Solar fluence in typical purple bacterial environmental niches can range from 0.1 W/m^2 to 1000 W/m^2, which corresponds to peak sunlight fluence at the equator. At the low end, photon absorption on our simulated membrane and physiological membranes occurs once in every 10 ms while in the high fluence limit, a photon is absorbed approximately once every 1 μs.[4] Even in the highest solar fluence, multi-exciton events are rare on purple bacterial ICMs because the exciton lifetime is maximally 200 ps[19] – orders of magnitude smaller than the photon absorption rate. Therefore, we investigate lifetime and number of exciton hops as functions of light fluence within the single exciton regime. However, if the final reduced product release of the exciton quenching process step (1-100 ms timescale for one exciton) is slower than the photon absorption rate, an incoming exciton cannot hop to an exciton dissociating RC to be quenched. This phenomenon is called RC blocking and it determines exciton lifetimes in the high fluence limit. We include RC blocking in our model by adopting a strategy similar to that of Fassioli *et al.*[4] RCs are blocked (transfer to RC is turned off) for a variable number of subsequent simulations after the RC traps an exciton. This number is denoted by N_{block}. The relationship between light fluence and number of subsequent blocked simulations depends on the membrane absorption cross-section and the exact turnover time of the RC and is given by:

$$N_{block} = \frac{I\sigma\lambda}{hc} * \frac{1}{r} = \frac{N_{photons}}{r} \ (Equation\ 2.2).$$

In this equation, h Planck's constant, λ is the incident wavelength (800nm), I is the light fluence, r is RC turnover rate, σ is cross section, c is the speed of light, and $N_{photons}$ is number of photons absorbed by the membrane per unit time.

RC turnover times were not measured in previous fluence-dependent exciton lifetime studies on purple bacterial ICMs[19, 33] and are not known for the samples used in those studies. NaCl concentration, light fluence and quinone availability have been shown to affect RC turnover rates and the turnover times in laboratory conditions for the samples used in the two previous studies could be different by an order of magnitude.[34, 35] In this study, we use an RC turnover time of 25 ms/exciton, consistent with previous independent experimental and theoretical works and across different species.[4, 34, 35] The ratio of the number of photons absorbed per second and the RC turnover rate yields N_{block}. In our approach we first calculate the full membrane absorption cross-section using the molar absorption coefficients of bacteriochlorophylls B800 and B850 in LH2 of 226 mM^{-1} cm^{-1} and 2.5 mM^{-1} cm^{-1} accordingly[36] at 800 nm and a partition ratio of 86:14[19] of excitons between LH2 and LH1. The membrane contains LH1s and LH2s in 1:2 ratios and 14 excitons are created on each LH1 for every 86 excitons created on each LH2. From these values, we calculate that 1.4×10^5 photons are absorbed per second at a 100 W/m^2 light fluence by our 24x24 hexagonal membrane.

To investigate if the supercomplex structure affects transfer-to-trap efficiency, we construct three lattice structures ("Random"; "Island" with groups of LH1s clustered together, and "Isolated" with all LH1s separated by LH2s) for further fluence-dependent Monte-Carlo exciton

dynamics simulations. The first lattice is a random arrangement of LH1s and LH2s in the 1:2 ratio, which represents the high-light membranes of bacteria such as *Rsp. photometricum* and *Rps. acidophila.*[17] Simulations for this structure are performed on 144 different random arrangements to obtain the data, shown in the paper. The second lattice consists of 2×4 LH1 islands surrounded by LH2 such that the LH1:LH2 ratio is 1:2. This arrangement represents many species in the *Rhodobacter* genus. The third is an idealized "Isolated" lattice of a two-dimensional hexagonal AB_2 arrangement that eliminates adjacent LH1 neighbors. Data collected on different ratios, defects and light fluences is averaged over 72,000,000 exciton trajectories across 144 spatial and energetic realizations of the membranes. We assume that membrane curvature does not strongly change exciton dynamics.[37-42] We note that while we assume the hopping rate k_h to be constant, it has been shown that intercomplex distance changes because of membrane curvature and the average hopping time between two LH2 complexes can range between 4 and 25 ps because of different intercomplex distances. Finally, we assume that the $\sim$150 cm^{-1} static disorder of LH complexes rules out resonance enhancement of Förster hopping for certain energy differences in accordance with earlier work by Jang[43] and Schulten[44] and co-workers.

First, we look at the effect of LH1:LH2 ratios on exciton dynamics. Exciton lifetimes from our simulations, as shown in *Figure 2.2a*, are in good agreement with earlier experimentally determined lifetimes for the different ratios of LH1 and LH2 expression.[19] An earlier theoretical work calculated a 50 ps lifetime for a 1:2.8 LH1:LH2 ratio.[6] As the LH1:LH2 ratio increases from 1:2 to 1:6, the exciton lifetime increases from ~60 ps to 82 ps (*Fig. 2.2a*). Our simulations also show that the increasing LH1:LH2 ratio leads to an increase in fluorescence quantum yield, or lower transfer-to-trap efficiency (*Fig. 2.2b*). Looking at the constituent hops of the average exciton trajectory (defined as hops between the two different types of LH complexes), we find that only

hops between LH2s increase significantly (*Fig. 2.2c*) as a function of LH2 expression and LH1 to LH1 hops decrease concomitantly. Irrespective of the LH1:LH2 ratio, exciton hopping from LH2 to LH1 and back-hopping from LH1 to LH2 do not change significantly (on average 1.46 to 1.62 times and 0.65 to 0.78 times, respectively, over an exciton's lifetime).

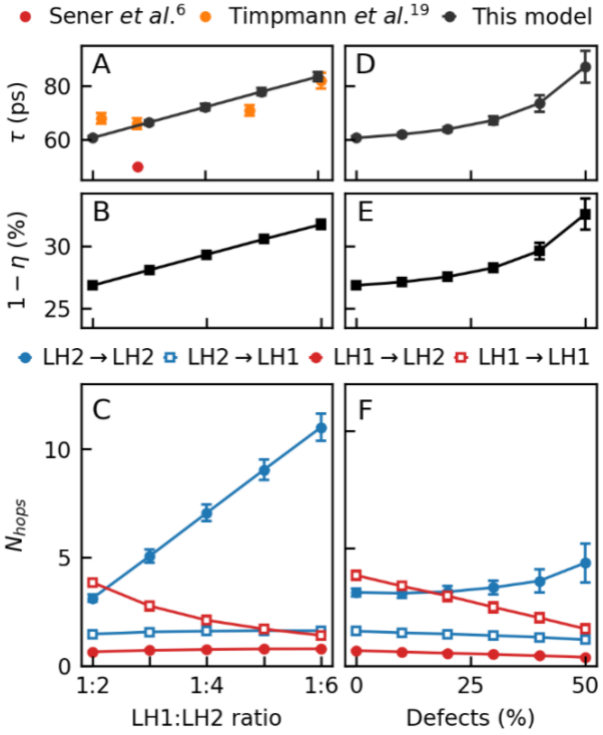

Fig 2.2: **a)** Trend of exciton lifetimes τ from our model plotted against experimentally obtained lifetimes by Timpmann *et al.*[19] and the theoretically calculated lifetime by Sener *et al.*[6] for different LH1:LH2 ratios **b)** Trend of fluorescence quantum yield $(1-\eta)$ values obtained from our simulations for different LH1:LH2 ratios **c)** Number of hops from LH2 to LH2, LH2 to LH1, LH1 to LH2 and LH1 to LH1 as a function of LH1:LH2 ratio **d)** Trend of exciton lifetimes τ as a function of percentage of defect sites on the membrane lattice **e)** Trend of quantum yield values as a function of percentage of defect sites **f)** Number of hops from LH2 to LH2, LH2 to LH1, LH1 to LH2 and LH1 to LH1. Error bars correspond to one standard deviation (SD).

Our simulations show that exciton lifetime increases with the percentage of defective lattice sites (*Fig. 2.2d*). For up to 30% defective sites, the transfer-to-trap efficiency of the

membrane decreases by only ~2% (*Fig. 2.2e*), after which it decreases more sharply. Looking at the types of exciton hops, we see that only hops between LH2s increase (*Fig. 2.2f*). Hops between LH1 decrease appreciably and hops from LH1 to LH2 and LH2 to LH1 show a small decrease with increasing percentage of defects.

We recover the experimentally observed trend of exciton lifetime as a function of light fluence.[19, 33] Using an RC turnover rate of 25 ms/exciton,[4, 34, 35] we find particularly good agreement with the experimental work of Borisov *et al.*[33] A saturation limit lifetime of 200 ps is obtained for the single exciton regime in accordance with our chosen LH1 fluorescence lifetime (*Fig. 2.3a*). A small increase is seen in hops between LH2s, from LH1 to LH2 and from LH2 to LH1. The largest increase is seen in inter-LH1 hops as a function of N_{block} (from ~4 to 16 hops, *Fig. 2.3b*). *Figure 2.3c* shows representative exciton trajectories on the lattice under low light ($N_{block} = 0$) and high light ($N_{block} = 10000$) conditions. We see that in high light, the diffusion region of the exciton increases, and there is a greater number of inter-LH1 hops.

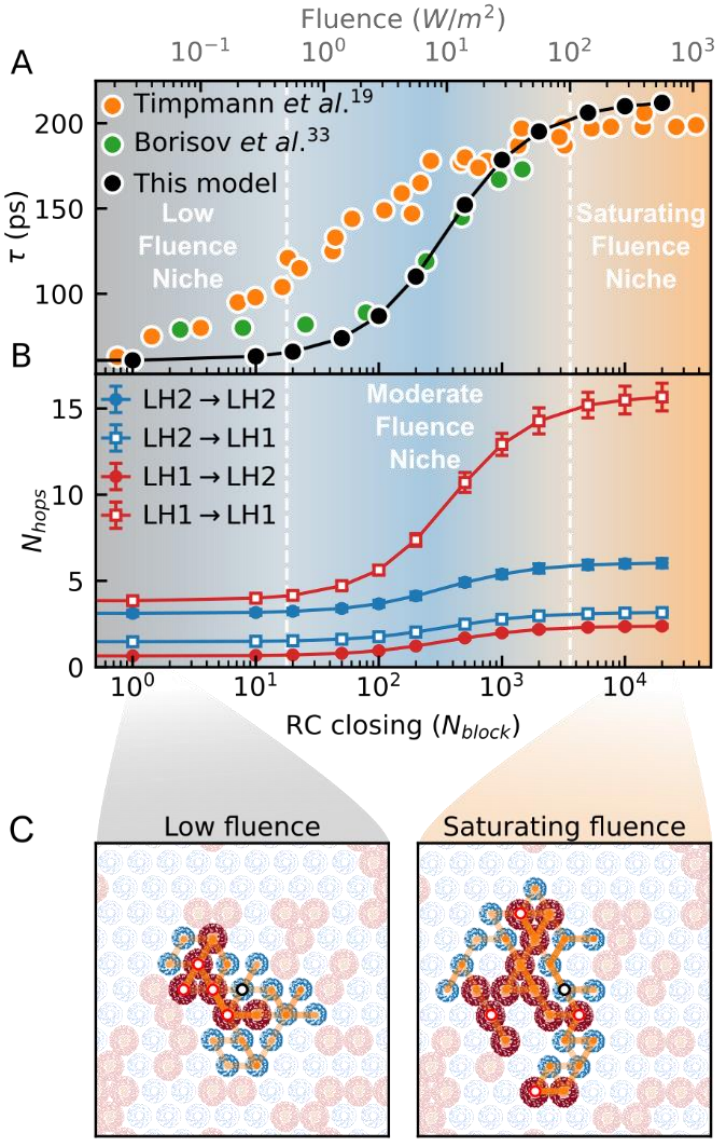

Fig 2.3: **a)** Trend of fluorescence lifetimes τ obtained from our simulations as a function of RC closing and light fluence plotted with experimentally measured lifetimes as a function of light fluence by Timpmann *et al.*[19] and Borisov *et al.*[33] **b**) Number of hops as a function of subsequent RC blocking iterations **c**) Four sample trajectories for RC closing (N_{block}) values of 0 and 10000. Trajectories start at the LH2 with a black outline circle and end at the circles with red outlines. Brightness of yellow lines indicates the number of hops between two pairs of complexes and highlights the increased inter-LH1 hops. Mean lifetime is preserved while randomly picking trajectories to represent. LH1, red; LH2, blue. Error bars show 1SD.

First, we look at the impact of LH1:LH2 ratios on exciton dynamics. The remarkable robustness of the energy funnel in purple bacteria is underlined by the stable rate of back-hopping from the low-energy LH1 pools to high-energy LH2s, even with high LH2 expression. Our observation that only inter-LH2 hops increase substantially for high LH2 ratios is consistent with earlier work showing that increased LH2 expression is not associated with enhanced exciton transfer from LH2 to LH1[20] (*Fig. 2.2c*). In the case of defects, up to 30% defects have only small effects on the different constituent hops, underlining the robustness of the ICM structure. In our simulations, we only model defects as sites to which the exciton cannot hop, but defective placement of bacteriochlorophylls can lead to LH1s or LH2s with very different energies or exciton hopping rates.[45] We do not incorporate the effect of these defects into our simulations.

In this study of the effect of fluence on transfer-to-trap efficiency, we observe a large increase in inter-LH1 hops in simulations of high RC blocking. This increase indicates that even in high light fluences — when most RCs are closed to incoming excitons — LH2s are effectively excluded from the diffusion region to maximize the probability of the exciton finding an open RC. This effect is clearly seen in *Fig. 2.3c*, where sample trajectories show that LH1s are sampled far more than LH2s in high light. It is worth noting that our *a priori* chosen RC turnover rate of 25 ms/exciton from Fassioli *et al*,[4] consistent with other experimental measurements,[34, 35] yields good agreement with fluence dependent lifetimes from the experimental work of Borisov *et al*,[33] shown in *Fig. 2.3a*. We further obtain a best fit RC turnover rate of 22.7 ms/exciton for the study by Borisov *et al*[33] and a best fit RC turnover rate of 143 ms/exciton for the study by Timpmann *et al.*[19] It is likely that different RC turnover rates in laboratory conditions among other factors could have led to differences in the fluence dependence of lifetimes measured by Borisov *et al*[33] and Timpmann *et al.*[19] Previous studies have suggested that quinone release, and not uptake is the rate

limiting step in the RC turnover making the physiological RC turnover of Random (*P. molischianum*)[46] and Island (*Rb. sphaeroides*)[47] comparable at 25 ms/exciton. At comparable RC turnover rates, the Island arrangement could provide *Rb. sphaeroides* with a transfer-to-trap efficiency advantage over other Random structures. It should be noted that pH and NaCl ionic strength strongly impact the RC turnover rate[34, 35, 48] in experimental conditions and a fluctuating RC turnover rate in turn impacts transfer-to-trap efficiency. Thus, our comparison of the two structures' transfer-to-trap efficiency as a function of light fluence is restricted to the case in which RC turnover rates are the same.

Efficiency differences between the Island, Random and Isolated arrangements (*Fig 2.4*) shed light on the effect of spatial arrangement on transfer-to-trap efficiencies in different light conditions. In the saturation limit, the three membranes show transfer-to-trap efficiency approaching 0% as all RCs are closed and almost all excitons fluoresce. The higher photosynthetic efficiency of the Isolated structure at low fluence is likely due to maximal encircling of every LH1 by LH2s, offering a possible one-hop pathway for excitons to reach an open LH1-embedded RC. These results are consistent with an earlier study[8] in which a similar "Isolated"-type structure was found to be more efficient for transfer-to-trap under low-light conditions than other structures. However, upon taking solar fluences into account, a single structure is not the clear winner in terms of transfer-to-trap efficiency. At the typical niche fluences between 0.5 and 100 W/m^2, the Island structure shows an enhanced transfer-to-trap efficiency by ~1%. Thus, if RC turnover rates are similar in Random and Island structures found in nature and limited by quinone release, the Island structure could provide an efficiency advantage over the Random arrangement.

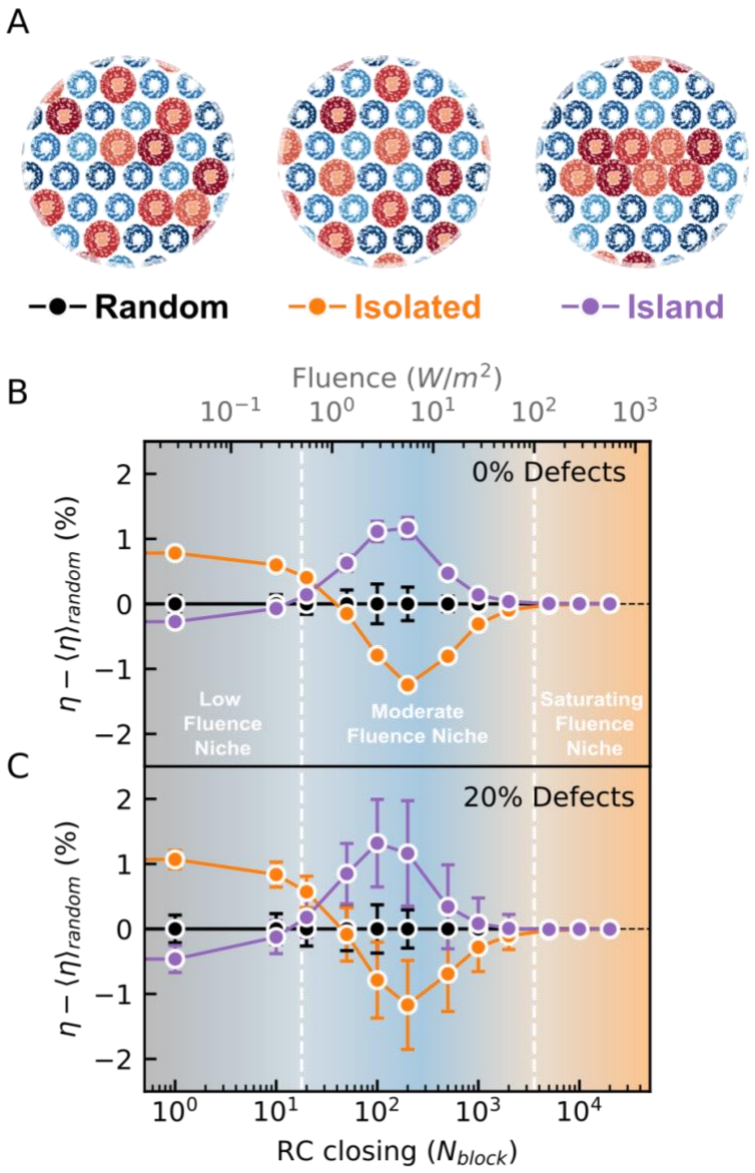

Fig 2.4: **a)** Representative sections of Random, Isolated and Island lattice structures. LH1s and LH2s are randomly distributed in a 1:2 ratio in the Random lattice, the Isolated and Island structures are repeated over the 24×24 membrane **b**) Random, Island and Isolated structure efficiency deviations from the average Random efficiency $\langle\eta\rangle_{random}$ as a function of N_{block} for a lattice without defects. **c**) Random, Island and Isolated structure efficiency deviations from the average Random efficiency $\langle\eta\rangle_{random}$ as a function of N_{block} for a lattice with 20% defects. Error bars show 1SD.

The replication of this trend with 20% defects, with faster hopping rates (see publication for details) suggests that this effect is robust to the placement of non-light harvesting proteins like cytochromes, defective proteins and to gaps induced due to the curvature of the membrane vesicle.[42] An earlier work on Photosystem I showed a similar robustness of the protein to chlorophyll *a* deletion, where the photosynthetic efficiency of the reaction center was not affected by more than 3% upon the random deletion of any chlorophyll molecule outside of the reaction center.[49]

Our finding that the Isolated LH1 arrangement performs better in low light is consistent with published membrane AFM images of species inhabiting low light environments. Isolated LH1 complexes are clearly seen in the "Random"-type arrangements found in these species. For example, *Roseobacter* species that inhabit temperate polar oceans and likely experience low light manifest prominent unconnected monomeric LH1 structures in AFM images;[50, 51] species observed in Antarctic seas at depths substantially below the depth at which only 1% of the surface light reaches show the presence of isolated LH1s.[52-55]

On the other hand, according to our findings, the formation of LH1 islands is deleterious to transfer-to-trap efficiency in low-light environments. In nature, while species with Random arrangements (e.g., *Rhodopseudomonas* genus) exist in niches with low, moderate and high solar fluences, species with prominent LH1 island arrangements, such as *Rhodobacter*, have been found only in medium and high fluence niches.

Further, within *Rb. sphaeroides*, the expression of RC-LH1-PufX dimers that form LH1 Islands has been shown to increase drastically in high light intensity growth[56] and suggests that LH1 Island formation is indeed light fluence driven. However, AFM images of low-light grown *Rb. sphaeroides* do not show a significant presence of monomeric LH1s.[57] It is likely that the

adaptive strategy we suggest manifests across different species. Therefore, we hypothesize that the remarkable 1% enhanced efficiency of the Island arrangement (compared to the Random arrangement) across a wide range of physiologically relevant light fluences (0.5 to 100 W/m^2) provides species of the *Rhodobacter* genus with a significant competitive advantage in well-lit environments. An extensive AFM based comparison between species will be needed to completely validate our hypothesis.

In summary, I demonstrate in this chapter the use of Miller-Abrahams weighting of exciton hopping on purple bacterial intracytoplasmic membranes. We observe that the formation of LH1 2x4 islands increases the transfer-to-trap efficiency of photosynthesis in moderate- to high-light environments while random arrangements work well in low-fluence environments. Our result explains the notable absence of species with aggregated LH1 structures in low light habitat and the drastic increase seen in the expression of dimeric LH1 complexes by Jones and co-workers.[56] This effect is robust against gaps induced by photosynthetic membrane curvature and the presence of non-photosynthetic proteins. We believe that the effect could be harnessed in future artificial photosynthesis design efforts because redox and electrochemistry are typically slower than exciton transport in materials.[1, 10]

Further details are included in Onizhuk, Sohoni*, Galli, Engel, J. Phys. Chem. Lett., 2021.*[58]

Bibliography

(1) Blankenship, R. E. Antenna Complexes and Energy Transfer Processes. In *Molecular Mechanisms of Photosynthesis*, Wiley, 2002; pp 61-94.
(2) Scholes, G. D.; Fleming, G. R.; Olaya-Castro, A.; van Grondelle, R. Lessons from Nature about Solar Light Harvesting. *Nature Chemistry* **2011**, *3* (10), 763-774.
(3) Lee, Y.; Gorka, M.; Golbeck, J. H.; Anna, J. M. Ultrafast Energy Transfer Involving the Red Chlorophylls of Cyanobacterial Photosystem I Probed through Two-Dimensional Electronic Spectroscopy. *Journal of the American Chemical Society* **2018**, *140* (37), 11631-11638.
(4) Fassioli, F.; Olaya-Castro, A.; Scheuring, S.; Sturgis, J. N.; Johnson, N. F. Energy Transfer in Light-Adapted Photosynthetic Membranes: From Active to Saturated Photosynthesis. *Biophysical Journal* **2009**, *97* (9), 2464-2473.
(5) Dahlberg, P. D.; Ting, P.-C.; Massey, S. C.; Allodi, M. A.; Martin, E. C.; Hunter, C. N.; Engel, G. S. Mapping the Ultrafast Flow of Harvested Solar Energy in Living Photosynthetic Cells. *Nature Communications* **2017**, *8* (1), 988.
(6) Şener, M. K.; Olsen, J. D.; Hunter, C. N.; Schulten, K. Atomic-level structural and functional model of a bacterial photosynthetic membrane vesicle. *Proceedings of the National Academy of Sciences* **2007**, *104* (40), 15723-15728.
(7) Ritz, T.; Park, S.; Schulten, K. Kinetics of Excitation Migration and Trapping in the Photosynthetic Unit of Purple Bacteria. *The Journal of Physical Chemistry B* **2001**, *105* (34), 8259-8267.
(8) Sturgis, J. N.; Niederman, R. A. Atomic Force Microscopy Reveals Multiple Patterns of Antenna Organization in Purple Bacteria: Implications for Energy Transduction Mechanisms and Membrane Modeling. *Photosynthesis Research* **2008**, *95* (2), 269-278.
(9) Sohail, S. H.; Dahlberg, P. D.; Allodi, M. A.; Massey, S. C.; Ting, P.-C.; Martin, E. C.; Hunter, C. N.; Engel, G. S. Communication: Broad manifold of excitonic states in light-harvesting complex 1 promotes efficient unidirectional energy transfer in vivo. *The Journal of Chemical Physics* **2017**, *147* (13).
(10) Proppe, A. H.; Li, Y. C.; Aspuru-Guzik, A.; Berlinguette, C. P.; Chang, C. J.; Cogdell, R.; Doyle, A. G.; Flick, J.; Gabor, N. M.; van Grondelle, R.; et al. Bioinspiration in light harvesting and catalysis. *Nature Reviews Materials* **2020**, *5* (11), 828-846.
(11) Cogdell, R. J.; Gall, A.; Köhler, J. The architecture and function of the light-harvesting apparatus of purple bacteria: from single molecules to in vivo membranes. *Quarterly Reviews of Biophysics* **2006**, *39* (3), 227-324.From Cambridge University Press Cambridge Core
(12) Wu, J.; Liu, F.; Shen, Y.; Cao, J.; Silbey, R. J. Efficient energy transfer in light-harvesting systems, I: optimal temperature, reorganization energy and spatial–temporal correlations. *New Journal of Physics* **2010**, *12* (10), 105012.
(13) Gellings, E.; Cogdell, R. J.; van Hulst, N. F. Room-Temperature Excitation–Emission Spectra of Single LH2 Complexes Show Remarkably Little Variation. *The Journal of Physical Chemistry Letters* **2020**, *11* (7), 2430-2435.
(14) Caycedo-Soler, F.; Rodríguez, F. J.; Quiroga, L.; Johnson, N. F. Interplay between excitation kinetics and reaction-center dynamics in purple bacteria. *New Journal of Physics* **2010**, *12* (9), 095008.

(15) Caycedo-Soler, F.; Rodríguez, F. J.; Quiroga, L.; Johnson, N. F. Light-Harvesting Mechanism of Bacteria Exploits a Critical Interplay between the Dynamics of Transport and Trapping. *Physical Review Letters* **2010**, *104* (15), 158302.
(16) Sundström, V.; Pullerits, T.; van Grondelle, R. Photosynthetic Light-Harvesting: Reconciling Dynamics and Structure of Purple Bacterial LH2 Reveals Function of Photosynthetic Unit. *The Journal of Physical Chemistry B* **1999**, *103* (13), 2327-2346.
(17) Bahatyrova, S.; Frese, R. N.; Siebert, C. A.; Olsen, J. D.; van der Werf, K. O.; van Grondelle, R.; Niederman, R. A.; Bullough, P. A.; Otto, C.; Hunter, C. N. The native architecture of a photosynthetic membrane. *Nature* **2004**, *430* (7003), 1058-1062.
(18) Scheuring, S.; Reiss-Husson, F.; Engel, A.; Rigaud, J. L.; Ranck, J. L. High resolution AFM topographs of *Rubrivivax gelatinosus* light harvesting complex LH2. *The EMBO Journal* **2001**, *20* (12), 3029-3035.
(19) Timpmann, K.; Chenchiliyan, M.; Jalviste, E.; Timney, J. A.; Hunter, C. N.; Freiberg, A. Efficiency of light harvesting in a photosynthetic bacterium adapted to different levels of light. *Biochimica et Biophysica Acta (BBA) - Bioenergetics* **2014**, *1837* (10), 1835-1846.
(20) Driscoll, B.; Lunceford, C.; Lin, S.; Woronowicz, K.; Niederman, R. A.; Woodbury, N. W. Energy transfer properties of *Rhodobacter sphaeroides* chromatophores during adaptation to low light intensity. *Physical Chemistry Chemical Physics* **2014**, *16* (32), 17133-17141. 10.1039/C4CP01981D
(21) Scheuring, S.; Rigaud, J. L.; Sturgis, J. N. Variable LH2 stoichiometry and core clustering in native membranes of *Rhodospirillum photometricum*. *The EMBO Journal* **2004**, *23* (21), 4127-4133.
(22) Olsen, J. D.; Adams, P. G.; Jackson, P. J.; Dickman, M. J.; Qian, P.; Hunter, C. N. Aberrant Assembly Complexes of the Reaction Center Light-harvesting 1 PufX (RC-LH1-PufX) Core Complex of *Rhodobacter sphaeroides* Imaged by Atomic Force Microscopy *Journal of Biological Chemistry* **2014**, *289* (43), 29927-29936.
(23) Miller, A.; Abrahams, E. Impurity Conduction at Low Concentrations. *Physical Review* **1960**, *120* (3), 745-755.
(24) Li, H.; Sini, G.; Sit, J.; Moulé, A. J.; Bredas, J.-L. Understanding charge transport in donor/acceptor blends from large-scale device simulations based on experimental film morphologies. *Energy & Environmental Science* **2020**, *13* (2), 601-615. 10.1039/C9EE03791H
(25) Singh, R.; Kim, M.; Lee, J.-J.; Ye, T.; Keivanidis, P. E.; Cho, K. Excimer formation effects and trap-assisted charge recombination loss channels in organic solar cells of perylene diimide dimer acceptors. *Journal of Materials Chemistry C* **2020**, *8* (5), 1686-1696. 10.1039/C9TC04955J
(26) Gilmore, R. H.; Winslow, S. W.; Lee, E. M. Y.; Ashner, M. N.; Yager, K. G.; Willard, A. P.; Tisdale, W. A. Inverse Temperature Dependence of Charge Carrier Hopping in Quantum Dot Solids. *ACS Nano* **2018**, *12* (8), 7741-7749.
(27) Lee, E. M. Y.; Tisdale, W. A.; Willard, A. P. Can Disorder Enhance Incoherent Exciton Diffusion? *The Journal of Physical Chemistry B* **2015**, *119* (30), 9501-9509.
(28) Rutkauskas, D.; Novoderezkhin, V.; Cogdell, R. J.; van Grondelle, R. Fluorescence Spectral Fluctuations of Single LH2 Complexes from Rhodopseudomonas acidophila Strain 10050. *Biochemistry* **2004**, *43* (15), 4431-4438.
(29) Schlau-Cohen, G. S.; Wang, Q.; Southall, J.; Cogdell, R. J.; Moerner, W. E. Single-molecule spectroscopy reveals photosynthetic LH2 complexes switch between emissive states. *Proceedings of the National Academy of Sciences* **2013**, *110* (27), 10899-10903.

(30) Law, C. J.; Cogdell, R. J. The effect of chemical oxidation on the fluorescence of the LH1 (B880) complex from the purple bacterium Rhodobium marinum. *FEBS Letters* **1998**, *432* (1-2), 27-30.
(31) Beyer, S. R.; Müller, L.; Southall, J.; Cogdell, R. J.; Ullmann, G. M.; Köhler, J. The Open, the Closed, and the Empty: Time-Resolved Fluorescence Spectroscopy and Computational Analysis of RC-LH1 Complexes from Rhodopseudomonas palustris. *The Journal of Physical Chemistry B* **2015**, *119* (4), 1362-1373.
(32) Pflock, T.; Dezi, M.; Venturoli, G.; Cogdell, R. J.; Köhler, J.; Oellerich, S. Comparison of the fluorescence kinetics of detergent-solubilized and membrane-reconstituted LH2 complexes from Rps. acidophila and Rb. sphaeroides. *Photosynthesis Research* **2008**, *95* (2), 291-298.
(33) Borisov, A. Y.; Freiberg, A. M.; Godik, V. I.; Rebane, K. K.; Timpmann, K. E. Kinetics of picosecond bacteriochlorophyll luminescence in vivo as a function of the reaction center state. *Biochimica et Biophysica Acta (BBA) - Bioenergetics* **1985**, *807* (3), 221-229.
(34) Comayras, F.; Jungas, C.; Lavergne, J. Functional Consequences of the Organization of the Photosynthetic Apparatus in *Rhodobacter sphaeroides*: II. A Study of *PufX* Membranes. *Journal of Biological Chemistry* **2005**, *280* (12), 11214-11223.
(35) Gerencsér, L.; Laczkó, G.; Maróti, P. Unbinding of Oxidized Cytochrome *c* from Photosynthetic Reaction Center of *Rhodobacter sphaeroides* Is the Bottleneck of Fast Turnover. *Biochemistry* **1999**, *38* (51), 16866-16875.
(36) Sturgis, J. N.; Hunter, C. N.; Niederman, R. A. Spectra and Extinction Coefficients of Near-Infrared Absorption Bands in Membranes of *Rhodobacter sphaeroides* Mutants Lacking Light-Harvesting and Reaction Center Complexes. *Photochemistry and Photobiology* **1988**, *48* (2), 243-247.
(37) Ogren, J. I.; Tong, A. L.; Gordon, S. C.; Chenu, A.; Lu, Y.; Blankenship, R. E.; Cao, J.; Schlau-Cohen, G. S. Impact of the lipid bilayer on energy transfer kinetics in the photosynthetic protein LH2. *Chemical Science* **2018**, *9* (12), 3095-3104. 10.1039/C7SC04814A
(38) Liu, L.-N.; Duquesne, K.; Oesterhelt, F.; Sturgis, J. N.; Scheuring, S. Forces guiding assembly of light-harvesting complex 2 in native membranes. *Proceedings of the National Academy of Sciences* **2011**, *108* (23), 9455-9459.
(39) Cleary, L.; Chen, H.; Chuang, C.; Silbey, R. J.; Cao, J. Optimal fold symmetry of LH2 rings on a photosynthetic membrane. *Proceedings of the National Academy of Sciences* **2013**, *110* (21), 8537-8542.
(40) Chandler, D. E.; Hsin, J.; Harrison, C. B.; Gumbart, J.; Schulten, K. Intrinsic Curvature Properties of Photosynthetic Proteins in Chromatophores. *Biophysical Journal* **2008**, *95* (6), 2822-2836.
(41) Singharoy, A.; Maffeo, C.; Delgado-Magnero, K. H.; Swainsbury, D. J. K.; Sener, M.; Kleinekathöfer, U.; Vant, J. W.; Nguyen, J.; Hitchcock, A.; Isralewitz, B.; et al. Atoms to Phenotypes: Molecular Design Principles of Cellular Energy Metabolism. *Cell* **2019**, *179* (5), 1098-1111.e1023.
(42) Şener, M.; Strümpfer, J.; Timney, J. A.; Freiberg, A.; Hunter, C. N.; Schulten, K. Photosynthetic Vesicle Architecture and Constraints on Efficient Energy Harvesting. *Biophysical Journal* **2010**, *99* (1), 67-75.
(43) Jang, S. J. Robust and Fragile Quantum Effects in the Transfer Kinetics of Delocalized Excitons between B850 Units of LH2 Complexes. *The Journal of Physical Chemistry Letters* **2018**, *9* (22), 6576-6583.

(44) Strümpfer, J.; Schulten, K. Light harvesting complex II B850 excitation dynamics. *The Journal of Chemical Physics* **2009**, *131* (22).
(45) Baghbanzadeh, S.; Kassal, I. Geometry, Supertransfer, and Optimality in the Light Harvesting of Purple Bacteria. *The Journal of Physical Chemistry Letters* **2016**, *7* (19), 3804-3811.
(46) Mascle-Allemand, C.; Lavergne, J.; Bernadac, A.; Sturgis, J. N. Organisation and function of the Phaeospirillum molischianum photosynthetic apparatus. *Biochimica et Biophysica Acta (BBA) - Bioenergetics* **2008**, *1777* (12), 1552-1559.
(47) Milano, F.; Agostiano, A.; Mavelli, F.; Trotta, M. Kinetics of the quinone binding reaction at the Q_B site of reaction centers from the purple bacteria Rhodobacter sphaeroides reconstituted in liposomes. *European Journal of Biochemistry* **2003**, *270* (23), 4595-4605.
(48) Osváth, S.; Maróti, P. Coupling of cytochrome and quinone turnovers in the photocycle of reaction centers from the photosynthetic bacterium Rhodobacter sphaeroides. *Biophysical Journal* **1997**, *73* (2), 972-982.
(49) Sener, M. K.; Lu, D.; Ritz, T.; Park, S.; Fromme, P.; Schulten, K. Robustness and Optimality of Light Harvesting in Cyanobacterial Photosystem I. *The Journal of Physical Chemistry B* **2002**, *106* (32), 7948-7960.
(50) Selje, N.; Simon, M.; Brinkhoff, T. A newly discovered Roseobacter cluster in temperate and polar oceans. *Nature* **2004**, *427* (6973), 445-448.
(51) Tang, K.; Zong, R.; Zhang, F.; Xiao, N.; Jiao, N. Characterization of the Photosynthetic Apparatus and Proteome of *Roseobacter denitrificans*. *Current Microbiology* **2010**, *60* (2), 124-133.
(52) *Modern Topics in the Phototrophic Prokaryotes*; Springer Cham, 2017.
(53) Scheuring, S.; Gonçalves, R. P.; Prima, V.; Sturgis, J. N. The Photosynthetic Apparatus of *Rhodopseudomonas palustris*: Structures and Organization. *Journal of Molecular Biology* **2006**, *358* (1), 83-96.
(54) Burke, C. M.; Burton, H. R. Photosynthetic bacteria in meromictic lakes and stratified fjords of the Vestfold Hills, Antarctica. *Hydrobiologia* **1988**, *165* (1), 13-23.
(55) El-Sayed, S. Z.; Biggs, D. C.; Holm-Hansen, O. Phytoplankton standing crop, primary productivity, and near-surface nitrogenous nutrient fields in the Ross Sea, Antarctica. *Deep Sea Research Part A. Oceanographic Research Papers* **1983**, *30* (8), 871-886.
(56) Crouch, L. I.; Jones, M. R. Cross-species investigation of the functions of the *Rhodobacter* PufX polypeptide and the composition of the RC–LH1 core complex. *Biochimica et Biophysica Acta (BBA) - Bioenergetics* **2012**, *1817* (2), 336-352.
(57) Adams, P. G.; Hunter, C. N. Adaptation of intracytoplasmic membranes to altered light intensity in *Rhodobacter sphaeroides*. *Biochimica et Biophysica Acta (BBA) - Bioenergetics* **2012**, *1817* (9), 1616-1627.
(58) Onizhuk, M.; Sohoni, S.; Galli, G.; Engel, G. S. Spatial Patterns of Light-Harvesting Antenna Complex Arrangements Tune the Transfer-to-Trap Efficiency of Excitons in Purple Bacteria. *The Journal of Physical Chemistry Letters* **2021**, *12* (29), 6967-6973.

Chapter 3

Phycobilisome's Exciton Transfer Efficiency Relies on an Energetic Funnel Driven by Chromophore-Linker Protein Interactions

Reproduced with permission from Sohoni, Lloyd, Hitchcock, MacGregor-Chatwin, Iwanicki, Ghosh, Shen, Hunter, Engel, J. Am. Chem. Soc., 2023

The phycobilisome is the primary light-harvesting antenna in cyanobacterial and red algal oxygenic photosynthesis. It maintains near-unity efficiency of energy transfer to reaction centers despite relying on slow exciton hopping along a relatively sparse network of highly fluorescent phycobilin chromophores. In this chapter, I try to answer how the complex maintains this high efficiency. Using a two-dimensional electronic spectroscopy polarization scheme that enhances energy transfer features, we directly watch energy flow in the phycobilisome complex of *Synechocystis* sp. PCC 6803 from the outer phycocyanin rods to the allophycocyanin core. The observed downhill flow of energy, previously hidden within congested spectra, is faster than timescales predicted by Förster hopping along single rod chromophores. We attribute the fast 8 ps energy transfer to interactions between the rod-core linker protein and the terminal phycocyanin trimer chromophores, which facilitate downhill, unidirectional energy flow to the core. This mechanism drives the high energy transfer efficiency in the phycobilisome and suggests that linker protein-chromophore interactions have likely evolved to shape this energetic landscape.

Cyanobacteria are oxygenic photosynthetic microorganisms. They produce about 40% of the world's oxygen and were responsible for the Great Oxygenation Event of our planet.[1-3] During

oxygenic photosynthesis in cyanobacteria, plants, and algae, solar energy absorbed by large networks of antenna pigments migrates to reaction centers, where it is converted to a charge separation. For example, excitons created in the $C_2S_2M_2$-LHCII complex of plants rapidly transfer to the reaction centers in photosystem II (PSII).[4, 5] In cyanobacteria, the ~5-8 MDa phycobilisome complex composed of multiple phycocyanin (PC) and allophycocyanin (APC) protein subunits serves as the primary light-harvesting antenna. It supplies excitations to both photosystems with near-unity efficiency.[6, 7] The phycobilisome complex from the model cyanobacterium *Synechocystis* sp. PCC 6803 consists of six PC hexamer rods attached by a linker protein onto a core made of three lateral APC hexamer assemblies (*Fig 3.1a*). The core sits atop the photosystems and funnels excitations to them.[6] The colorless linker proteins do not participate in light harvesting but provide structural integrity to this megacomplex by connecting the rods to the core.[4, 8-15] In high light fluences, the orange carotenoid protein (OCP) attaches to the phycobilisome core to efficiently quench excitations before they reach the photosystems.[15]

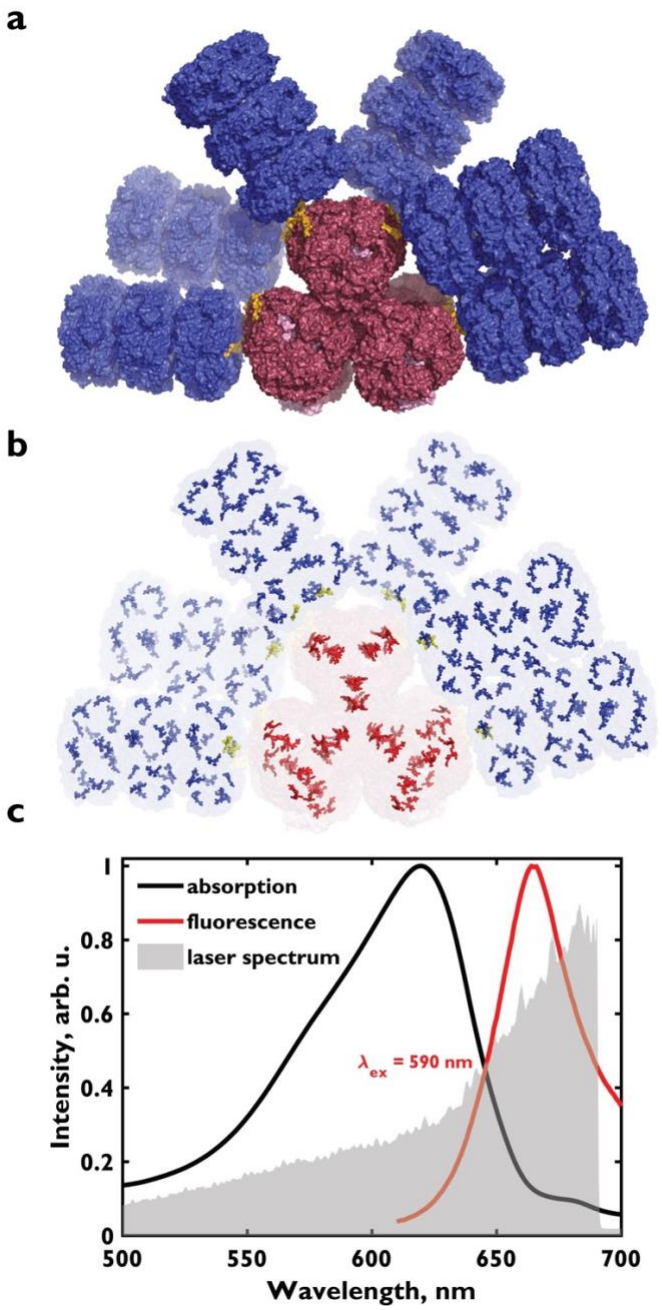

Fig 3.1: **a)** Cryo-electron microscopy structure of the *Synechocystis* sp. PCC 6803 phycobilisome rendered using coordinates from Kerfeld and coworkers:[15] Six hexameric C-phycocyanin rods (blue) are assembled on the three lateral allophycocyanin cores (red). **b)** The arrangement of phycocyanobilin chromophores in the phycobilisome (blue) with terminal rod chromophores (gold) strongly associated with the CpcG rod-core linker protein, and core allophycocyanin chromophores (red). **c)** Absorption (black) and fluorescence (red) spectra overlaid with the laser spectrum (gray) used in our broadband two-dimensional spectroscopy experiments.

Despite seemingly deleterious slow exciton hopping over the sparse arrangement of highly fluorescent chromophores, the complex maintains near-unity exciton-transfer efficiency.[6, 7] As detailed in numerous studies, the mechanisms yielding this high transfer efficiency are not well known.[4, 8-13] Electron microscopy (EM) advances in recent years have driven detailed structural elucidation of these megacomplexes and provide many clues about the underlying mechanisms.[8, 12, 14-17] However, progress in resolving energy transfer dynamics using time-resolved spectroscopy has been slower owing to massive spectral congestion from hundreds of phycobilisome pigments.[18-26] Small energetic separations in the donor and acceptor chromophores in the network confound isolation of signal kinetics from individual pigments or complexes, hiding the principles driving high transfer efficiencies that operate on the supercomplex or quaternary level. An alternative to using spectral resolution to reveal excitonic pathways is to use the different dipole directions of the linear phycocyanobilin chromophores in the complex through polarization dependent spectroscopy. Conveniently, the bilins in the core proximal to the rods sit at about 60 degrees to those in the rods.[13]

To selectively obtain signals associated with energy transfer along the chromophore network, we perform polarization-controlled broadband two-dimensional electronic spectroscopy (2DES) on the cyanobacterial phycobilisome complex. Using a previously reported polarization sequence[27, 28] in 2DES, we suppress signals from interactions with parallel transition dipole moments removing the spectral congestion, dynamic Stokes shift of chromophores and excited state absorption in this antenna. The suppression allows us to watch energy transfer selectively and directly from the rods of the phycobilisome to the inner core. We find that downhill energy transfer along the complex occurs on a much faster timescale (~8 ps) than suggested by previous time-resolved experiments and Förster calculations. We attribute the fast energy transfer to key

interactions between chromophores and the aromatic residues of the CpcG linker protein that connects PC rods to the lateral APC core. These interactions lower the energy of chromophores that form the rod-to-core connection in the excitonic pathway. This redshift has been characterized extensively by fluorescence measurements by Sauer and Pizarro.[29] They observe an emission redshift of about 150 cm^{-1} from the terminal phycocyanobilin chromophores in PC rods.[29] Multiple cryo-EM structures show that the interactions with the terminal chromophore are conserved across phycobilisomes of cyanobacterial and red-algal species.[8, 9, 12, 14-17] This redshift of the terminal chromophore promotes unidirectional downhill energy flow and minimizes exciton random walk along isoenergetic chromophores, in turn minimizing the probability of fluorescence and trapping. These results unearth a previously hidden photosynthetic design principle operating on the quaternary or supercomplex level that supports robust near-unity exciton transfer efficiency in oxygenic photosynthesis. We also find that upon reaching the core, the excitations remain in the higher energy core proteins for at least 800 ps, which is the majority of the phycobilisome fluorescence lifetime. Recent photoprotected cryo-EM structures show that these proteins are sites of photoprotection through OCP attachment.[15] The structures suggest that our observed long stay of excitons in the higher energy core proteins provides robust photoprotection opportunities to the antenna.

Phycobilisome absorption is tuned to 600-660 nm, which is outside of the main chlorophyll absorption bands (*Fig 3.1c*). Enhanced absorption in this region of the solar spectrum has in part driven cyanobacteria to become prolific and widespread photosynthesizers in marine and terrestrial habitats.[30-32] Unlike most other light-harvesting antennas, the spatial arrangement of about 300-400 chromophores in this complex is relatively sparse (*Fig 3.1b*) with the average distance between neighboring chromophores exceeding 2.5 nm.[5, 8, 9] Therefore, incoherent Förster type excitation

energy transfer (FRET) is the dominant energy transfer mechanism between pigments.[19, 33-36] The primary light-absorbing pigments in phycobilisomes are derivatives of open-chain tetrapyrrole molecules bound covalently to the protein backbone. These chromophores have a significantly higher fluorescence quantum yield *in vitro* than chlorophyll derivatives found in other antennas. In coherent time-resolved spectra, the phycobilisome shows a broad photoinduced absorption (PIA) feature suggested to arise from an electrochromic shift coupling[21, 37, 38] of excited and ground-state chromophores, which masks the red-most absorption and complete emission profile.[18, 21, 39] Previous time-resolved studies have suggested that excitations created in the rods travel downhill to the higher-energy ApcA and ApcB (hereafter called APC_{660} for their emission maxima) core proteins on the 30-50 ps timescale and from APC_{660} to the core terminal emitters bound to ApcD, ApcE and ApcF (hereafter called APC_{680}) proteins, on the 100 ps timescale before fluorescing with a ~1-2 ns lifetime in detached complexes.[15, 19, 21, 22, 26] APC_{680} terminal emitters transfer excitations to the photosystems that lie beneath the phycobilisomes.[40, 41] A new study by Beck and coworkers uses global analysis of 2DES data and suggests that excitons travel to the core in 13 ps.[20] The exact timescale of the rod-to-core transfer remains a topic of debate and differs in different global analyses. Many of the FRET steps along the way to the allophycocyanin core have time constants longer than 10 ps.[33] A bottleneck is predicted at the rod-to-core transfer step due to the large interchromophore distance, which makes backward hopping into the rod more favorable[15] and confounds our understanding of the high transfer efficiency of the complex. In this chapter, I investigate the basis for high energy transfer efficiency in the phycobilisome by directly monitoring energy flow in the phycobilisome complex of *Synechocystis* sp. PCC 6803 using polarization-controlled 2DES.

Two-dimensional Electronic Spectroscopy with Identically Polarized Pulses: Two-dimensional spectra of the phycobilisome obtained with identically linearly polarized pulses at 0.2, 2, 20 and 200 ps (*Fig 3.2a*) show dynamics in agreement with past measurements and significant spectral congestion.[18-22] The elongated positive feature along the diagonal from 590 to 670 nm in these spectra at early times corresponds to ground-state bleach and stimulated emission of all chromophores. Phycocyanobilin, the only bilin type in the *Synechocystis* sp. PCC 6803 phycobilisome, has different spectral properties in different protein environments, which gives rise to a broad and elongated lineshape along the diagonal. Each phycocyanin rod hexamer contains six β_{155} bilin chromophores in the β subunit that absorb maximally at 594 nm and six pairs of β_{84} and α_{84} chromophores arranged in close proximity that absorb at 625 nm and 618 nm, respectively.[42, 43] Each allophycocyanin trimer in the core also contains three β_{84} - α_{84} chromophore pairs absorbing maximally at 651 nm.[21] The maximal emission of the rods is at 645 nm[44] and the entire phycobilisome complex emits at ~665 nm. These features cannot be deconvolved at room temperature because of the broad lineshapes, as seen with other large photosynthetic proteins.[45, 46] Low-temperature studies of the phycobilisome are challenging because of the propensity of the complex to disassemble[4] and only a few fluorescence studies have been reported.[47-50] Similar diagonal elongation in 2D spectra is also observed in other light-harvesting antennae like PSI[45] and LHCII-CP29-CP24.[46] The negative feature seen below the diagonal at detection wavelengths (λ_{det}) between 660 and 680 nm has previously been attributed to an electrochromic shift of the excited states of neighboring chromophores, which induces a PIA feature.[21] A rounding out and downward movement in the 610-630 nm excitation region is seen in the positive feature at later times.

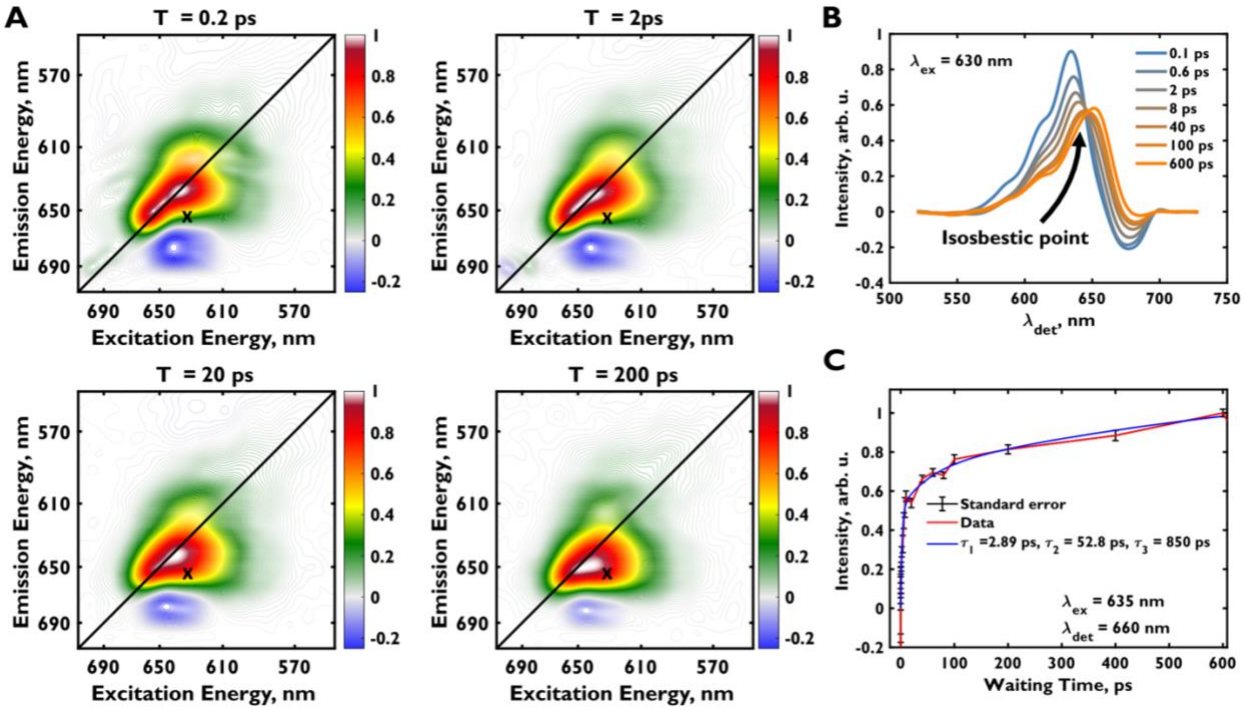

Fig 3.2: **a)** Purely absorptive real-valued two-dimensional electronic spectra of the phycobilisome at 0.2, 2, 20 and 200 ps in the {0 º 0 º 0 º 0 º}, or all-parallel pulse sequence. Spectra are frame-normalized. The positive features represent ground state bleach and stimulated emission, negative features represent photoinduced absorption. **b)** Cross-section of the two-dimensional spectra at various waiting times at λ_{ex} = 630 nm. **c)** Multi-exponential fit for the off-diagonal point, λ_{ex} = 635 nm, λ_{det} = 660 nm.

Downhill energy transfer from phycocyanin to allophycocyanin should appear as a cross-peak centered at excitation wavelength λ_{ex} = 618-635 nm and λ_{det} = 658 nm, based on chromophore excitation and emission energies. We cannot isolate the rise of this cross-peak because this region is also congested with the decaying PIA feature,[21] a dynamic Stokes shift in the phycocyanin and allophycocyanin pigments,[51] and the dynamics of the broad diagonal peak. *Figure 2.2b* shows a cross-section at λ_{ex} = 630 nm to illustrate this point. Three rising exponentials are needed to accurately fit this region (*Fig 2.2c*). The salient isosbestic point at λ_{det} ~ 647 nm, observed in the cross-section in *Figure 2.2b*, strongly suggests that a decaying spectral signature is giving rise to a new spectral signature. In previous studies, a ~50 ps time constant has been attributed to the

downward flow of energy from the rods to the core[19, 21] but this time constant could easily arise from differences between kinetics of the three processes described above. The first time constant, 2.89 ps, has been attributed to energy transfer along phycocyanin hexamers,[19, 21] but could also arise from the large dynamic Stokes shift of 30 nm in phycocyanin rods.[51] The longest time constant, 850 ps, has been attributed to the fluorescence lifetime and the decay of the PIA feature.[19] However, spectral congestion from numerous spectroscopic signals prohibits us from attributing these time constants to specific processes.

Two-dimensional Electronic Spectroscopy in the Diagonal Suppressing Pulse Polarization Sequence: Previous studies have used many different methods to deconvolve 2DES dynamics in spectrally congested systems including global analysis,[45] lifetime density analysis,[52] and cross-peak enhancing pulse sequences.[27] Polarization control has also been leveraged in many 2DES and 2D infrared spectroscopy studies to extract chiral,[53] coherence-specific[54, 55] and cross-peak-specific[27, 28, 56-60] dynamics. To suppress spectral congestion and selectively watch energy transfer dynamics within the phycobilisome, we used a 2DES pulse sequence that suppresses signals arising from four interactions with parallel transition dipole moments. The suppression is achieved by independently controlling the polarization of all pulses.[59] The diagonal suppressing sequence is encoded into the beam polarizations as {90º 60º 120º 0º}[27, 28] or {60º 120º 0º 0º}[59, 60] where the first two pulses are pump pulses, the third is the probe, and the fourth is the local oscillator pulse. Suppressed signals include diagonal signals as well as off-diagonal signals arising from Stokes shifts and ultrafast solvation, as these processes typically do not strongly reorient the transition dipole. Similarly, for linear molecules, ESA signals from the same chromophore are strongly suppressed. We perform 2DES on the phycobilisome complex with both diagonal-suppressing pulse sequences and obtain identical dynamics, which we attribute to energy transfer in the

complex. Throughout this work, we refer to diagonal peaks as peaks arising from the same dipole moments as the excitation, and cross-peaks as peaks arising from interactions with dipole moments with orientations that differ from those originally excited. Both polarization combinations show identical dynamics because they report on energy transfer between non-parallel stationary dipoles occurring over time.

Figure 3.3a shows two-dimensional spectra in the {90º 60º 120º 0º} pulse sequence at 0.2, 2, 20 and 200 ps. As expected, no signal is seen at early times because of diagonal suppression. At later times, a cross-peak centered at λ_{ex} = ~631 nm and λ_{det} = ~657 nm (*Fig 3.3b*) rises on the ~8 ps timescale (*Fig 3.3c*). The feature remains stationary and does not arise from reorientation during a dynamics Stokes shift. We attribute this feature to downhill energy transfer from the phycocyanin rods to the allophycocyanin core. The signal decays with a few ns time constant when data is collected up to 800 ps, verifying this assignment. This decay is in excellent agreement with the known fluorescence lifetime of the phycobilisome core.[21, 22, 26] Our observed timescale of ~8 ps is closer to the 13 ps timescale suggested by the global analysis of 2DES data by Beck and coworkers[20] but much faster than timescales obtained from other similar compartmental models.[19, 21, 22, 26] Moreover, Moran and co-workers do not see a signal redder than λ_{det} = ~645 nm along the detection axis in photon echo peak shift spectra of C-phycocyanin.[36] The phycocyanin emission maximum is also at 645 nm.[44] The signal extends to the blue side of 600 nm in the excitation domain, which is outside of the allophycocyanin absorption, confirming that excitation primarily occurs in the rods. The emission maximum of the peak lies on the emission maximum of the allophycocyanin proteins, ApcA and ApcB. No dynamic Stokes shift is seen even at the earliest times,[51, 61] which would be the case if the signal were due to transfer between C-phycocyanin trimers. Such a signal, which would peak at 645 nm, is clearly seen in the study by

Moran and co-workers to occur on the 120 fs timescale.[36] Finally, our phycobilisome sample emits at λ_{max} = 664 nm in accordance with earlier literature.[62] The cross-peak has a λ_{max} of ~657 nm on the detection axis which corresponds to emission from the upper rods of the core, in accordance with the emission profile of the quenched phycobilisome in the same work,[62] further confirming that the primary signal we isolate arises from energy transfer from rods to the first sites in the core. We do not see the small, few nm dynamic Stokes shift of allophycocyanin because this process is fast compared to excitations moving to the core, nor do we see a shifting peak from phycocyanin relaxation because the direction of the dipole moment does not change during this process.

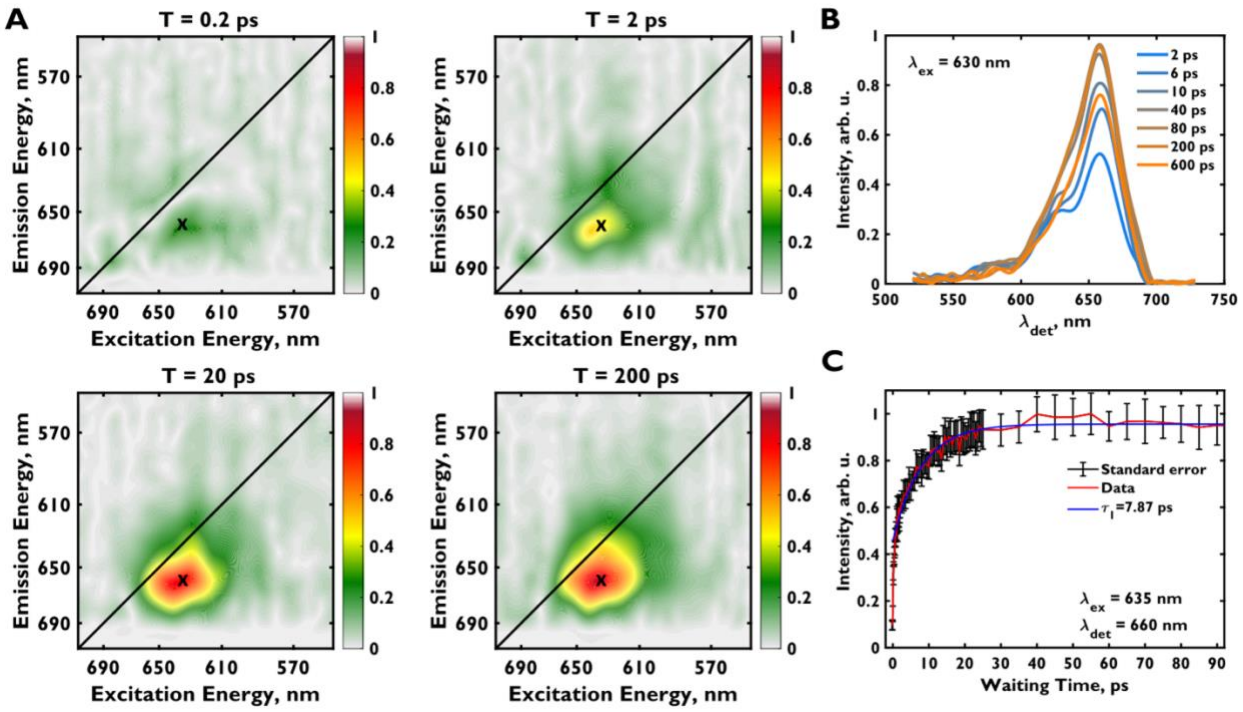

Fig 3.3: **a)** Diagonal suppressed two-dimensional electronic spectra ({90 º 60 º 120 º 0 º} pulse sequence) of the phycobilisome at 0.2, 2, 20 and 200 ps. Spectra are normalized to the maximum of the entire data cube. **b)** Cross-section of the two-dimensional spectra at various waiting times at λ_{ex} = 630 nm. **c)** Multi-exponential fit for the off-diagonal point, λ_{ex} = 635 nm, λ_{det} = 660 nm.

We do not observe signal at early and zero times at the spectral position of the negative signal seen in the all-parallel polarized spectra (**Fig 2**). We attribute the lack of T = 0 signal, which would be indicative of direct coupling between transitions to two factors: the sparse arrangement of the chromophores leading to relatively localized states and the small fraction of rod chromophores that are coupled to the core. The signal at longer times is effectively amplified because energy absorbed into any rod chromophore eventually traverses from rod to core giving rise to the energy transfer signal. Therefore, the negative signal observed in pump-probe spectra and parallel 2DES is attributed to ESA from $S_1 \rightarrow S_n$, which must have a transition dipole moment nearly parallel to the $S_0 \rightarrow S_1$ transition. This assumption is reasonable because phycocyanobilin is an approximately linear molecule. It has been recently shown by Beck and coworkers[20] that excitations in phycocyanin hexamers remain delocalized over the α_{84}-β_{84} chromophore pair. In their scheme, the canceling of the ESA feature suggests that the X1→X2 and X2→X3 transition dipoles are nearly parallel. If the PIA signal were a photoinduced absorption from an electric field-induced shift on a neighboring molecule, this signal would appear from T = 0 in the diagonal-suppressing sequence as well. Tensor component analysis by Mukamel and co-workers[63] confirms that a signal from a non-parallel dipole would not be cancelled by our pulse sequence. A similar red ESA feature is observed in an earlier transient absorption study with parallel polarized pump and probe pulses on free phycocyanobilin in solution, which also supports our ESA assignment.[64] Our dataset is further supported by a cross-peak observed at λ_{ex} = ~600 nm and λ_{det} = ~635 nm, corresponding to energy transfer from the β_{155} chromophore to the β_{84} chromophore and calculated to be 25 ps by Sauer and Scheer.[33] We see a rise of 17 ps and attribute the discrepancy to inter-rod pathways near the core ends[65] of the rods where β_{155} chromophores are proximal to β_{84}

chromophores from other rods. We note that minor contributions from spectral congestion from the broad signal of the main cross-peak likely also influence the time constant.

Suppressing the diagonal peaks isolates the intercomplex energy transfer signals from rods to cores and allows us to attribute a timescale to this process. Previous studies have attributed a timescale of 50 ps for downhill energy flow or rod-core equilibration using decay-associated spectra of pump-probe measurements.[15, 19, 21] However, we observe a significantly faster rise time of the cross-peak and steady intensity up to ~150 ps, after which the signal starts to decay. Our obtained dynamics in the all-parallel data acquisition sequence match earlier reports and compartmental models yielding a sub-5 ps component, a ~50 ps component and a ~1 ns component. Similar dynamics have been observed in many studies[15,18-23,25,26] by fitting transient absorption and time-resolved emission decay traces. Our cross-peak specific spectra show distinctly different dynamics from these reports and our own all-parallel 2DES because the pulse sequence selects the cross-peak signal, or the stimulated emission from energy transfer while suppressing the highly wavelength-dependent dynamics of the other three signatures. In all-parallel 2DES and transient absorption, the time-dependent change of signal intensity is a convolution of the different dynamics of all these processes making the selective isolation of energy transfer unreliable. The large background of the diagonal signal overwhelms the dynamic response in transient absorption and all-parallel 2DES.

Based on the Förster calculations of Sauer and Scheer,[33] energy flow along rods of phycocyanin hexamers should occur primarily through intertrimer exciton hopping between adjacent β_{84}^{1} and β_{84}^{4} rod chromophores. This hop occurs with a FRET rate of 1/(2.5 ps).[18, 33] To rationalize the fast downhill energy transfer rate, we initially used a random hopping model of excitons along four isoenergetic β_{84} sites with a wall on one end and an allophycocyanin sink on

the other. Four sites are used based on the negative staining EM images of Gao and coworkers[9] and other TEM and theoretical studies of phycocyanin assembly and rod-length as functions of light intensity used for cellular growth, which also suggest that two-hexamers or four trimers are most commonly found in intact phycobilisome structures.[66, 67] Considering the allophycocyanin as a sink is not easily justified because many studies suggest that the bottleneck for excitation transfer in the phycobilisome is from the rod to the core because of the large interchromophore distance.[8, 15] However, even assuming an allophycocyanin sink, we retrieve only a mean phycocyanin to allophycocyanin transfer time of 16 ps which does not agree with our measurements.

Next, we consider a model in which the last β_{84} chromophore closest to the allophycocyanin core, or the core-proximal β_{84} chromophore, is of lower energy and, as such, an intermediate trap state. Further, the allophycocyanin core is placed at an energy lower than this terminal β_{84} chromophore. In this case, a random walk is allowed between the two most distant chromophores, but excitons effectively move unidirectionally to the core-proximal chromophore from the third chromophore and from this core-proximal β_{84} chromophore to the allophycocyanin core. With this model, we obtain a rod-to-core transfer time of 8.8 ps, in excellent agreement with our measured time constant of 7.9 ps (see simulation details in publication). *Fig 3.4* shows a cartoon schematic of this model, which is based on numerous spectroscopic and structural studies: recent cryo-EM structures suggest that aromatic and charged residues of the CpcG rod-core linker protein form a pocket around core-proximal β_{84} chromophores, lowering their energy and forming a conduit through which energy is funneled to the core (*Fig 3.4*).[9, 15] Sui and co-workers have previously suggested that this feature is conserved across phycobilisome complexes of cyanobacteria and red algae, and it is also consistent with spectroscopic characterization of the CpcG-C-phycocyanin linker protein complex.[8, 12] Pertinently, Sauer and Pizarro[29] and Glazer and coworkers[68] have

characterized the CpcG-phycocyanin complex spectroscopically and a redshift of 12 nm and 6 nm is seen in the absorption and emission profiles, respectively, of the C-phycocyanin trimer upon CpcG binding. Based on the relative intensity weights of fluorescence peaks, fluorescence spectra of the CpcG-C-phycocyanin complex[29] suggest that two of the three terminal chromophores redshift due to interactions with CpcG. The recent cryo-EM structures of the megacomplex suggest that these two chromophores are also the closest contacts to the allophycocyanin core although systematic electronic structure calculations will be needed to obtain the spectra of each chromophore.[9, 15] We also modify our model to incorporate FRET rates based on the absorption and emission spectra of the isolated CpcG-C-phycocyanin complex.[29] We note however that these spectra contain emission from both redshifted and non-redshifted chromophores, which increases back-hopping rates in our calculations and yields an energy transfer time constant of 9.6 ps. Our model incorporates the known redshift of the terminal C-phycocyanin in the FRET rates but is otherwise a simplified FRET model similar to the recent work of Kerfeld and coworkers.[15] Single-molecule fluorescence studies on this complex may isolate emission from the redshifted chromophores.[69] Beck and coworkers have recently shown that excitons hopping along phycocyanin rods are delocalized over the tightly coupled α_{84}-β_{84} chromophore pair and that intertrimer transfer predominates localization.[20] In the case of the core-proximal β_{84} chromophore, the lower energy would likely suppress the superposition of the α_{84}-β_{84} states and localize the excitation on the β_{84} chromophore, creating an even more unidirectional flow of energy along the rod.

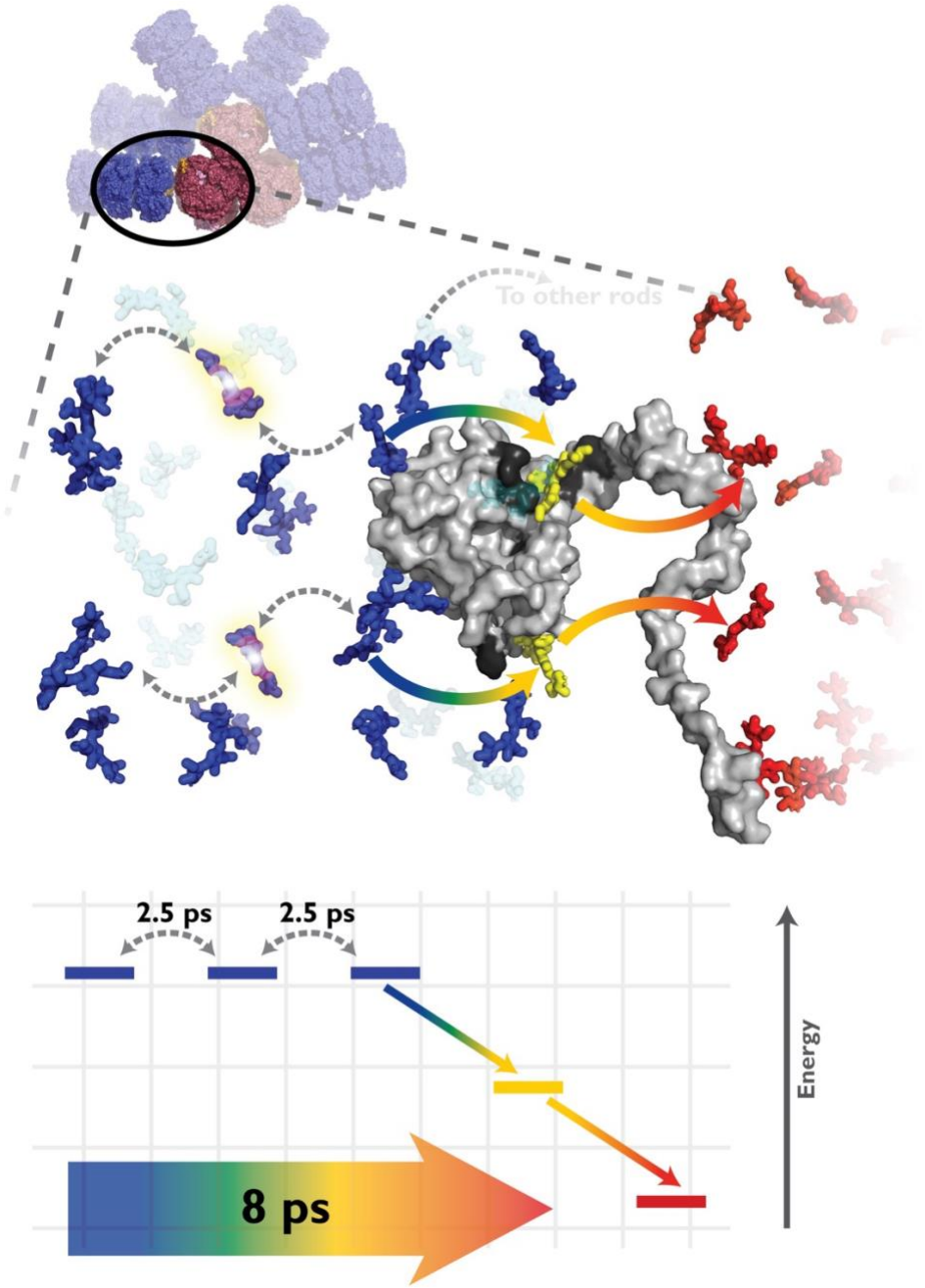

Fig 3.4: Phycocyanobilin rod chromophores in a single phycobilisome rod (blue) and the nearest allophycocyanin core chromophores (red). Chromophores shown in bold transfer energy directly to the core-proximal chromophores (gold). CpcG, the rod-core linker protein is shown in grey and its aromatic and charged residues (shown in dark grey) surround the core-proximal rod chromophores (gold). All structures are rendered using coordinates from Kerfeld and coworkers.[15] Chromophore-residue interactions lower the energy of the core-proximal chromophores by ~250 cm^{-1} to facilitate unidirectional flow from the rod to the core.[29]

On average, two β_{84} chromophores of the core-proximal trimer are within 4 nm of the core chromophores. Energy transfer between β_{84} chromophores in the same trimer is slow (1/(25 ps)).[33] Therefore, an explanation is needed for fast transfer from the third chain of β_{84} chromophores. A few possibilities arise: recent theoretical studies[11, 65] strongly suggest that inter-rod transfer pathways play a dominant role in funneling excitations to the core. Most importantly, the recent down-down and up-down TEM and cryo-EM structures seen by Kerfeld and coworkers[15] reveal these dominant inter-rod exciton hopping pathways and strongly suggest that excitons are not limited to FRET hopping within single phycocyanin hexamers and rods. From their cryo-EM structures, they calculate that about 70% of phycobilisome complexes have at least one rod in the down conformation. FRET calculations in the same work indicate prominent inter-rod energy transfer pathways. The work by Kerfeld and coworkers[15] does not suggest that inter-rod transfer significantly speeds up energy transfer to the core because they do not incorporate red-shifted core-proximal chromophores in their modeling. However, up to 10% exciton transfer to each rod from the down-shifted rod is suggested in their calculations.[15] Another cryo-EM[16] structure suggests that linker protein interactions laterally shift phycocyanin hexamers with respect to each other along the rod axis. This shift could also lead to more favorable FRET rates.

Finally, the detection maximum of the signal in the cross-peak-specific spectra remains 657 nm until at least 800 ps, at which time it shifts to the fluorescence maximum of 664 nm. This observation suggests that over the bulk of the exciton lifetime, excitations stay in the APC_{660} pigments. Global analysis on time-resolved fluorescence spectra of the same phycobilisome complex by Amerongen and co-workers suggests that APC_{680} is reached in 43 ps in rod-less CK phycobilisomes, but this movement was not clearly resolved in wild-type phycobilisomes[22]. We find that in our wild-type phycobilisomes, bulk excitons from APC_{660} reach the terminal emitters

on a much slower timescale. Our observation of the long lifetime of the APC_{660} is also consistent with the study of Beck and co-workers, who suggest that exciton localization may occur in the upper chromophores of the core.[20] It has been previously shown that the APC_{680} proteins are not involved in OCP-based photoprotection.[48] The cryo-EM structures of this phycobilisome[15] show that four OCPs bind to the sides of the core and are suitably placed to quench the majority of the APC_{660} subunits. These observations together suggest that the long staying time of the excitations in the APC_{660} subunits serves as a design strategy to allow efficient OCP-based quenching.

The phycobilisome antenna differs from the LHCII and LH2 complexes found in plants, algae, and purple phototrophs in that the arrangement of chromophores in the rods and cores is sparse and the chromophores themselves are more fluorescent than chlorophyll derivatives. Unlike the other complexes, the phycobilisome does not exploit dense packing of chromophores and quantum mechanical delocalization of excitonic states.[5] The near-unity efficiency of energy transfer along the phycobilisome is therefore remarkable. What the phycobilin chromophores lack in energy absorption and retention capabilities in comparison to chlorophyll derivatives, they make up for with facile absorption and emission wavelength tunability through their local protein environment, variable conjugation length, and tunable charge-separated states. The known redshifted core-proximal chromophores increase the probability of excitation energy transfer to the core, reminiscent of similarly placed red chromophores in other systems such as the red chlorophylls in PSI[44] and bacteriochlorophylls in LH1 in purple bacteria.[70, 71] However, in this case, the known redshifted chromophores are energetic intermediates in relation to the phycobilisome rod and allophycocyanin core chromophores (*Fig. 4*),[29] so rather than retarding exciton transfer to the next component they improve spectral overlap and speed up energy transfer.

While multiple time-resolved spectroscopic studies have tried to observe site-specific excitation transfer in large and physiologically important light-harvesting antennas, spectral congestion of several antenna components obscures the dynamics. In this study, we suppress diagonal features in 2DES to directly watch exciton flow across tens of nanometers between the components of the phycobilisome megacomplex. This pulse sequence suppresses both strong diagonal signal and PIA near the cross-peak, isolating off-diagonal cross-peaks indicative of energy transfer.

Our results show that, despite slow FRET rates within phycocyanin trimers on the order of 10-30 ps and large interchromophore distances, most rod excitations reach the core of the phycobilisome with a ~8 ps time constant before decaying with a few ns decay constant matching the fluorescence lifetime of the core. Previous studies have pointed out that the rod-to-core transfer is the biggest bottleneck in downhill energy movement in the phycobilisome,[15, 72] but cross-peak specific spectra suggest that this bottleneck is averted by limiting the active random walk region available to the excitation in a rod, and by facilitating spectral overlap with the core. Because random walk time scales as N^2 for N sites in one-dimension (higher for larger dimensions) as assumed for a rod, the rate of transfer doubles when the spectroscopically characterized redshifted core-proximal chromophore holds excitations to prevent them from escaping back into the random walk region. Reducing the random walk time minimizes the probability of trapping, fluorescence, and exciton annihilation[18, 19] and increases the efficiency of the excitation transfer process. In other words, creating a continuous or fine-tuned spatioenergetic funnel allows largely unidirectional energy flow and enhanced transfer efficiencies. Moreover, inter-rod energy transfer between closely situated chromophores in different rods further lowers reliance on the slow FRET rates within a phycocyanin trimer. The recently observed down-down phycobilisome structures may

play a significant role in enhancing this effect.[15] These interactions are conserved across red algal and cyanobacterial phycobilisomes,[8] suggesting that they are an evolutionary design feature that drives unidirectional and near-unity efficient energy transfer from phycobilisome rods to cores. Finally, while energy transfers swiftly from rods to the core, the transfer from APC_{660} core proteins to the terminal emitters in APC_{680} (ApcD, ApcE, ApcF) is slow and likely allows efficient OCP-based photoprotection. Therefore, the bottleneck in the exciton transfer through the phycobilisome is not the rod-to-core transfer but transfer to the APC_{680} terminal emitters from APC_{660} chromophores. Recent cryo-EM structures of OCP-attached phycobilisome cores from Kerfeld and co-workers[15] and our observation that excitons spend the bulk of their lifetime in the APC_{660} pigments in the phycobilisome strongly suggest that the bottleneck of energy transfer to the terminal emitters is not an inefficiency, but a design principle that provides robust and self-contained photoprotection to any protein that should receive excitations from the phycobilisome.

Methods

UV-vis Absorption Spectroscopy: Absorption spectra are collected in a 1 mm vial in a Cary 5000 spectrometer. Spectra are collected before and after time-resolved data acquisition.

Fluorescence Spectroscopy: Fluorescence spectra are collected on a Horiba JobinYvon spectrometer with an excitation wavelength of 590 nm, entrance and exit slits of 3 nm and an integration time of 0.1 s.

We note that while our fluorescence spectrum indicates sample intactness, the cross-peak polarized spectra by themselves are further proof of sample intactness because the cross-peak for C-

phycocyanin absorption and APC_{660} emission would not have occurred without energy transfer between these chromophores.

Two-dimensional Electronic Spectroscopy and Pump-Probe Spectroscopy: Two-dimensional spectroscopic experiments were performed using a setup described previously.[53] Briefly, a Ti:sapphire mode-locked oscillator (Coherent Micra) operating at 80 MHz seeds a Ti:sapphire regenerative amplifier (Coherent Legend Elite) to produce 35 fs pulses centered at 800 nm at a 5 kHz repetition rate. This output is passed through a pressurized argon tube held at ~16 pounds per square inch above atmosphere to generate a white light continuum. The 800 nm light remaining after white light generation is rejected with a bandpass filter, and the white light is compressed using two pairs of chirped mirrors (Laser Quantum) to ~8 fs fwhm. 2D spectra are collected in the fully non-collinear BOXCARS geometry with a beam diameter of 290 μm at the focus at the sample and heterodyned with an attenuated local oscillator pulse. Powers are kept to 15 nJ per pulse in our experiments. At this fluence, annihilation is minimal although annihilation does not affect downhill energy transfer dynamics.[18-20] Broadband half-waveplates (Union Optic) are used to independently control the polarization of each pulse. Two-dimensional spectra were obtained by collecting coherence time data from -90 to 90 fs in 1.5 fs time-steps. Hann and Tukey windows were used for apodization and windowing in rephasing time and coherence time respectively. Fully-absorptive 2D spectra were obtained for the parallel polarization sequence using the projection-slice theorem after acquisition of separate pump-probe spectra at identical waiting times to determine the absolute signal phase for every waiting time frame independently. A 200 μm flow cell was used and the sample was flowed throughout data acquisition.

Further details are included in Sohoni, Lloyd, Hitchcock, MacGregor-Chatwin, Iwanicki, Ghosh, Shen, Hunter and Engel, J. Am. Chem. Soc., 2021[73]

Bibliography

(1) Blankenship, R. E. Antenna Complexes and Energy Transfer Processes. In *Molecular Mechanisms of Photosynthesis*, Wiley, 2002; pp 61-94.
(2) Kasting, J. F.; Siefert, J. L. Life and the Evolution of Earth's Atmosphere. *Science* **2002**, *296* (5570), 1066-1068.
(3) Schirrmeister, B. E.; de Vos, J. M.; Antonelli, A.; Bagheri, H. C. Evolution of multicellularity coincided with increased diversification of cyanobacteria and the Great Oxidation Event. *Proceedings of the National Academy of Sciences* **2013**, *110* (5), 1791-1796.
(4) *Light-Harvesting Antennas in Photosynthesis*; Springer, 2003.
(5) Scholes, G. D.; Fleming, G. R.; Olaya-Castro, A.; van Grondelle, R. Lessons from Nature about Solar Light Harvesting. *Nature Chemistry* **2011**, *3* (10), 763-774.
(6) Liu, H.; Zhang, H.; Niedzwiedzki, D. M.; Prado, M.; He, G.; Gross, M. L.; Blankenship, R. E. Phycobilisomes Supply Excitations to Both Photosystems in a Megacomplex in Cyanobacteria. *Science* **2013**, *342* (6162), 1104-1107.
(7) Kolodny, Y.; Avrahami, Y.; Zer, H.; Frada, M. J.; Paltiel, Y.; Keren, N. Phycobilisome Light-harvesting Efficiency in Natural Populations of the Marine Cyanobacteria *Synechococcus* Increases with Depth. *Communications Biology* **2022**, *5* (1), 727.
(8) Sui, S.-F. Structure of Phycobilisomes. *Annual Review of Biophysics* **2021**, *50* (Volume 50, 2021), 53-72.
(9) Zheng, L.; Zheng, Z.; Li, X.; Wang, G.; Zhang, K.; Wei, P.; Zhao, J.; Gao, N. Structural insight into the mechanism of energy transfer in cyanobacterial phycobilisomes. *Nature Communications* **2021**, *12* (1), 5497.
(10) Harris, D.; Bar-Zvi, S.; Lahav, A.; Goldshmid, I.; Adir, N. The Structural Basis for the Extraordinary Energy-Transfer Capabilities of the Phycobilisome. In *Membrane Protein Complexes: Structure and Function*, Harris, J. R., Boekema, E. J. Eds.; Springer Singapore, 2018; pp 57-82.
(11) Kolodny, Y.; Zer, H.; Propper, M.; Yochelis, S.; Paltiel, Y.; Keren, N. Marine cyanobacteria tune energy transfer efficiency in their light-harvesting antennae by modifying pigment coupling. *The FEBS Journal* **2021**, *288* (3), 980-994.
(12) Ma, J.; You, X.; Sun, S.; Wang, X.; Qin, S.; Sui, S.-F. Structural basis of energy transfer in *Porphyridium purpureum* phycobilisome. *Nature* **2020**, *579* (7797), 146-151.
(13) Marx, A.; David, L.; Adir, N. Piecing Together the Phycobilisome. In *The Structural Basis of Biological Energy Generation*, Hohmann-Marriott, M. F. Ed.; Springer Netherlands, 2014; pp 59-76.
(14) Peng, P.-P.; Dong, L.-L.; Sun, Y.-F.; Zeng, X.-L.; Ding, W.-L.; Scheer, H.; Yang, X.; Zhao, K.-H. The Structure of Allophycocyanin B from *Synechocystis* PCC 6803 Reveals the Structural Basis for the Extreme Redshift of the Terminal Emitter in Phycobilisomes. *Acta Crystallographica Section D* **2014**, *70* (10), 2558-2569.
(15) Domínguez-Martín, M. A.; Sauer, P. V.; Kirst, H.; Sutter, M.; Bína, D.; Greber, B. J.; Nogales, E.; Polívka, T.; Kerfeld, C. A. Structures of a Phycobilisome in Light-harvesting and Photoprotected States. *Nature* **2022**, *609* (7928), 835-845.

(16) Kawakami, K.; Hamaguchi, T.; Hirose, Y.; Kosumi, D.; Miyata, M.; Kamiya, N.; Yonekura, K. Core and rod structures of a thermophilic cyanobacterial light-harvesting phycobilisome. *Nature Communications* **2022**, *13* (1), 3389.
(17) Chang, L.; Liu, X.; Li, Y.; Liu, C.-C.; Yang, F.; Zhao, J.; Sui, S.-F. Structural organization of an intact phycobilisome and its association with photosystem II. *Cell Research* **2015**, *25* (6), 726-737.
(18) Navotnaya, P.; Sohoni, S.; Lloyd, L. T.; Abdulhadi, S. M.; Ting, P.-C.; Higgins, J. S.; Engel, G. S. Annihilation of Excess Excitations along Phycocyanin Rods Precedes Downhill Flow to Allophycocyanin Cores in the Phycobilisome of Synechococcus elongatus PCC 7942. *The Journal of Physical Chemistry B* **2022**, *126* (1), 23-29.
(19) van Stokkum, I. H. M.; Gwizdala, M.; Tian, L.; Snellenburg, J. J.; van Grondelle, R.; van Amerongen, H.; Berera, R. A Functional Compartmental Model of the *Synechocystis* PCC 6803 Phycobilisome. *Photosynthesis Research* **2018**, *135* (1), 87-102.
(20) Sil, S.; Tilluck, R. W.; Mohan T. M, N.; Leslie, C. H.; Rose, J. B.; Domínguez-Martín, M. A.; Lou, W.; Kerfeld, C. A.; Beck, W. F. Excitation Energy Transfer and Vibronic Coherence in Intact Phycobilisomes. *Nature Chemistry* **2022**, *14* (11), 1286-1294.
(21) Fălămaș, A.; Porav, S. A.; Tosa, V. Investigations of the Energy Transfer in the Phycobilisome Antenna of *Arthrospira platensis* Using Femtosecond Spectroscopy. *Applied Sciences* **2020**, *10* (11), 4045.
(22) Tian, L.; Gwizdala, M.; van Stokkum, Ivo H. M.; Koehorst, Rob B. M.; Kirilovsky, D.; van Amerongen, H. Picosecond Kinetics of Light Harvesting and Photoprotective Quenching in Wild-Type and Mutant Phycobilisomes Isolated from the Cyanobacterium *Synechocystis* PCC 6803. *Biophysical Journal* **2012**, *102* (7), 1692-1700.
(23) Hirota, Y.; Serikawa, H.; Kawakami, K.; Ueno, M.; Kamiya, N.; Kosumi, D. Ultrafast energy transfer dynamics of phycobilisome from *Thermosynechococcus vulcanus*, as revealed by ps fluorescence and fs pump-probe spectroscopies. *Photosynthesis Research* **2021**, *148* (3), 181-190.
(24) Nganou, C.; David, L.; Adir, N.; Mkandawire, M. Linker proteins enable ultrafast excitation energy transfer in the phycobilisome antenna system of *Thermosynechococcus vulcanus*. *Photochemical & Photobiological Sciences* **2016**, *15* (1), 31-44.
(25) Gwizdala, M.; Berera, R.; Kirilovsky, D.; van Grondelle, R.; Krüger, T. P. J. Controlling Light Harvesting with Light. *Journal of the American Chemical Society* **2016**, *138* (36), 11616-11622.
(26) Tian, L.; van Stokkum, I. H. M.; Koehorst, R. B. M.; Jongerius, A.; Kirilovsky, D.; van Amerongen, H. Site, Rate, and Mechanism of Photoprotective Quenching in Cyanobacteria. *Journal of the American Chemical Society* **2011**, *133* (45), 18304-18311.
(27) Zanni, M. T.; Ge, N.-H.; Kim, Y. S.; Hochstrasser, R. M. Two-dimensional IR Spectroscopy can be Designed to Eliminate the Diagonal peaks and Expose only the Crosspeaks Needed for Structure Determination. *Proceedings of the National Academy of Sciences* **2001**, *98* (20), 11265-11270.
(28) Fidler, A. F.; Singh, V. P.; Long, P. D.; Dahlberg, P. D.; Engel, G. S. Probing Energy Transfer Events in the Light Harvesting Complex 2 (LH2) of *Rhodobacter sphaeroides* with Two-dimensional Spectroscopy. *The Journal of Chemical Physics* **2013**, *139* (15).
(29) Pizarro, S. A.; Sauer, K. Spectroscopic Study of the Light-harvesting Protein C-Phycocyanin Associated with Colorless Linker Peptides. *Photochemistry and Photobiology* **2001**, *73* (5), 556-563.
(30) *The Molecular Biology of Cyanobacteria*; Springer, 1994.

(31) Flombaum, P.; Gallegos, J. L.; Gordillo, R. A.; Rincón, J.; Zabala, L. L.; Jiao, N.; Karl, D. M.; Li, W. K. W.; Lomas, M. W.; Veneziano, D.; et al. Present and future global distributions of the marine Cyanobacteria *Prochlorococcus* and *Synechococcus*. *Proceedings of the National Academy of Sciences* **2013**, *110* (24), 9824-9829.
(32) Garcia-Pichel, F.; Belnap, J.; Neuer, S.; Schanz, F. Estimates of global cyanobacterial biomass and its distribution. *Algological Studies* **2003**, *109* (1), 213-227. USGS Publications Warehouse
(33) Sauer, K.; Scheer, H. Excitation Transfer in C-phycocyanin. Förster Transfer Rate and Exciton Calculations based on New Crystal Structure Data for C-phycocyanins from *Agmenellum quadruplicatum* and *Mastigocladus laminosus*. *Biochimica et Biophysica Acta (BBA) - Bioenergetics* **1988**, *936* (2), 157-170.
(34) Riter, R. E.; Edington, M. D.; Beck, W. F. Isolated-Chromophore and Exciton-State Photophysics in C-Phycocyanin Trimers. *The Journal of Physical Chemistry B* **1997**, *101* (13), 2366-2371.
(35) Womick, J. M.; Moran, A. M. Exciton Coherence and Energy Transport in the Light-Harvesting Dimers of Allophycocyanin. *The Journal of Physical Chemistry B* **2009**, *113* (48), 15747-15759.
(36) Womick, J. M.; Moran, A. M. Nature of Excited States and Relaxation Mechanisms in C-Phycocyanin. *The Journal of Physical Chemistry B* **2009**, *113* (48), 15771-15782.
(37) Matsuura, K.; Shimada, K. Electrochromic spectral band shift of carotenoids in the photosynthetic membranes of *Rhodospirillum molischianum* and *Rhodospirillum photometricum*. *Biochimica et Biophysica Acta (BBA) - Bioenergetics* **1993**, *1140* (3), 293-296.
(38) Bukartė, E.; Paleček, D.; Edlund, P.; Westenhoff, S.; Zigmantas, D. Dynamic band-shift signal in two-dimensional electronic spectroscopy: A case of bacterial reaction center. *The Journal of Chemical Physics* **2021**, *154* (11).
(39) Niedzwiedzki, D. M.; Bar-Zvi, S.; Blankenship, R. E.; Adir, N. Mapping the excitation energy migration pathways in phycobilisomes from the cyanobacterium Acaryochloris marina. *Biochimica et Biophysica Acta (BBA) - Bioenergetics* **2019**, *1860* (4), 286-296.
(40) Ho, M.-Y.; Niedzwiedzki, D. M.; MacGregor-Chatwin, C.; Gerstenecker, G.; Hunter, C. N.; Blankenship, R. E.; Bryant, D. A. Extensive remodeling of the photosynthetic apparatus alters energy transfer among photosynthetic complexes when cyanobacteria acclimate to far-red light. *Biochimica et Biophysica Acta (BBA) - Bioenergetics* **2020**, *1861* (4), 148064.
(41) Rast, A.; Schaffer, M.; Albert, S.; Wan, W.; Pfeffer, S.; Beck, F.; Plitzko, J. M.; Nickelsen, J.; Engel, B. D. Biogenic regions of cyanobacterial thylakoids form contact sites with the plasma membrane. *Nature Plants* **2019**, *5* (4), 436-446.
(42) Mimuro, M.; Füglistaller, P.; Rümbeli, R.; Zuber, H. Functional assignment of chromophores and energy transfer in C phycocyanin isolated from the thermophilic cyanobacterium *Mastigocladus laminosus*. *Biochimica et Biophysica Acta (BBA) - Bioenergetics* **1986**, *848* (2), 155-166.
(43) Demidov, A. A.; Mimuro, M. Deconvolution of C-phycocyanin beta-84 and beta-155 chromophore absorption and fluorescence spectra of cyanobacterium *Mastigocladus laminosus*. *Biophysical Journal* **1995**, *68* (4), 1500-1506.
(44) Sauer, K.; Scheer, H.; Sauer, P. Förster Transfer Calculations Based on Crystal Structure Data from *Agmenellum quadruplicatum* C-Phycocyanin. *Photochemistry and Photobiology* **1987**, *46* (3), 427-440.

(45) Lee, Y.; Gorka, M.; Golbeck, J. H.; Anna, J. M. Ultrafast Energy Transfer Involving the Red Chlorophylls of Cyanobacterial Photosystem I Probed through Two-Dimensional Electronic Spectroscopy. *Journal of the American Chemical Society* **2018**, *140* (37), 11631-11638.
(46) Do, T. N.; Nguyen, H. L.; Akhtar, P.; Zhong, K.; Jansen, T. L. C.; Knoester, J.; Caffarri, S.; Lambrev, P. H.; Tan, H.-S. Ultrafast Excitation Energy Transfer Dynamics in the LHCII–CP29–CP24 Subdomain of Plant Photosystem II. *The Journal of Physical Chemistry Letters* **2022**, *13* (19), 4263-4271.
(47) Calzadilla, P. I.; Muzzopappa, F.; Sétif, P.; Kirilovsky, D. Different roles for ApcD and ApcF in Synechococcus elongatus and Synechocystis sp. PCC 6803 phycobilisomes. *Biochimica et Biophysica Acta (BBA) - Bioenergetics* **2019**, *1860* (6), 488-498.
(48) Jallet, D.; Gwizdala, M.; Kirilovsky, D. ApcD, ApcF and ApcE are not required for the Orange Carotenoid Protein related phycobilisome fluorescence quenching in the cyanobacterium *Synechocystis* PCC 6803. *Biochimica et Biophysica Acta (BBA) - Bioenergetics* **2012**, *1817* (8), 1418-1427.
(49) Kuzminov, F. I.; Bolychevtseva, Y. V.; Elanskaya, I. V.; Karapetyan, N. V. Effect of ApcD and ApcF subunits depletion on phycobilisome fluorescence of the cyanobacterium *Synechocystis* PCC 6803. *Journal of Photochemistry and Photobiology B: Biology* **2014**, *133*, 153-160.
(50) Ashby, M. K.; Mullineaux, C. W. The role of ApcD and ApcF in energy transfer from phycobilisomes to PS I and PS II in a cyanobacterium. *Photosynthesis Research* **1999**, *61* (2), 169-179.
(51) Petkov, B. K.; Gellen, T. A.; Farfan, C. A.; Carbery, W. P.; Hetzler, B. E.; Trauner, D.; Li, X.; Glover, W. J.; Ulness, D. J.; Turner, D. B. Two-Dimensional Electronic Spectroscopy Reveals the Spectral Dynamics of Förster Resonance Energy Transfer. *Chem* **2019**, *5* (8), 2111-2125.
(52) Song, Y.; Sechrist, R.; Nguyen, H. H.; Johnson, W.; Abramavicius, D.; Redding, K. E.; Ogilvie, J. P. Excitonic structure and charge separation in the heliobacterial reaction center probed by multispectral multidimensional spectroscopy. *Nature Communications* **2021**, *12* (1), 2801.
(53) Lloyd, L. T.; Wood, R. E.; Mujid, F.; Sohoni, S.; Ji, K. L.; Ting, P.-C.; Higgins, J. S.; Park, J.; Engel, G. S. Sub-10 fs Intervalley Exciton Coupling in Monolayer MoS2 Revealed by Helicity-Resolved Two-Dimensional Electronic Spectroscopy. *ACS Nano* **2021**, *15* (6), 10253-10263.
(54) Schlau-Cohen, G. S.; Ishizaki, A.; Calhoun, T. R.; Ginsberg, N. S.; Ballottari, M.; Bassi, R.; Fleming, G. R. Elucidation of the timescales and origins of quantum electronic coherence in LHCII. *Nature Chemistry* **2012**, *4* (5), 389-395.
(55) Thyrhaug, E.; Tempelaar, R.; Alcocer, M. J. P.; Žídek, K.; Bína, D.; Knoester, J.; Jansen, T. L. C.; Zigmantas, D. Identification and characterization of diverse coherences in the Fenna–Matthews–Olson complex. *Nature Chemistry* **2018**, *10* (7), 780-786.
(56) Mehlenbacher, R. D.; McDonough, T. J.; Kearns, N. M.; Shea, M. J.; Joo, Y.; Gopalan, P.; Arnold, M. S.; Zanni, M. T. Polarization-Controlled Two-Dimensional White-Light Spectroscopy of Semiconducting Carbon Nanotube Thin Films. *The Journal of Physical Chemistry C* **2016**, *120* (30), 17069-17080.
(57) Westenhoff, S.; Paleček, D.; Edlund, P.; Smith, P.; Zigmantas, D. Coherent Picosecond Exciton Dynamics in a Photosynthetic Reaction Center. *Journal of the American Chemical Society* **2012**, *134* (40), 16484-16487.
(58) Read, E. L.; Engel, G. S.; Calhoun, T. R.; Mančal, T.; Ahn, T. K.; Blankenship, R. E.; Fleming, G. R. Cross-peak-specific two-dimensional electronic spectroscopy. *Proceedings of the National Academy of Sciences* **2007**, *104* (36), 14203-14208.

(59) Farrell, K. M.; Yang, N.; Zanni, M. T. A polarization scheme that resolves cross-peaks with transient absorption and eliminates diagonal peaks in 2D spectroscopy. *Proceedings of the National Academy of Sciences* **2022**, *119* (6), e2117398119.
(60) Tokmakoff, A. Orientational correlation functions and polarization selectivity for nonlinear spectroscopy of isotropic media. I. Third order. *The Journal of Chemical Physics* **1996**, *105* (1), 1-12.
(61) Moya, R.; Norris, A. C.; Kondo, T.; Schlau-Cohen, G. S. Observation of Robust Energy Transfer in the Photosynthetic Protein Allophycocyanin Using Single-molecule Pump–probe Spectroscopy. *Nature Chemistry* **2022**, *14* (2), 153-159.
(62) Stadnichuk, I. N.; Yanyushin, M. F.; Maksimov, E. G.; Lukashev, E. P.; Zharmukhamedov, S. K.; Elanskaya, I. V.; Paschenko, V. Z. Site of non-photochemical quenching of the phycobilisome by orange carotenoid protein in the cyanobacterium *Synechocystis* sp. PCC 6803. *Biochimica et Biophysica Acta (BBA) - Bioenergetics* **2012**, *1817* (8), 1436-1445.
(63) Dreyer, J.; Moran, A. M.; Mukamel, S. Tensor Components in Three Pulse Vibrational Echoes of a Rigid Dipeptide. *Bulletin-Korean Chemical Society* **2003**, *24* (8), 1091-1096.
(64) Bischoff, M.; Hermann, G.; Rentsch, S.; Strehlow, D.; Winter, S.; Chosrowjan, H. Excited-State Processes in Phycocyanobilin Studied by Femtosecond Spectroscopy. *The Journal of Physical Chemistry B* **2000**, *104* (8), 1810-1816.
(65) Padyana, A. K.; Ramakumar, S. Lateral energy transfer model for adjacent light-harvesting antennae rods of C-phycocyanins. *Biochimica et Biophysica Acta (BBA) - Bioenergetics* **2006**, *1757* (3), 161-165.
(66) Chenu, A.; Keren, N.; Paltiel, Y.; Nevo, R.; Reich, Z.; Cao, J. Light Adaptation in Phycobilisome Antennas: Influence on the Rod Length and Structural Arrangement. *The Journal of Physical Chemistry B* **2017**, *121* (39), 9196-9202.
(67) de Lorimier, R. M.; Smith, R. L.; Stevens, S. E., Jr. Regulation of Phycobilisome Structure and Gene Expression by Light Intensity 1. *Plant Physiology* **1992**, *98* (3), 1003-1010.
(68) Lundell, D. J.; Williams, R. C.; Glazer, A. N. Molecular architecture of a light-harvesting antenna. In vitro assembly of the rod substructures of *Synechococcus* 6301 phycobilisomes. *Journal of Biological Chemistry* **1981**, *256* (7), 3580-3592.
(69) Squires, A. H.; Moerner, W. E. Direct single-molecule measurements of phycocyanobilin photophysics in monomeric C-phycocyanin. *Proceedings of the National Academy of Sciences* **2017**, *114* (37), 9779-9784.
(70) van Grondelle, R.; Novoderezhkin, V. I. Energy transfer in photosynthesis: experimental insights and quantitative models. *Physical Chemistry Chemical Physics* **2006**, *8* (7), 793-807. 10.1039/B514032C
(71) Sohail, S. H.; Dahlberg, P. D.; Allodi, M. A.; Massey, S. C.; Ting, P.-C.; Martin, E. C.; Hunter, C. N.; Engel, G. S. Communication: Broad manifold of excitonic states in light-harvesting complex 1 promotes efficient unidirectional energy transfer in vivo. *The Journal of Chemical Physics* **2017**, *147* (13).
(72) Adir, N.; Bar-Zvi, S.; Harris, D. The amazing phycobilisome. *Biochimica et Biophysica Acta (BBA) - Bioenergetics* **2020**, *1861* (4), 148047.
(73) Sohoni, S.; Lloyd, L. T.; Hitchcock, A.; MacGregor-Chatwin, C.; Iwanicki, A.; Ghosh, I.; Shen, Q.; Hunter, C. N.; Engel, G. S. Phycobilisome's Exciton Transfer Efficiency Relies on an Energetic Funnel Driven by Chromophore–Linker Protein Interactions. *Journal of the American Chemical Society* **2023**, *145* (21), 11659-11668.

Chapter 4

Resonant Vibrational Enhancement of Downhill Energy Transfer in the C-Phycocyanin Chromophore Dimer

Note: This work was pursued in collaboration with coworker Ping-Jui Wu, who performed the Redfield simulations. The simulation development methodology will be discussed in detail in his thesis.

Energy transfer between electrostatically coupled photosynthetic light-harvesting antenna pigments is frequently assisted by protein and chromophore nuclear motion. This energy transfer mechanism, called the Redfield mechanism, operates in the intermediate bath-coupling regime. Vibrational spectral densities coupling to the visible transitions of the chromophores govern the energy transfer rate in this process. In this work, we perform finely sampled broadband pump-probe spectroscopy on the phycobilisome antenna complex with sub-10 fs pump and probe pulses. The spectral density obtained by Fourier transforming the pump-probe time-domain signal is used to perform modified Redfield rate calculations to check for vibrational enhancement of energy transfer in a coupled chromophore dimer in the C-phycocyanin protein of the phycobilisome antenna. We find two low frequency vibrations to be in near-resonance with the interexcitonic energy gap and a few-fold enhancement in the interexcitonic energy transfer rate due to these resonances at room temperature. Our observations and calculations explain the fast downhill energy transfer process in C-phycocyanin. We also observe high-frequency vibrations involving chromophore-protein residue interactions on the excited state of the phycocyanobilin

chromophore. We suggest that these vibrations lock the chromophore nuclear configuration of the excited state and prevent energetic relaxation that blocks energy transfer.

Energy transfers from antenna pigments to reaction centers in photosynthesis with near-unity quantum efficiency.[1-3] The photosynthetic antenna pigment network for electronic excitation flow is coupled to the protein and chromophore nuclear bath. Therefore, energy capture, or downhill energy transfer, occurs through bath-mediated processes in photosynthesis. Over large distances, energy transfers primarily through a cascade of dipole-dipole interactions between pigments.[4-6] This process is called Förster Resonance energy transfer (FRET). However, when chromophores are separated by sub-nm distances and are electrostatically coupled, nuclear bath motion can assist fast energy transfer between chromophores. This mechanism of bath-assisted energy transfer is referred to as the Redfield mechanism,[7-11] and it provides significant enhancement to the net energy transfer rate.[12-15]

FRET rates are calculated with relative ease when protein cryo-EM structures are known.[16-18] They require the knowledge of dipole orientations, the interchromophore distance, and the absorption and emission spectra and dipole moments of the donor and acceptor chromophores.[19] In comparison, the assistance provided by bath vibrations to energy transfer is not calculated in a straightforward manner because the low-frequency (0-800 cm^{-1}) vibrations coupling to the energy transfer process are not easily characterized through ultrafast Raman,[20] resonance Raman,[21] or ultrafast IR spectroscopy.[22, 23] Typically, broad Ohmic spectral densities are used as bath proxies that couple to the transfer process.[24-28] An Ohmic spectral density does not account for the role of particular vibrations[12, 24, 26] that are in near-resonance[29, 30] with the interexcitonic energy gap between the donor and acceptor chromophores. Near-resonance selectively spikes the

interexcitonic energy-transfer rate[9, 29] and therefore it is an important consideration for the rate calculation.

In this chapter, I explore the earliest energy transfer processes in the phycobilisome light-harvesting antenna of cyanobacteria.[4, 18, 31] The phycobilisome antenna utilizes phycocyanobilin as its light absorbing chromophore (*Fig 4.1a*). Unlike chlorophyll, phycocyanobilin is floppy and highly spectrally tunable.[32, 33] π- conjugation in phycocyanobilin depends on the chromophore configuration and increasing conjugation redshifts the absorption and emission wavelengths. The antenna is composed of rods of trimers of C-phycocyanin (CPC, shown in blue in *Fig 4.1b*) and a lateral core assembly of trimers of allophycocyanin (APC, shown in red in *Fig 4.1c*). Spectral tunability provides the phycobilisome antenna a broad absorption feature in 600-650 nm and a fluorescence feature at ~664 nm (*Fig 4.1c*). Within each CPC/APC trimer, two phycocyanobilin chromophores, covalently linked to the α_{84} and β_{84} sites, are within 2 nm of each other[18] and are therefore electrostatically coupled (*Fig 4.1d, e*). The α_{84} chromophore has a lower energy than β_{84} due to a more planar chromophore structure in the α pocket. CPC absorbs maximally at 620 nm and emits at 645 nm. APC absorbs at ~650 nm and emits at 660 nm.[34] Pump-probe spectra of the phycobilisome antenna have been reported numerous times[34, 35] and feature a prominent excited-state absorption feature between 660 and 680 nm.[4]

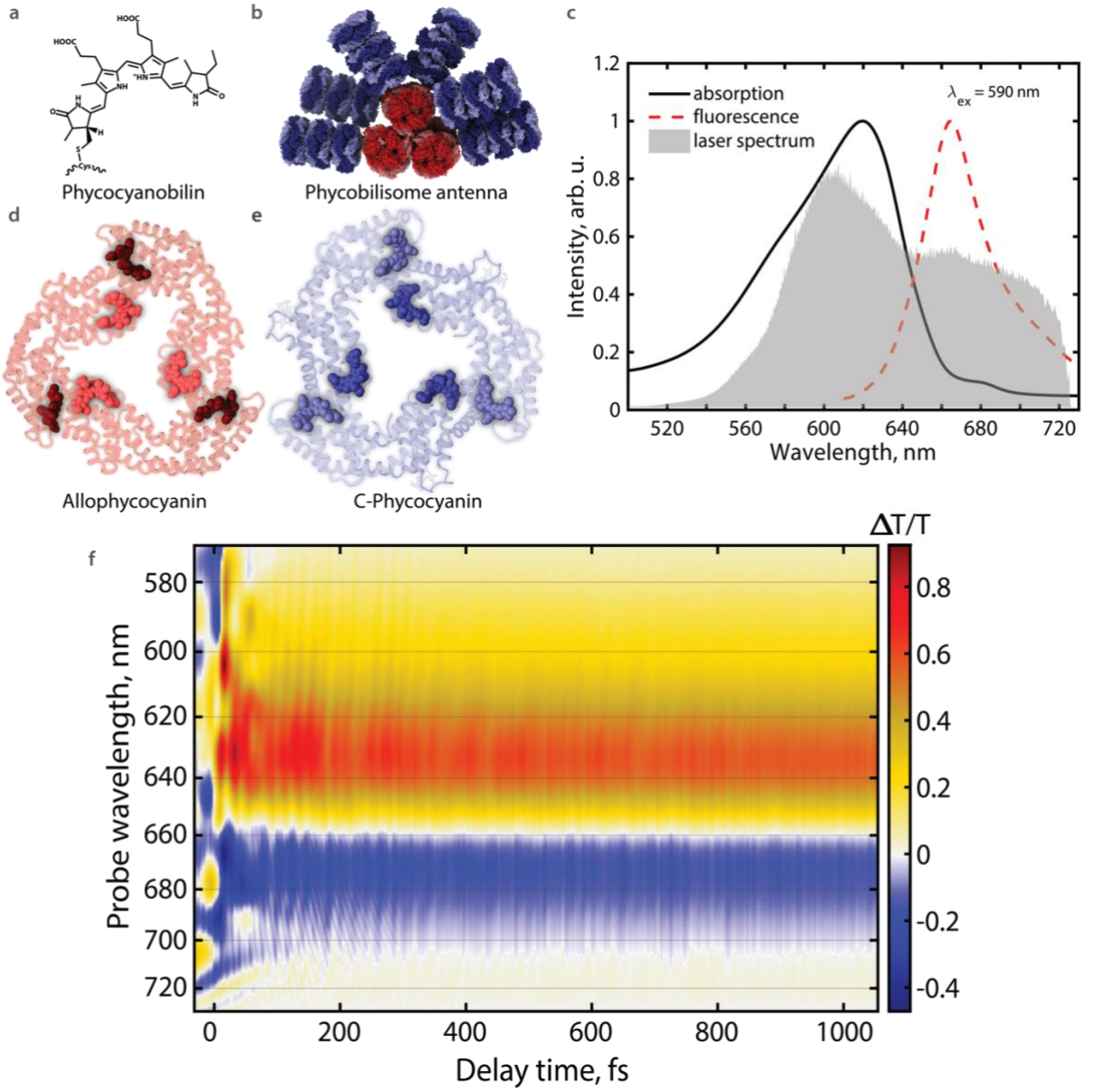

Fig 4.1: **a)** Chemical structure of the phycocyanobilin chromophore **b)** cryo-EM structure[18] of the *Synechocystis* 6803 phycobilisome antenna with C-phycocyanin rods colored blue and allophycocyanin cores colored red **c)** The absorption and emission spectra of *Synechocystis* 6803 phycobilisome antenna (adapted from [4]). The laser spectrum used for experiments in this work is shown in grey **d)** Allophycocyanin trimer protein structure with the coupled chromophore dimer highlighted **e)** C-phycocyanin trimer protein structure **f)** Transient transmission spectrum of the *Synechocystis* 6803 phycobilisome antenna up to 1.1 ps in time steps of 3 fs. Negative signal is excited-state absorption, positive signal is ground-state bleach and stimulated emission.

To study energy transfer within the coupled chromophores, we develop a method to obtain the profile of the low-frequency spectral density of the nuclear modes coupling to Franck-Condon excitation, and therefore energy transfer, for use in modified-Redfield theory calculations. Specifically, we perform finely sampled broadband pump-probe spectroscopy on the intact phycobilisome antenna complex with sub-10 fs pulses (*Fig 4.1f*). We Fourier transform the obtained time-domain data across the probe wavelength axis. Normalized frequency domain data for multiple probe wavelengths is plotted in *Fig 4.2*. The Fourier transform (FT) data matches within our spectral resolution with resonance Raman experiments on phycocyanobilin based systems in the high-frequency regime.[20, 21, 36-39] Notably, this method allows Rayleigh scatter-free characterization of the low-frequency vibrational modes that are Franck-Condon active[40] and hence couple to electronic excitation. We fit the obtained FT peaks with generalized Brownian oscillator functions[41] and use the functional form as the spectral density in numerical simulations of modified-Redfield theory calculations of interexcitonic energy transfer in the excitonically coupled dimer of CPC.

We find two vibrational modes, at 387 cm^{-1} and 437 cm^{-1}, to be in resonance with reported literature values of the C-phycocyanin interexcitonic energy gap.[27, 42] Modified Redfield theory calculations show a many-fold enhancement in the interexcitonic energy transfer rate due to the involvement these modes in the transfer process. This approach provides a broadly applicable method to incorporate realistic vibrational spectral densities in energy transfer calculations. Separately, the excited-state absorption feature[4] in phycobilisomes allows us to selectively observe active vibrational modes that lock the chromophore configuration in the excited state and prevent energetic relaxation to promote energy transfer.[43] Specifically, we observe that chromophore-residue hydrogen bonding prevents relaxation of the phycocyanobilin excited state so that transfer

precedes trapping.[44] Our characterization of the vibrations coupled to the excitons in the phycobilisome antenna highlights the role of both tertiary and primary protein structure in regulating and promoting the energy capture process in oxygenic photosynthesis.

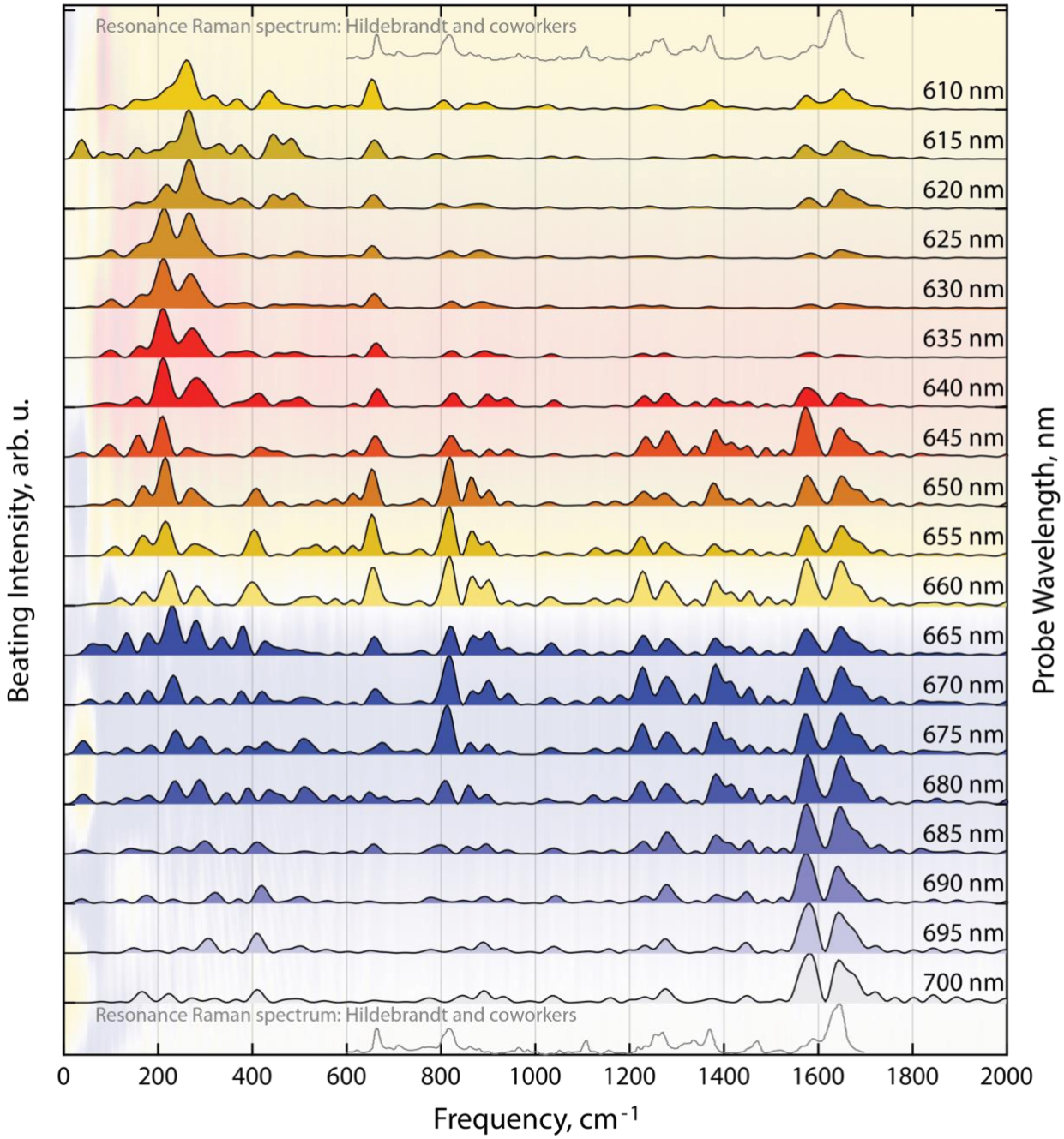

Fig 4.2: Normalized Fourier transforms of time traces of the phycobilisome pump-probe signal at different wavelengths. The x- axis shows the vibrational beating frequency. Intensity is normalized to maximum at each wavelength. The resonance Raman spectrum of C-phycocyanin is shown for comparison from work by Hildebrandt and coworkers[36] (digitized with WebPlotDigitizer[45])

We find two vibrational modes, at 387 cm^{-1} and 437 cm^{-1}, to be in resonance with reported literature values of the C-phycocyanin interexcitonic energy gap.[27, 42] Modified Redfield theory calculations show a many-fold enhancement in the interexcitonic energy transfer rate due to the involvement these modes in the transfer process. This approach provides a broadly applicable method to incorporate realistic vibrational spectral densities in energy transfer calculations. Separately, the excited-state absorption feature[4] in phycobilisomes allows us to selectively observe active vibrational modes that lock the chromophore configuration in the excited state and prevent energetic relaxation to promote energy transfer.[43] Specifically, we observe that chromophore-residue hydrogen bonding prevents relaxation of the phycocyanobilin excited state so that transfer precedes trapping.[44] Our characterization of the vibrations coupled to the excitons in the phycobilisome antenna highlights the role of both tertiary and primary protein structure in regulating and promoting the energy capture process in oxygenic photosynthesis.

Pump-probe acquisition: Phycobilisome isolation and steady-state characterization for this work are reported elsewhere.[4] Sub-40 fs laser pulses centered at ~800 nm with an average power of 2.7 W and a repetition rate of 5 kHz are generated in a Ti:sapphire Coherent Legend Elite regenerative amplifier seeded by a Coherent Micra Ti:sapphire oscillator. The laser beam is focused in argon gas at 18 psi. The resulting white-light supercontinuum is compressed to sub-10 fs using a combination of two DCM10 chirped mirror pairs from Laser Quantum. A representative laser spectrum is shown in *Fig 4.1c*. The compressed pulse is split into pump and probe beams with a 90/10 beam splitter. The pump beam is passed through a mechanical delay stage (Aerotech) and chopped at 2.5 kHz (Newport Corp.). The pump and probe are focused into a 200 μm thickness sample cell. The sample is flowed through data acquisition to minimize photodamage. The spot size at the sample cell is ~250 μm and the fluence is kept at ~15 nJ per pump pulse using reflective

neutral density filters. Annihilation is not a concern because it occurs largely beyond the 1 ps delay time of our measurements.[34] Pump and probe polarizations are kept identical. The probe passes through an iris to be aligned onto a Shamrock spectrometer with a Teledyne Dalsa Spyder 3 CCD camera. 19 averages are performed to achieve a high signal-to-noise ratio. Spectra are windowed in rephasing time (inverse of detection wavelength) to remove pump-probe scatter. Frequency domain data is obtained by Fourier transforming the obtained time-domain data across the probe wavelength axis after six-fold zero-padding. Zero-padding is performed to aid curve fitting with Brownian oscillators in MATLAB. No claims regarding shifts smaller than the original frequency resolution without zero padding are made in the chapter. Simulation and curve-fitting details will follow in the thesis of Ping-Jui Wu.

In spectrally congested photosynthetic antenna systems, the obtained FT map of the pump-probe spectrum provides information similar to two-dimensional electronic-vibrational spectroscopy[30, 46, 47] with vibrational resolution along the visible probe axis instead of the pump axis. For example, low frequency modes change systematically across 630 nm to 660 nm clearly indicating two different species in this spectroscopic region, which we know to be C-phycocyanin and allophycocyanin respectively. This information cannot be accessed through steady-state spectroscopy and is not clearly visible in time-domain pump probe measurements. To calculate vibration-mediated energy transfer rates, we use the FT at 620 nm because this wavelength has low overlap with APC spectral features.

The extracted spectral density is shown in *Fig 4.3a*. One can find most of the peaks located at low frequency area and the highest peak shows up at 260 cm^{-1}. Given the Coulomb coupling is -175 cm^{-1}, the lowest possible excitonic energy gap of dimer system is 350 cm^{-1}, therefore, we are particularly interested in the 370 and 437 cm^{-1} peaks. The 807 cm^{-1} HOOP mode also appears in

the extracted spectral density; however, we can see it has low relative intensity in comparison to the low frequency mode. Additionally, the energy gap of chromophore dimer in CPC is much lower to its frequency, so we expect the HOOP mode shows no significant role in the excitation energy transfer of dimer in CPC.

The excitation energy transfer of dimer is calculated as a function of reorganization energy of the multimode Brownian oscillator (MBO) bath and the site energy gap between two monomers. We plot the rates as a 2D map in *Fig 4.3b*. An intense and clear resonant peak shows up at excitonic energy gap of 370 cm^{-1} and a less pronounced resonant peak appears around 437 cm^{-1}. The calculated rates at 200 cm^{-1} reorganization energy are 10.96 ps^{-1} ($\tau = 91$ fs) and 8.23 ps^{-1} ($\tau = 121$ fs) for site energy of 370 and 430 respectively, which these time constants are much faster than the experimental reported time constant (500 fs). This is mainly due to the ignorance of dynamic localization in the modified Redfield theory. Nevertheless, modified Redfield theory still provide a correct trend for us to explore the effect of protein bath modes toward energy transfer process. The overestimation of the energy transfer rates could be fixed by adopting a more advanced theoretical method e.g., the hierarchical equations of motion (HEOM). But the computational cost will increase significantly and thus we stick to using modified Redfield theory throughout this work.

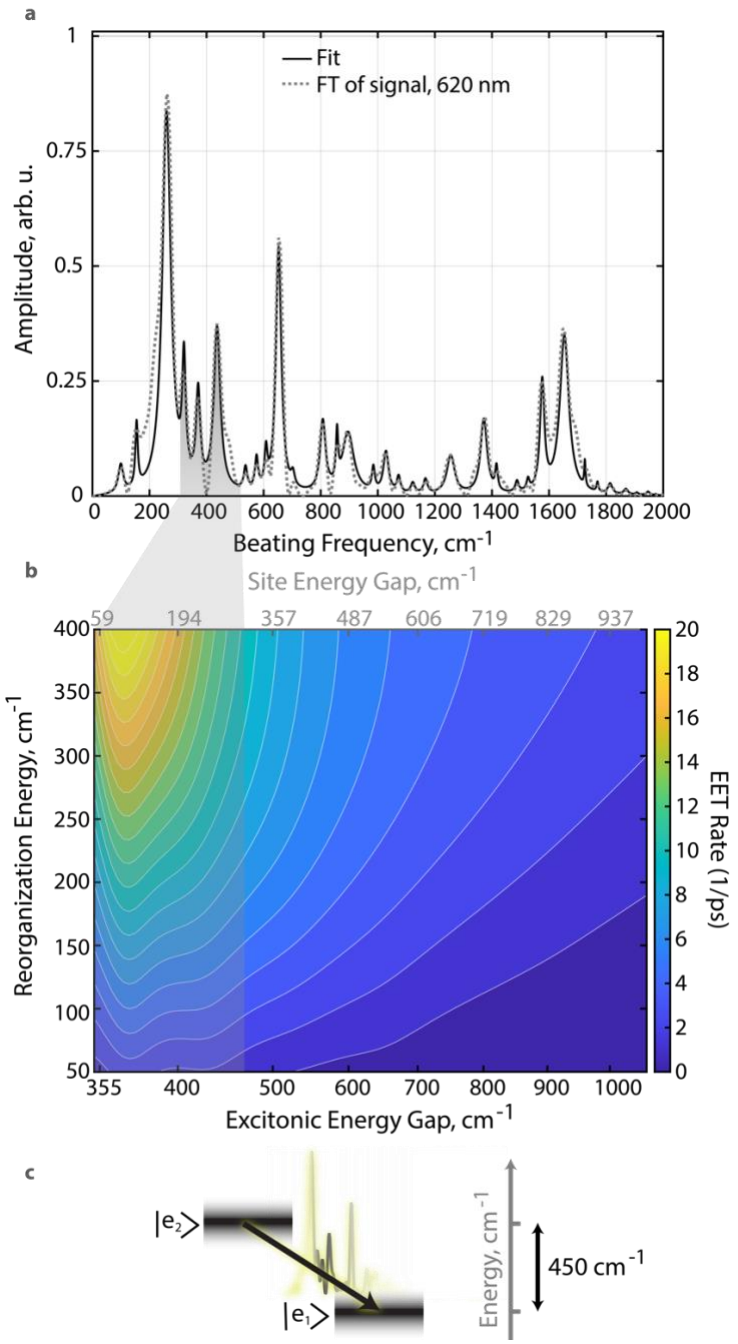

Fig 4.3: **a)** Fourier transform of the probe signal at 620 nm, which we use as the spectral density for C-phycocyanin. The Fourier transformed 'vibrational spectrum' is fit with multiple Brownian oscillator peaks **b)** Calculated modified-Redfield rates using the Fourier-transformed spectrum in **b** as the spectral density **c)** Cartoon depicting vibrationally enhanced energy transfer between the excitonic states: a resonance between the vibrational energies and the interexciton energy gap drives fast energy transfer

The matching of these two excitonic energy gaps to frequency of extracted mode from FT of phycobilisome pump-probe spectrum implies the vibrational enhancement of excitation energy transfer of the chromophore dimer in CPC. This resonance also demonstrates the importance of utilizing structural spectral density. While the commonly used spectral densities like Drude-Lorentz form or Ohmic form statistically describe protein environmental effect, they obscure the details of bath mode distribution in the protein. Therefore, observation of vibrational enhancement becomes impossible and the importance of specific protein bath modes or chromophore vibrational modes is hidden.

Interestingly, one can notice the resonant peaks in *Fig 4.3b* fade out and redshift with increasing reorganization energy: this effect is due to the multiphonon effect. It allows the combination of a low frequency mode and either 370 or 437 cm^{-1} mode to induce the downhill transition. Therefore, the broadening and redshift occur at high reorganization energy condition where multiphonon effects are more probable.

Separately, our previous work has shown that the prominent negative feature observed in the time-resolved spectra of the phycobilisome complex[31, 35, 48] arises from an excited-state absorption (ESA) process in the phycocyanobilin chromophore.[4] When we Fourier-transform the time domain signal at the ESA wavelengths, we can selectively observe the vibrations that couple to the excited state of the phycocyanobilin as it is placed in various cavities in the phycobilisome antenna. We observe that two high-frequency modes, at ~1580 cm^{-1} and ~1640 cm^{-1}, are strongly active on the excited state, implying that the excited-state remains bound along these vibrational coordinates. These phycocyanobilin modes are well-characterized in many previous studies, in which they were observed through resonance Raman,[36-39] time-resolved Raman,[20] and two-dimensional infrared spectroscopy.[22, 49] Both C-PC and APC show this negative ESA feature in

their time-resolved spectra. Therefore, it is not possible to assign these vibrations selectively to APC or C-PC excited states. Mutated structures will be required for specific studies. However, these modes are observed on the ground electronic state of both[50] APC and C-PC chromophores and important conclusions about protein-cofactor interactions can still be drawn.

Recently, Schlau-Cohen and coworkers[43] demonstrated with single-molecule pump-probe spectroscopy experiments on APC trimers that energy-transfer precedes chromophore relaxation in the phycobilisome antenna. This finding is important because the floppy phycocyanobilin molecule relaxes to a highly redshifted state in free solution.[39] It shows that the protein environment actively slows this relaxation process. Our selective observation of the excited-state vibrational modes allows us to identify the protein-chromophore interactions that prevent chromophore relaxation in the protein pocket.

The 1580 cm^{-1} mode has been assigned to N-H in-plane modes of the inner rings that hydrogen-bond with the Asp^{87} residue.[36] This mode has also been shown to disappear when the chromophore's inner rings are deprotonated.[37] The mode at 1642 cm^{-1} is assigned backbone methine bridge stretching. pH dependent studies on the chromophore have shown that relaxation to the so-called far-red trap state in the phycobilin chromophore requires an intermediate in which the chromophore is deprotonated.[38, 44] From this information, we infer that relaxation of the excited-state landscape to a red emission is prevented by the Asp^{87} residue holding the inner rings of the chromophore in place through hydrogen bonding, thereby preventing nuclear motion of the methine bridges to a more conjugated and relaxed configuration. In other words, these modes are strongly active on the excited state with minimal anharmonic shift because the excited state potential is bound along these coordinates, thus preventing rolling to a globally relaxed minimum. This configuration locking prevents the chromophore to enter a highly-conjugated, planar, relaxed

state that emits redder than chlorophyll absorption. The locking therefore prevents the formation of traps along the photosynthetic pathway. *Fig 4.4* shows a cartoon for the mechanism that locks the phycocyanobilin chromophores of C-PC in a high-energy configuration.

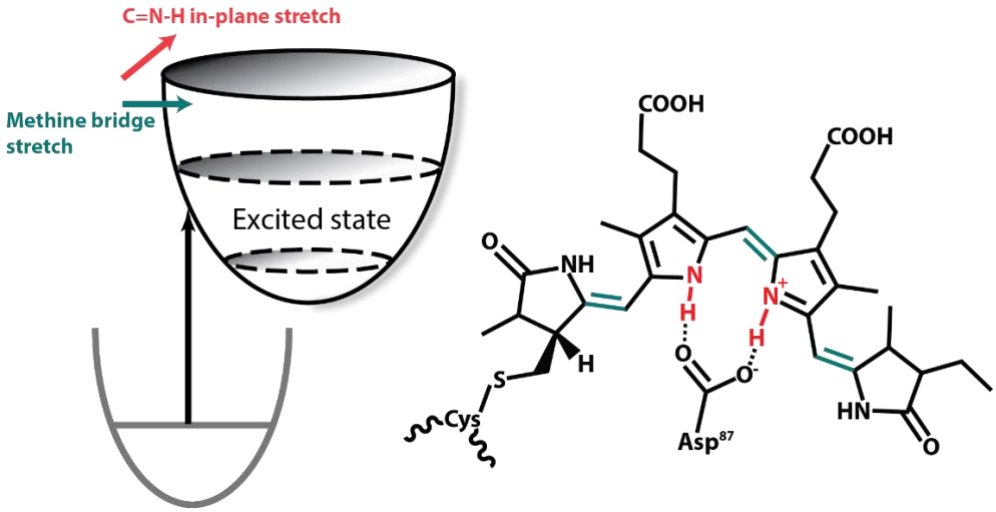

Figure 4.4: The excited-state potential energy surface remains bound along the 1570 and 1640 cm^{-1} modes corresponding to methine bridge stretching and C=N-H stretch modes. The Asp^{87} residue that hydrogen bonds with rings B and C of the phycocyanobilin chromophore prevents deprotonation and chromophore relaxation.

In this chapter, I explore the role of cofactor-amino acid interactions in driving effective energy capture. We observe that residue Asp^{87} of C-PC and APC proteins plays a crucial role in ensuring that absorbed light energy traverses through the phycobilisome complex to reach the photosystem reaction centers. It hydrogen-bonds directly with the pigment to prevent its nuclear relaxation to a red-emitting state that cannot participate in photosynthetic light harvesting. Excited-state-specific Raman spectra of the chromophores show that the excited state remains bound in local bond potentials that involve hydrogen bonding with the amino acid residue. Further, I successfully demonstrate a method to extract the vibrational spectral densities that directly couple to the excitonic states of the light-harvesting pigments. This density provides cross-sections for

scattering processes that involve phonon release coupled to downhill energy transfer. We observe that the low frequency modes that can effectively propel the energy capture process vary between C-phycocyanin and allophycocyanin, although both proteins display great homology otherwise. We find that two modes with strong Raman activity, at 370 or 437 cm^{-1}, likely drive the fast downhill energy transfer process that is well-known in C-phycocyanin.[27, 42] In this case, amino acid-cofactor interactions are more subtle as opposed to the hydrogen-bonding scenario. The overall tertiary folding of the protein dictates these modes, and our observations suggest that tertiary folding could be tuned through evolution towards effective energy capture.

Bibliography

(1) Blankenship, R. E. Antenna Complexes and Energy Transfer Processes. In *Molecular Mechanisms of Photosynthesis*, Wiley, 2002; pp 61-94.
(2) Scholes, G. D.; Fleming, G. R.; Olaya-Castro, A.; van Grondelle, R. Lessons from Nature about Solar Light Harvesting. *Nature Chemistry* **2011**, *3* (10), 763-774.
(3) Kolodny, Y.; Avrahami, Y.; Zer, H.; Frada, M. J.; Paltiel, Y.; Keren, N. Phycobilisome Light-harvesting Efficiency in Natural Populations of the Marine Cyanobacteria *Synechococcus* Increases with Depth. *Communications Biology* **2022**, *5* (1), 727.
(4) Sohoni, S.; Lloyd, L. T.; Hitchcock, A.; MacGregor-Chatwin, C.; Iwanicki, A.; Ghosh, I.; Shen, Q.; Hunter, C. N.; Engel, G. S. Phycobilisome's Exciton Transfer Efficiency Relies on an Energetic Funnel Driven by Chromophore–Linker Protein Interactions. *Journal of the American Chemical Society* **2023**, *145* (21), 11659-11668.
(5) Dahlberg, P. D.; Ting, P.-C.; Massey, S. C.; Allodi, M. A.; Martin, E. C.; Hunter, C. N.; Engel, G. S. Mapping the Ultrafast Flow of Harvested Solar Energy in Living Photosynthetic Cells. *Nature Communications* **2017**, *8* (1), 988.
(6) Otto, J. P.; Wang, L.; Pochorovski, I.; Blau, Samuel M.; Aspuru-Guzik, A.; Bao, Z.; Engel, G. S.; Chiu, M. Disentanglement of Excited-state Dynamics with Implications for FRET Measurements: Two-dimensional Electronic Spectroscopy of a BODIPY-Functionalized Cavitand. *Chemical Science* **2018**, *9* (15), 3694-3703. 10.1039/C8SC00818C
(7) Novoderezhkin, V. I.; Palacios, M. A.; van Amerongen, H.; van Grondelle, R. Energy-Transfer Dynamics in the LHCII Complex of Higher Plants: Modified Redfield Approach. *The Journal of Physical Chemistry B* **2004**, *108* (29), 10363-10375.
(8) Yang, M.; Fleming, G. R. Influence of Phonons on Exciton Transfer Dynamics: Comparison of the Redfield, Förster, and Modified Redfield Equations. *Chemical Physics* **2002**, *282* (1), 163-180.
(9) Hwang-Fu, Y.-H.; Chen, W.; Cheng, Y.-C. A Coherent Modified Redfield Theory for Excitation Energy Transfer in Molecular Aggregates. *Chemical Physics* **2015**, *447*, 46-53.
(10) Chang, Y.; Cheng, Y.-C. On the Accuracy of Coherent Modified Redfield Theory in Simulating Excitation Energy Transfer Dynamics. *The Journal of Chemical Physics* **2015**, *142* (3).
(11) Seibt, J.; Mančal, T. Ultrafast Energy Transfer with Competing Channels: Non-equilibrium Förster and Modified Redfield theories. *The Journal of Chemical Physics* **2017**, *146* (17).
(12) Kolli, A.; O'Reilly, E. J.; Scholes, G. D.; Olaya-Castro, A. The Fundamental Role of Quantized Vibrations in Coherent Light Harvesting by Cryptophyte Algae. *The Journal of Chemical Physics* **2012**, *137* (17).
(13) O'Reilly, E. J.; Olaya-Castro, A. Non-classicality of the Molecular Vibrations Assisting Exciton Energy Transfer at Room Temperature. *Nature Communications* **2014**, *5* (1), 3012.
(14) Dean, J. C.; Mirkovic, T.; Toa, Z. S. D.; Oblinsky, D. G.; Scholes, G. D. Vibronic Enhancement of Algae Light Harvesting. *Chem* **2016**, *1* (6), 858-872.
(15) Mohseni, M.; Rebentrost, P.; Lloyd, S.; Aspuru-Guzik, A. Environment-assisted Quantum Walks in Photosynthetic Energy Transfer. *The Journal of Chemical Physics* **2008**, *129* (17).
(16) Sauer, K.; Scheer, H. Excitation Transfer in C-phycocyanin. Förster Transfer Rate and Exciton Calculations based on New Crystal Structure Data for C-phycocyanins from *Agmenellum quadruplicatum* and *Mastigocladus laminosus*. *Biochimica et Biophysica Acta (BBA) - Bioenergetics* **1988**, *936* (2), 157-170.

(17) Akhtar, P.; Caspy, I.; Nowakowski, P. J.; Malavath, T.; Nelson, N.; Tan, H.-S.; Lambrev, P. H. Two-Dimensional Electronic Spectroscopy of a Minimal Photosystem I Complex Reveals the Rate of Primary Charge Separation. *Journal of the American Chemical Society* **2021**, *143* (36), 14601-14612.
(18) Domínguez-Martín, M. A.; Sauer, P. V.; Kirst, H.; Sutter, M.; Bína, D.; Greber, B. J.; Nogales, E.; Polívka, T.; Kerfeld, C. A. Structures of a Phycobilisome in Light-harvesting and Photoprotected States. *Nature* **2022**, *609* (7928), 835-845.
(19) van Amerongen, H.; van Grondelle, R.; Valkunas, L. *Photosynthetic Excitons*; World Scientific, 2000. DOI: doi:10.1142/3609.
(20) Dasgupta, J.; Frontiera, R. R.; Taylor, K. C.; Lagarias, J. C.; Mathies, R. A. Ultrafast Excited-State Isomerization in Phytochrome Revealed by Femtosecond Stimulated Raman Spectroscopy. *Proceedings of the National Academy of Sciences* **2009**, *106* (6), 1784-1789.
(21) Andel, F.; Murphy, J. T.; Haas, J. A.; McDowell, M. T.; van der Hoef, I.; Lugtenburg, J.; Lagarias, J. C.; Mathies, R. A. Probing the Photoreaction Mechanism of Phytochrome through Analysis of Resonance Raman Vibrational Spectra of Recombinant Analogues. *Biochemistry* **2000**, *39* (10), 2667-2676.
(22) Buhrke, D.; Michael, N.; Hamm, P. Vibrational Couplings between Protein and Cofactor in Bacterial Phytochrome Agp1 Revealed by 2D-IR Spectroscopy. *Proceedings of the National Academy of Sciences* **2022**, *119* (31), e2206400119.
(23) Roy, P. P.; Leonardo, C.; Orcutt, K.; Oberg, C.; Scholes, G. D.; Fleming, G. R. Infrared Signatures of Phycobilins within the Phycocyanin 645 Complex. *The Journal of Physical Chemistry B* **2023**, *127* (20), 4460-4469.
(24) Higgins, J. S.; Lloyd, L. T.; Sohail, S. H.; Allodi, M. A.; Otto, J. P.; Saer, R. G.; Wood, R. E.; Massey, S. C.; Ting, P.-C.; Blankenship, R. E.; et al. Photosynthesis Tunes Quantum-mechanical Mixing of Electronic and Vibrational States to Steer Exciton Energy Transfer. *Proceedings of the National Academy of Sciences* **2021**, *118* (11), e2018240118.
(25) Kell, A.; Feng, X.; Reppert, M.; Jankowiak, R. On the Shape of the Phonon Spectral Density in Photosynthetic Complexes. *The Journal of Physical Chemistry B* **2013**, *117* (24), 7317-7323.
(26) Womick, J. M.; Moran, A. M. Exciton Coherence and Energy Transport in the Light-Harvesting Dimers of Allophycocyanin. *The Journal of Physical Chemistry B* **2009**, *113* (48), 15747-15759.
(27) Womick, J. M.; Moran, A. M. Nature of Excited States and Relaxation Mechanisms in C-Phycocyanin. *The Journal of Physical Chemistry B* **2009**, *113* (48), 15771-15782.
(28) Womick, J. M.; Moran, A. M. Vibronic Enhancement of Exciton Sizes and Energy Transport in Photosynthetic Complexes. *The Journal of Physical Chemistry B* **2011**, *115* (6), 1347-1356.
(29) Policht, V. R.; Niedringhaus, A.; Willow, R.; Laible, P. D.; Bocian, D. F.; Kirmaier, C.; Holten, D.; Mančal, T.; Ogilvie, J. P. Hidden Vibronic and Excitonic Structure and Vibronic Coherence Transfer in the Bacterial Reaction Center. *Science Advances* **2022**, *8* (1), eabk0953.
(30) Yang, S.-J.; Arsenault, E. A.; Orcutt, K.; Iwai, M.; Yoneda, Y.; Fleming, G. R. From Antenna to Reaction Center: Pathways of Ultrafast Energy and Charge Transfer in Photosystem II. *Proceedings of the National Academy of Sciences* **2022**, *119* (42), e2208033119.
(31) Sil, S.; Tilluck, R. W.; Mohan T. M, N.; Leslie, C. H.; Rose, J. B.; Domínguez-Martín, M. A.; Lou, W.; Kerfeld, C. A.; Beck, W. F. Excitation Energy Transfer and Vibronic Coherence in Intact Phycobilisomes. *Nature Chemistry* **2022**, *14* (11), 1286-1294.

(32) Gisriel, C. J.; Elias, E.; Shen, G.; Soulier, N. T.; Flesher, D. A.; Gunner, M. R.; Brudvig, G. W.; Croce, R.; Bryant, D. A. Helical Allophycocyanin Nanotubes Absorb Far-red Light in a Thermophilic Cyanobacterium. *Science Advances* **2023**, *9* (12), eadg0251.
(33) Peng, P.-P.; Dong, L.-L.; Sun, Y.-F.; Zeng, X.-L.; Ding, W.-L.; Scheer, H.; Yang, X.; Zhao, K.-H. The Structure of Allophycocyanin B from *Synechocystis* PCC 6803 Reveals the Structural Basis for the Extreme Redshift of the Terminal Emitter in Phycobilisomes. *Acta Crystallographica Section D* **2014**, *70* (10), 2558-2569.
(34) van Stokkum, I. H. M.; Gwizdala, M.; Tian, L.; Snellenburg, J. J.; van Grondelle, R.; van Amerongen, H.; Berera, R. A Functional Compartmental Model of the *Synechocystis* PCC 6803 Phycobilisome. *Photosynthesis Research* **2018**, *135* (1), 87-102.
(35) Fălămaș, A.; Porav, S. A.; Tosa, V. Investigations of the Energy Transfer in the Phycobilisome Antenna of *Arthrospira platensis* Using Femtosecond Spectroscopy. *Applied Sciences* **2020**, *10* (11), 4045.
(36) Mroginski, M. A.; Mark, F.; Thiel, W.; Hildebrandt, P. Quantum Mechanics/Molecular Mechanics Calculation of the Raman Spectra of the Phycocyanobilin Chromophore in α-C-Phycocyanin. *Biophysical Journal* **2007**, *93* (6), 1885-1894.
(37) Kneip, C.; Hildebrandt, P.; Schlamann, W.; Braslavsky, S. E.; Mark, F.; Schaffner, K. Protonation State and Structural Changes of the Tetrapyrrole Chromophore during the Pr → Pfr Phototransformation of Phytochrome: A Resonance Raman Spectroscopic Study. *Biochemistry* **1999**, *38* (46), 15185-15192.
(38) Mroginski, M. A.; von Stetten, D.; Kaminski, S.; Escobar, F. V.; Michael, N.; Daminelli-Widany, G.; Hildebrandt, P. Elucidating Photoinduced Structural Changes in Phytochromes by the Combined Application of Resonance Raman Spectroscopy and Theoretical Methods. *Journal of Molecular Structure* **2011**, *993* (1), 15-25.
(39) Fodor, S. P. A.; Lagarias, J. C.; Mathies, R. A. Resonance Raman analysis of the Pr and Pfr forms of phytochrome. *Biochemistry* **1990**, *29* (50), 11141-11146.
(40) Liebel, M.; Schnedermann, C.; Wende, T.; Kukura, P. Principles and Applications of Broadband Impulsive Vibrational Spectroscopy. *The Journal of Physical Chemistry A* **2015**, *119* (36), 9506-9517.
(41) Meier, C.; Tannor, D. J. Non-Markovian Evolution of the Density Operator in the Presence of Strong Laser Fields. *The Journal of Chemical Physics* **1999**, *111* (8), 3365-3376.
(42) Womick, J. M.; West, B. A.; Scherer, N. F.; Moran, A. M. Vibronic Effects in the Spectroscopy and Dynamics of C-phycocyanin. *Journal of Physics B: Atomic, Molecular and Optical Physics* **2012**, *45* (15), 154016.
(43) Moya, R.; Norris, A. C.; Kondo, T.; Schlau-Cohen, G. S. Observation of Robust Energy Transfer in the Photosynthetic Protein Allophycocyanin Using Single-molecule Pump–probe Spectroscopy. *Nature Chemistry* **2022**, *14* (2), 153-159.
(44) Mroginski, M. A.; Murgida, D. H.; Hildebrandt, P. The Chromophore Structural Changes during the Photocycle of Phytochrome: A Combined Resonance Raman and Quantum Chemical Approach. *Accounts of Chemical Research* **2007**, *40* (4), 258-266.
(45) Rohatgi, A. *WebPlotDigitizer, Version 4.6*. 2022. https://automeris.io/WebPlotDigitizer (accessed.
(46) Wu, E. C.; Arsenault, E. A.; Bhattacharyya, P.; Lewis, N. H. C.; Fleming, G. R. Two-dimensional Electronic Vibrational Spectroscopy and Ultrafast Excitonic and Vibronic Photosynthetic Energy Transfer. *Faraday Discussions* **2019**, *216* (0), 116-132. 10.1039/C8FD00190A

(47) Nguyen, H. H.; Song, Y.; Maret, E. L.; Silori, Y.; Willow, R.; Yocum, C. F.; Ogilvie, J. P. Charge Separation in the Photosystem II Reaction Center Resolved by Multispectral Two-dimensional Electronic Spectroscopy. *Science Advances* **2023**, *9* (18), eade7190.
(48) Navotnaya, P.; Sohoni, S.; Lloyd, L. T.; Abdulhadi, S. M.; Ting, P.-C.; Higgins, J. S.; Engel, G. S. Annihilation of Excess Excitations along Phycocyanin Rods Precedes Downhill Flow to Allophycocyanin Cores in the Phycobilisome of Synechococcus elongatus PCC 7942. *The Journal of Physical Chemistry B* **2022**, *126* (1), 23-29.
(49) Buhrke, D.; Lahav, Y.; Rao, A.; Ruf, J.; Schapiro, I.; Hamm, P. Transient 2D IR Spectroscopy and Multiscale Simulations Reveal Vibrational Couplings in the Cyanobacteriochrome Slr1393-g3. *Journal of the American Chemical Society* **2023**, *145* (29), 15766-15775.
(50) Szalontai, B.; Gombos, Z.; Csizmadia, V.; Bagyinka, C.; Lutz, M. Structure and Interactions of Phycocyanobilin Chromophores in Phycocyanin and Allophycocyanin from an Analysis of their Resonance Raman Spectra. *Biochemistry* **1994**, *33* (39), 11823-11832.

Chapter 5

Observation of Chirality-Controlled Exciton Dynamics in LH2

Our notion of chirality in chemistry is generally restricted to the arrangement of nuclei in molecules and proteins, and the associated asymmetries in chemical reaction rates involving the rearrangement of these nuclei.[1] Electrons in chiral materials also demonstrate a susceptibility to differential interactions with left- and right-circularly polarized light. This effect is called circular dichroism.[2] Typically, circular dichroism is thought of as being a static effect arising from the chiral nuclear arrangement in a system, but recent explorations suggest that it could play dynamic roles in governing chemistry.[3]

In this chapter, I describe experiments that demonstrate the presence of chirality-dependent excited-state dynamics in the antenna protein, LH2 of purple bacteria. The pigment-protein complex LH2 is a remarkable model protein to study spectroscopically because it has a near-C_9 symmetry in most purple bacterial species.[4] A cartoon of the cryo-EM structure from *Rb. sphaeroides*[5] is shown in *Fig 5.1a*. LH2 utilizes bacteriochlorophyll *a* pigments to absorb NIR light between 800 and 900 nm. A representative absorption spectrum of the complex used in our experiments is shown in *Fig 5.1b*.

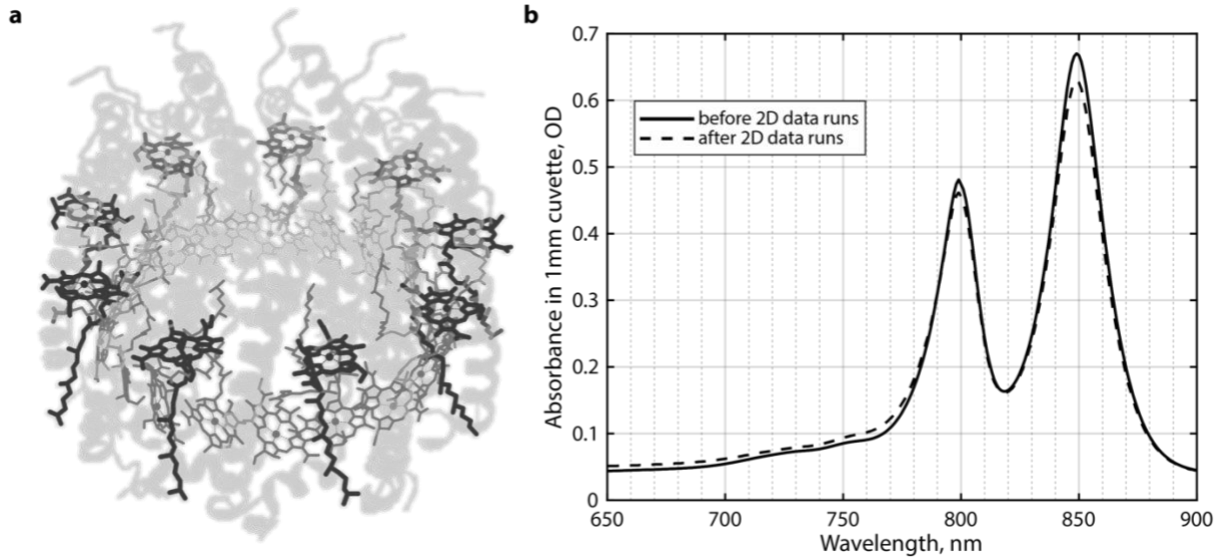

Fig 5.1: a) cryo-EM structure of LH2 from *Rb. sphaeroides*. b) The absorption spectrum of the LH2 used in experiments presented in this chapter. Chromophores shown in black in *a* are separated from each other by 21 Å, resulting in weak coupling, and a corresponding absorption band at 800 nm, seen in *b*. Chromophores in the lower half of the complex shown in grey are separated from each other by 7 Å. These chromophores are strongly coupled to each other, and result in an absorption band at 850 nm seen in *b*.

The LH2 complex of *Rb. sphaeroides* is a transmembrane protein made of nine apoprotein subunits, and has a roughly C_9 symmetry. The inner α apoprotein and the outer β apoprotein in a subunit bind three bacteriochlorophyll molecules between them. Two chromophores are bound noncovalently through the sidechain of a conserved His residue, forming a ring of nine bacteriochlorophyll *a* dimers perpendicular to the membrane plane. This ring faces the periplasmic side in the intracytoplasmic membrane and is called the B850 ring, based on its maximal absorption at 850 nm. Each αβ subunit also binds an additional bacteriochlorophyll a molecule with the formylated N- terminal of the α polypeptide. These chromophores form a ring of nine weakly coupled bacteriochlorophyll *a* molecules that lies roughly in the membrane plane, and faces the cytoplasmic side. This ring is referred to as the B800 ring, after its absorption peak at 800 nm. Head-to-head alignment of the transition dipole moments of the chromophores in the rings causes

J- like coupling in both rings, which leads to the redshift to 800 nm and 850 nm respectively.[6, 7] The dimers of bacteriochlorophylls in the B850 ring are in close contact with each other, with a nearest neighbor distance of around 9 Å, which leads to strong coupling of the order of 200 cm^{-1} vis-à-vis a static disorder of around 100 cm^{-1} in these chromophores.[5, 7, 8] Chromophores in the B800 ring are weakly coupled to each other due to a large interchromophore distance of 21 Å between adjacent chromophores. The interchromophore coupling in the B800 ring is estimated to be 30 cm^{-1} as opposed to a static disorder of 150 cm^{-1}.[7] B850 excitations are delocalized across the ring upon initial photoexcitation because of the strong coupling between chromophores. These excitons can be described as particles on a ring and can be assigned positive and negative angular momentum values from the solutions of the particle-on-a-ring model.[9] The distance between the B800 and B850 rings is ~1.7 nm,[5] allowing bath-mediated downhill energy transfer from B800 to B850.[10-12] Exciton delocalization along the B850 ring creates a strong and conserved circular dichroism signal suggesting a spectral shift between the absorption of right- and left-handed B850 excitonic states. *Fig 5.2* shows the circular dichroism (CD) spectrum for the sample used in our experiments. We note here that although the arrangement of chromophores in the B800 and B850 rings is perpendicular, the transition dipole moments are close to parallel so that fast energy transfer is allowed.[13]

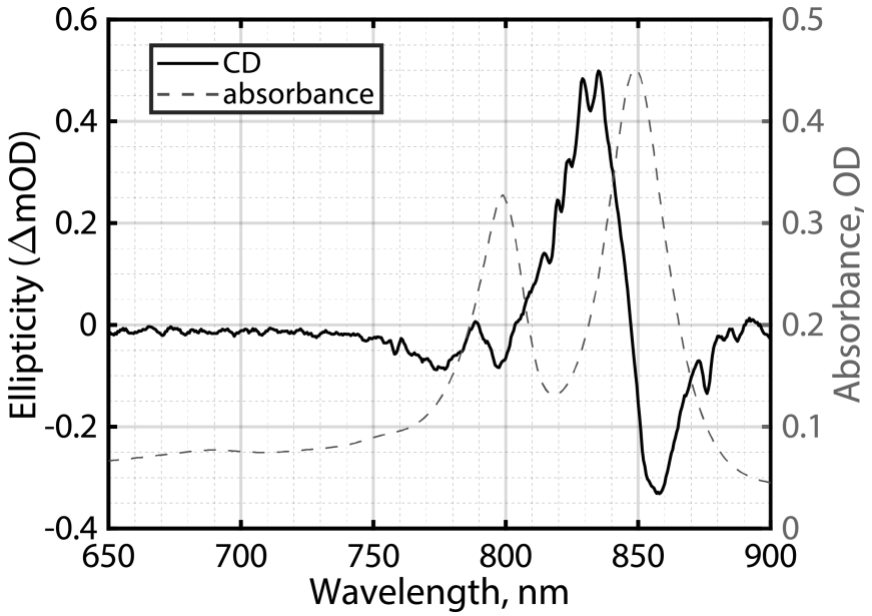

Fig 5.2: Circular dichroism spectrum of LH2. $Abs_L - Abs_R$ is plotted. The circular dichroism arises almost completely from the B850 band.[14]

The circular dichroism spectrum of LH2 shows two prominent bands, the main band with a dispersive shape at 850 nm, and another band between 780 nm and 800 nm. CD experiments on B800-less LH2 mutants have suggested that the 780-800 nm CD band is a mixture of bands from B800 and higher-lying B850 states.[14] Higher-lying delocalized excited states also exist in the related complex LH1,[15] and they have been observed to play a role in energy capture.

The B800 ring displays a small circular dichroism signal[14] and previous theoretical studies have found weak delocalization and coupling between B800 ring chromophores.[11] These findings together suggest that the particle-on-a-ring model can also be invoked to describe B800 excitons, at least immediately upon excitation with broadband, coherent light. Rapid exciton localization occurs in B800 to single chromophores, whereas dephasing in B850 is somewhat slower, occurring on the 100-200 fs timescale.[9] Electronic structure of the B800 and B850 rings in the delocalized angular momentum basis set is shown in *Fig 5.3.*

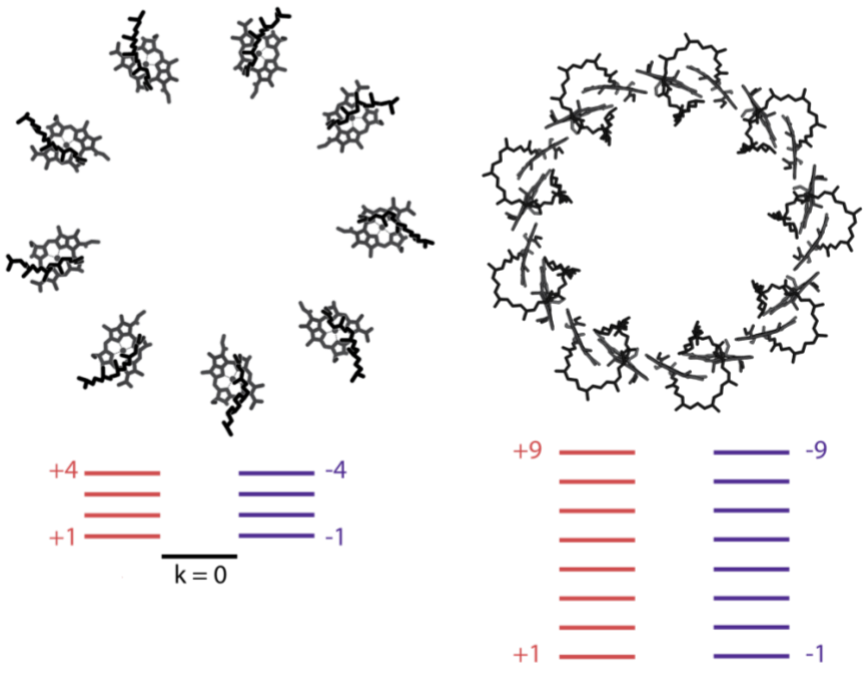

Fig 5.3: The delocalized basis sets of B800 and B850 excitons. On the left, nine chromophores weakly couple to form a new delocalized excitonic basis set described by particle-on-a-ring states with positive and negative angular momenta. The y- axis, energy, is not to scale. On the right, the B850 ring is shown. In this ring, chromophores are strongly coupled (300-800 cm^{-1}) and result in a circular delocalization even at room temperature.[9, 11, 16]

Energy transfer from B800 to B850 has been extensively studied with two-dimensional electronic spectroscopy and occurs with a 500-650 fs time constant.[17, 18] It is well-known that this transfer process is assisted by bath interactions and disorder.[7, 10, 11, 19]

Interestingly, previous work from our group observed spectral signatures that suggested that energy transfer from left- and right-handed B800 states to corresponding B850 rates had different dynamics.[20] In that work, the authors performed two-dimensional circular dichroism spectroscopy on LH2 with an XYYY pulse sequence.[20] In the XYYY pulse sequence, the polarization of beam 1 (first pump interaction) is set perpendicular to the other three pulses. In the chiral basis, the polarization of the first pulse is expressed as $L - R$ with respect to the other pulses' polarizations.[21-23] Here, L and R represent left- and right-circularly polarized light. Therefore, this

pulse sequence yields weak, dipole-disallowed signal corresponding to the change in the circular dichroism as a function of the waiting time. This signal is typically 10000 times weaker than dipole-allowed signal. The authors obtained direct evidence for delocalized acceptor states in the energy transfer process. In their work, they observed that the 800 nm region had a larger chiral signal compared to the 850 nm region, reflecting that the higher-lying B850* states with higher angular momentum contribute strongly to the ultrafast CD signal.

The measurements in this earlier work demonstrated that LH2 has a time-resolved circular dichroism signal. However, because they directly measured the $L - R$ component in that work, their measurements could not reveal if the differential signal occurred due to different oscillator strengths of the left- and right-handed states or due to their different decay dynamics.

In this chapter, I describe 2DES experiments I preformed using LXXX and RXXX pulse sequences on LH2 to untangle the effects of oscillator strength and dynamics on the ultrafast CD signal. The first pump pulse is left-circularly polarized in LXXX experiments and is right-circularly polarized in RXXX experiments. These pulse sequences selectively excite left- and right-handed angular momentum states of LH2 shown in *Fig 5.3.*

The circular polarization purity of our pulses is confirmed with a Glan-Thompson analyzer at the sample position with measurements of beam power made every 10^{o}. Polarizing optics generating the circular polarization are tuned for minimal change of power through the entire Glan-Thompson rotation. A combination of broadband half- and quarter-waveplates from Union Optic, Wuhan is used to ensure high polarization purity. *Fig 5.4* shows a representative polarization-purity scan.

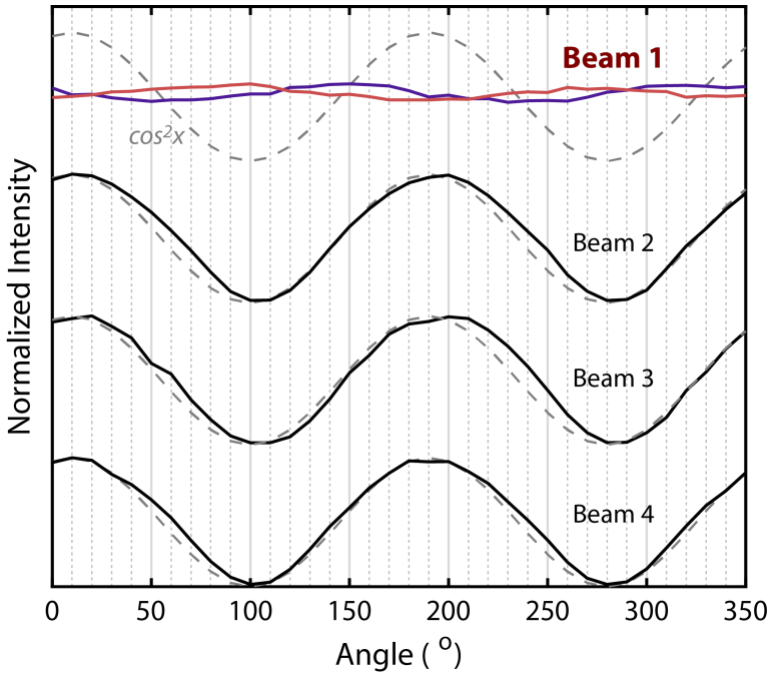

Fig 5.4: Polarization purities of all beams in the 2DES experiment. Beam 1 does not show power change as a function of the analyzer angle, indicating clean circularly polarized light with ellipticity > 0.99.

In the 2DES experiments, we observe left- and right-handed exciton states of B800 display both different initial oscillator strengths and different energy transfer dynamics to B850. We also observe that the bath coupling of right-handed states is stronger than the bath coupling of the left-handed states, leading to faster energy transfer due to vibronic resonance. *Figs 5.5* and *5.6* show representative 2DES spectra for different waiting times for RXXX and LXXX respectively. Comparing the 520 fs frames shows clearly that energy transfer in the right-handed states is faster than in the left-handed states. We confirm that the ellipticity of beam 1 is >0.99 to observe this effect.

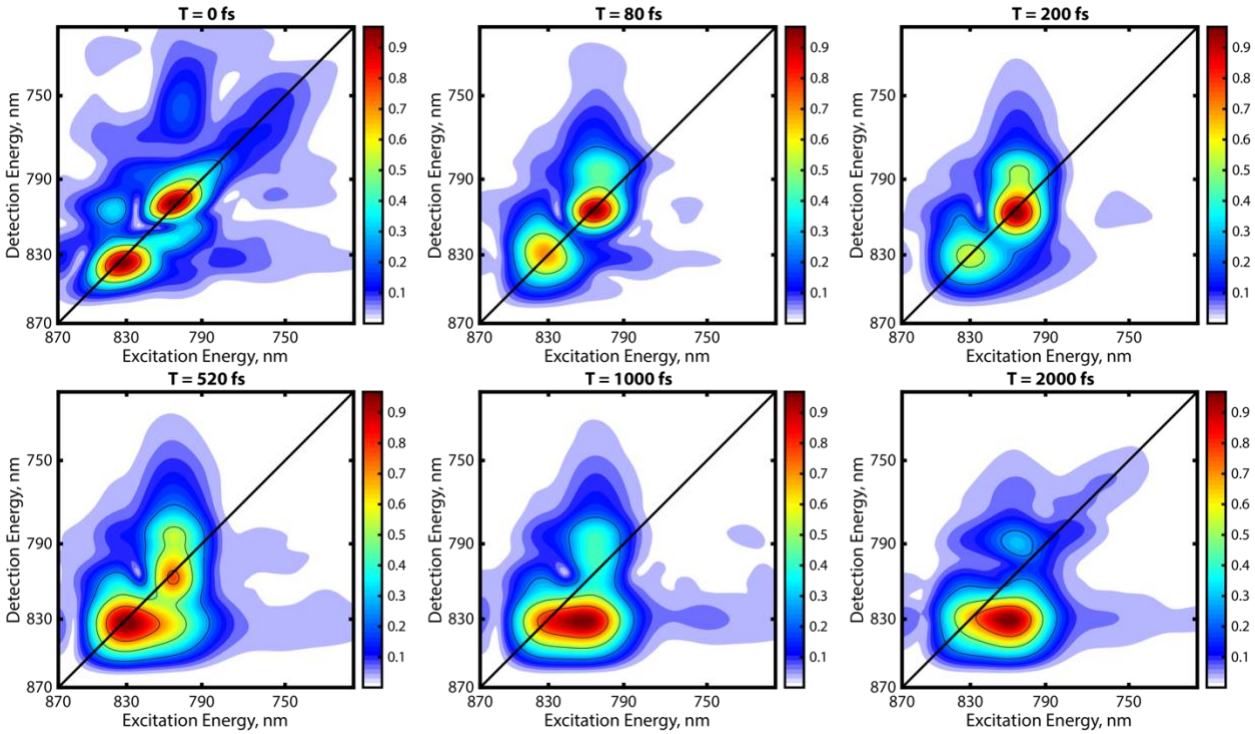

Fig 5.5: Representative 2DES frames obtained with an RXXX pulse sequence on LH2

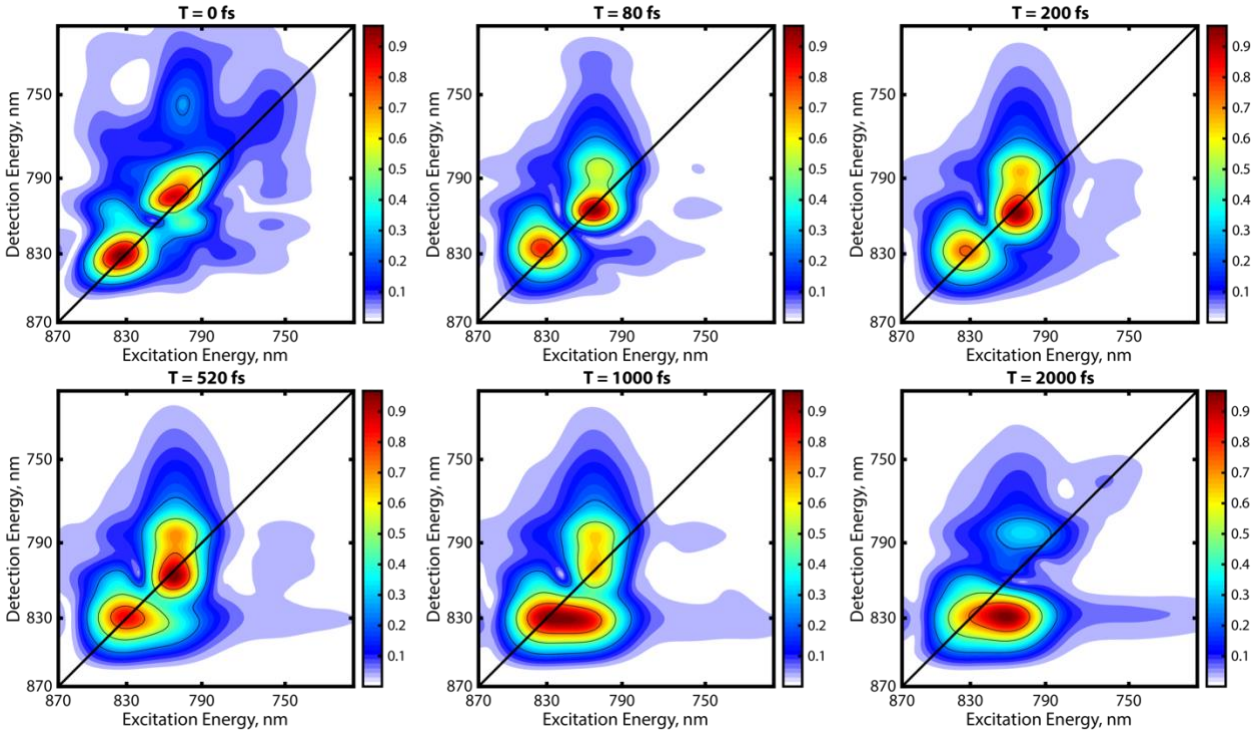

Fig 5.6: Representative 2DES frames obtained with an LXXX pulse sequence on LH2

Signal at the 804 nm diagonal point is plotted as a function of waiting time in *Fig 5.7*, and we observe that the right-handed states decay with a time-constant ~90 fs faster than the left-handed states.

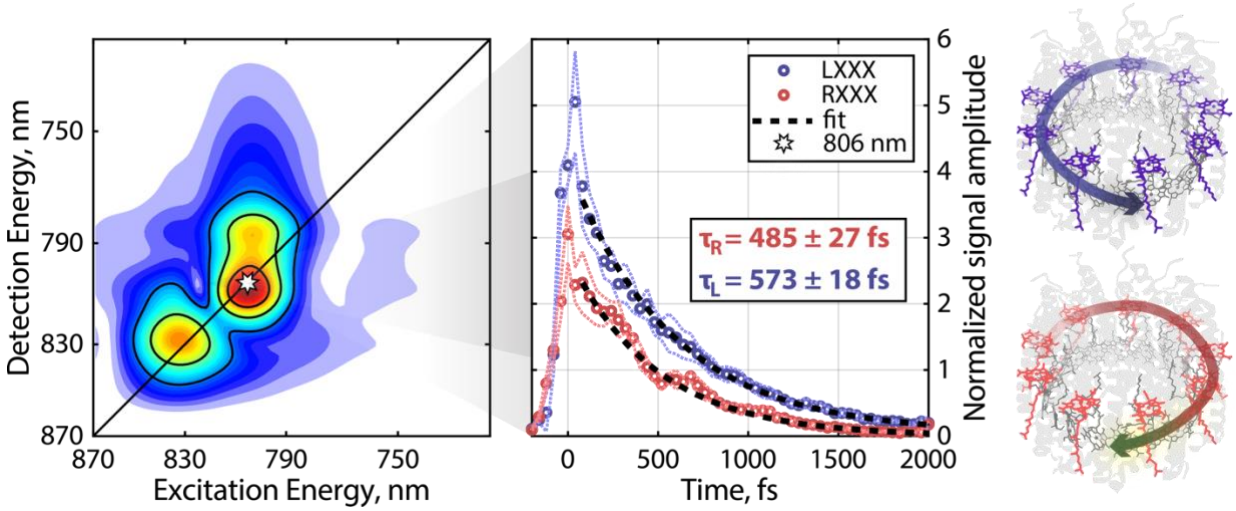

Fig 5.7: LH2 2DES signal as a function of waiting time at the 806 nm diagonal for the RXXX and LXXX pulse sequences. Plotted time traces are unnormalized. It is observed that the LXXX sequence has a larger signal intensity and that the RXXX signal decays significantly faster.

T-statistics reveal that the probability of the two datasets arising from the overall population is 0.000027, strongly suggesting that the decay constants of left- and right-handed experiments arise from different processes. Further, we observe that an 85 cm^{-1} vibration couples strongly with the right-handed states but does not couple with the left-handed states. This vibration is shown in *Fig 5.8. Fig 5.9* shows the amplitude of the vibronic beating across the 2D spectra. We observe that the 85 cm^{-1} mode is most active at the 800 nm diagonal feature.

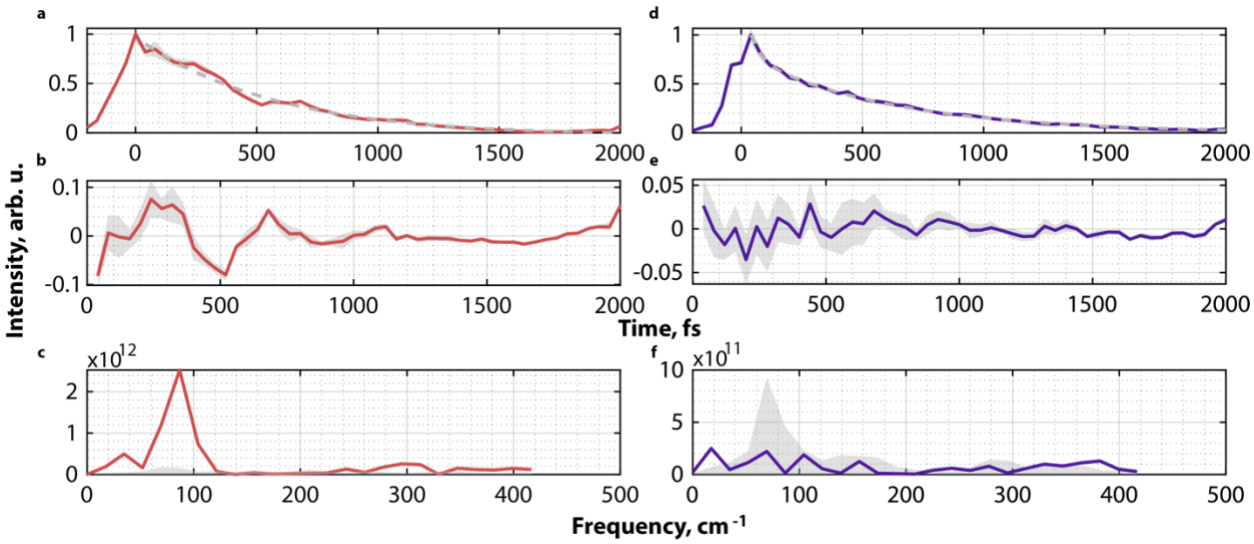

Fig 5.8: **a)** Time-trace of signal at the 804 nm diagonal with a biexponential fit **b)** Residuals after subtracting the biexponential fit **c)** Fourier transform of residual, for RXXX **d)** Time-trace of signal at the 804 nm diagonal with a biexponential fit **e)** Residuals after subtracting the biexponential fit **f)** Fourier transform of residual, for LXXX

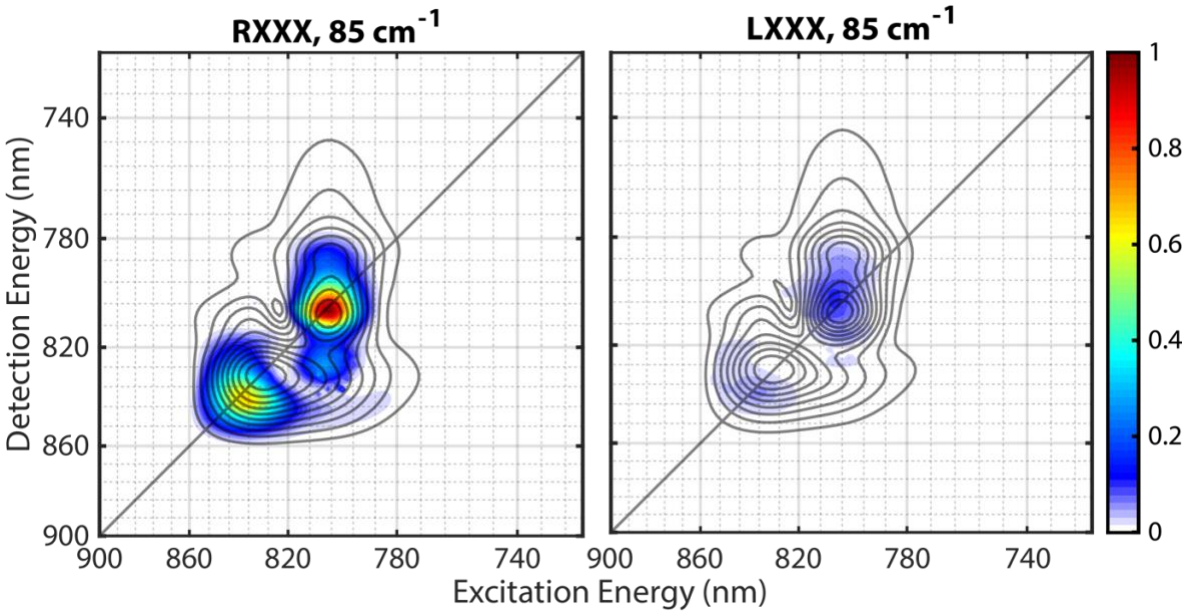

Fig 5.9: Fourier transforms of all time-traces across the 2D spectral map for RXXX (left) and LXXX (right) pulse sequences. We observe that the 85 cm^{-1} mode is only active in the 800 nm diagonal region for the RXXX pulse sequence.

An important aspect to consider in describing the observed chiral dynamics is that the chromophores in the B800 ring are weakly coupled to each other, with an average interchromophore coupling of 30 cm^{-1}.[7] At room temperature, it is therefore expected that excitations in the B800 ring are localized to single chromophores, and are not chiral in nature. Therefore, the observation of chiral dynamics originating from the B800 is surprising. We hypothesize that chirality is induced in the B800 excitons in our experiments due to the large chiral impulse of our pulses. A previous theoretical study has shown that chiral activity can be orders of magnitude larger than the optical activity if the incident exciting field is highly chiral.[24] Recent experiments by Bonetti and coworkers[25] have shown that a strong, chiral light pulse can induce magnetization and multiferroicity in materials due to handed interactions. Therefore, we propose a mechanism in which the strong magnetic field of our circularly polarized exciting pulse drives the B800 excitons into a chiral basis. Upon the creation of chiral B800 excitations, faster transfer occurs to right-handed higher-energy B850* states through a vibronic resonance which is not accessible to the left-handed states. The B850* left- and right-handed states then relax to B850 low angular momentum states and localize to a few chromophores[9]. This mechanism is illustrated in *Fig 5.10.*

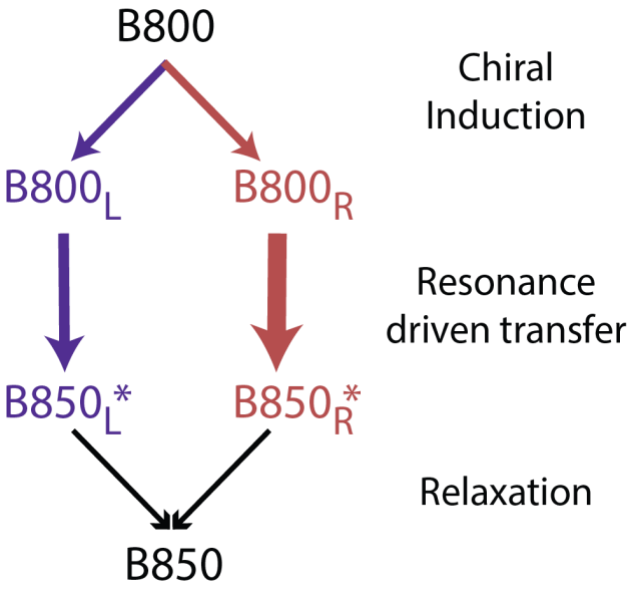

Fig 5.10: Proposed mechanism for chirality-controlled energy transfer in LH2. Ground-state B800 chromophores are excited with highly chiral light so that resulting excited states retain chiral memory. Right-handed B800 states transfer energy faster to B850* states due to vibronic resonance compared to left-handed states as seen in our experiments. Both states then relax to localized B850 states.

To test our hypothesis of induced chirality in the B800 states, I performed 2DES experiments in which the pump (beams 1 and 2) spectrum is made significantly narrower in the frequency domain to not interact with the B850 band. In these experiments, the impulse of the exciting pulses would be lower, and moreover magnetization of the B850 ring would be absent. The pump and probe spectra for narrowband pump excitation 2DES experiments is shown in *Fig 5.11*.

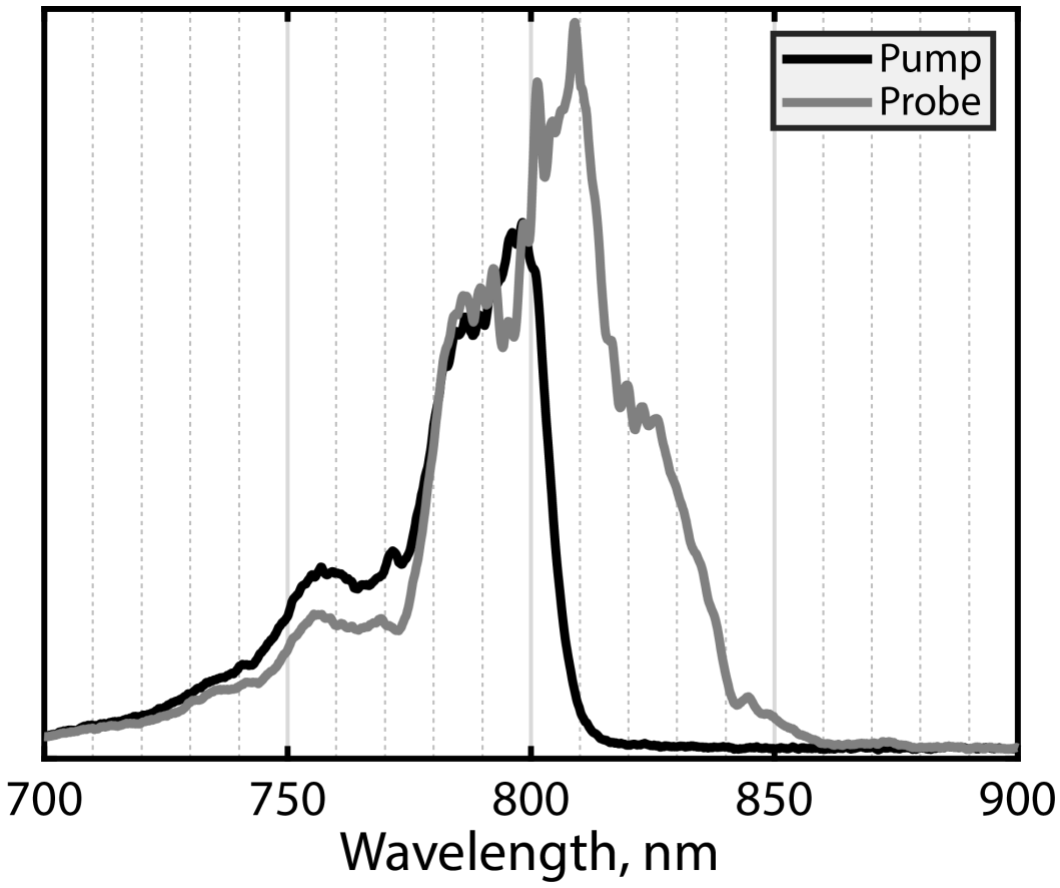

Fig 5.11: Pump and probe spectra for narrowband-excitation 2DES experiments in which beams 1 and 2 do not interact with the B850 ring. The pump spectrum is filtered with a 45^{o} angle-tuned shortpass filter from Thorlabs. This filter is added in the beam path of the copropagating beams 1 and 2.

As is expected, the B850 diagonal feature is not observed in 2DES spectra in these experiments. Representative spectra at different waiting times are shown in *Figs 5.12* for the RXXX sequence.

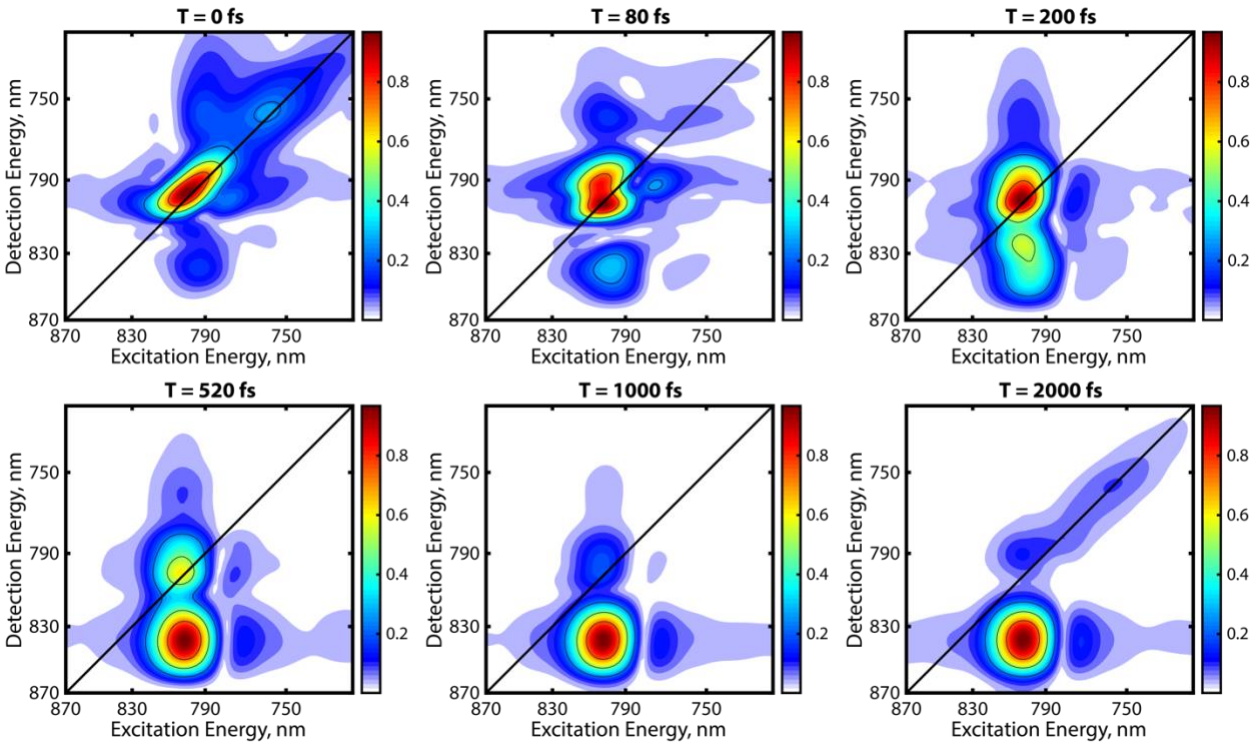

Fig 5.12: Representative 2DES spectra obtained in the RXXX pulse sequence with narrowband pump excitation at different waiting times. The B850 diagonal peak is not observed in this experiment because 850 nm light has been filtered out. The formation of the off-diagonal peak over waiting times indicates the energy transfer from B800 to B850.

Fig 5.13 compares all the data runs performed with broad and narrow pump pulses. The time constant obtained for each run is plotted as a point along with the 5% confidence interval of the fit. We observe that for experiments with narrowband pump pulses, the time constants obtained for the LXXX sequence do not fall outside of the 5% confidence interval of the RXXX experiments, not allowing us to accept the hypothesis that the time constants for RXXX and LXXX narrowband experiments are different. Interestingly, RXXX narrowband experiments yield a larger average time constant within error as compared to LXXX experiments, further suggesting that all RXXX and LXXX experiments yield time constants from the same overall process. Both findings confirm that chirality-control of energy transfer is not present when narrowband excitation is used.

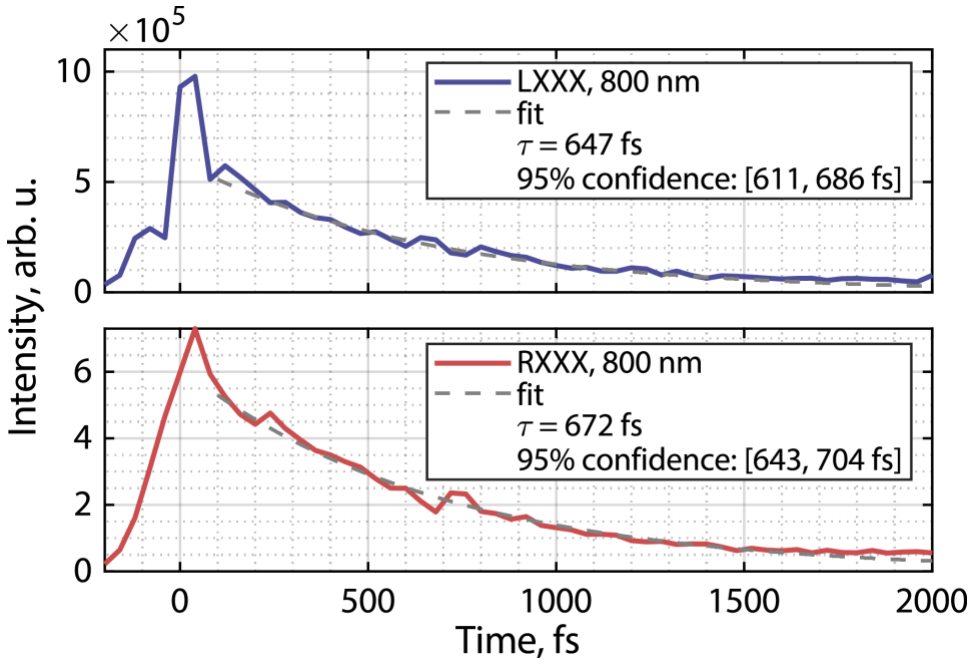

Fig 5.13: Statistical comparison of obtained time constants for the peak at 800 nm in the narrowband pump experiments between RXXX and LXXX pulse sequences. We observe that the time constants are not outside of the 95% confidence interval of each other. The signal intensity difference between RXXX and LXXX observed in broadband experiments is not observed in this pulse sequence apart from an early-time artefact in the LXXX sequence.

From these experiments, it is clear that the large impulse of broadband pump excitation is required to observe chiral control of energy transfer dynamics. Two factors should be considered in understanding this phenomenon. First, at the 2 nm distance, the point-dipole approximation of B850 excitons' effect on B800 excitons breaks down. Therefore, a significant non-resonant magnetization of the B850 ring can occur with broadband light, even in the one exciton limit, to transiently influence the electronic structure of B800 excitons, now creating a chiral basis for them even at room temperature. Second, optical current in the B850 ring can drive anomalously high chirality in the B800 ring as demonstrated theoretically by Cohen and coworkers.[24] In their theoretical description, small molecules resting on a silver mirror display anomalously high chiral activity due to the reflection of CPL from the mirror, especially when a CPL node hits the mirror. Effectively, the B850 ring could act as a mirror-like element in our experiments to induce this

anomalously high chiral effect. Further calculations of the induced fields will be required to confirm these hypotheses and will be performed in the future. Finally, Govorov and coworkers[26] expanded the theory of circular dichroism to include nanoparticle-chiral chromophore interaction-induced enhancement. In their theoretical study, they claim that the circular dichroism of a chromophore-nanoparticle system is enhanced due to two factors. They describe the first factor as being an enhancement in the helical current in the chiral center of the molecule due to the large electric field change driven by the plasmon effect of the nanoparticle. This effect enhances CD at the chromophore's absorption wavelength. The second factor is the creation of a helical current in the nanoparticle's electrons from the chirality of the chromophore. This effect enhances CD at the plasmon transition. These two effects could be used to model the current observations in LH2 if the B850 ring is thought of as a semiconducting/metallic ring which enhances helical currents in the B800 ring.

In summary, I show in this chapter that the protein scaffold of the LH2 protein creates a transient magnetization effect that allows us to control the chemical rate of energy transfer with only the polarization of light as opposed to its intensity or spectrum. This mechanism could unlock the optical degree of freedom for spintronics[27] and could possibly have also played a role in chiral selection over the development of life.[28]

Methods

Two-dimensional Electronic Spectroscopy: Two-dimensional spectroscopic experiments were performed using a setup described previously. Briefly, a Ti:sapphire mode-locked oscillator (Coherent Micra) operating at 80 MHz seeds a Ti:sapphire regenerative amplifier (Coherent

Legend Elite) to produce 35 fs pulses centered at 800 nm at a 5 kHz repetition rate. This output is passed through a pressurized argon tube held at ~12 pounds per square inch above atmosphere to generate a white light continuum. The remaining fundamental 800 nm light after white light generation is rejected with an iris, and the white light is compressed using two pairs of chirped mirrors (Laser Quantum) to ~8 fs fwhm and a 1 cm fused silica cuvette with water. 2D spectra are collected in the fully non-collinear BOXCARS geometry with a beam diameter of 290 μm at the focus at the sample and heterodyned with an attenuated local oscillator pulse. Powers are kept to 15 nJ per pulse in our experiments. Broadband half-waveplates (Union Optic) are used to independently control the polarization of each pulse. A quarter waveplate is placed before the sample position to make beam 1 circularly polarized. Half-waveplates of beams 2, 3 and 4 rotate their polarizations so that they pass through the axis of the quarter waveplate and remain linearly polarized[29]. Two-dimensional spectra were obtained by collecting coherence time data from -90 to 90 fs in 1.5 fs time-steps. Hann and Tukey windows were used for apodization and windowing in rephasing time and coherence time respectively. A 200 μm flow cell was used and the sample was flowed throughout data acquisition.

Bibliography

(1) Cahn, R. S.; Ingold, C.; Prelog, V. Specification of Molecular Chirality. *Angewandte Chemie International Edition in English* **1966**, *5* (4), 385-415.
(2) Berova, N.; Nakanishi, K.; Woody, R. W. *Circular Dichroism: Principles and Applications*; Wiley, 2000.
(3) Brixner, T.; Hildner, R.; Köhler, J.; Lambert, C.; Würthner, F. Exciton Transport in Molecular Aggregates – From Natural Antennas to Synthetic Chromophore Systems. *Advanced Energy Materials* **2017**, *7* (16), 1700236.
(4) Blankenship, R. E. Antenna Complexes and Energy Transfer Processes. In *Molecular Mechanisms of Photosynthesis*, Wiley, 2002; pp 61-94.
(5) Qian, P.; Swainsbury, D. J. K.; Croll, T. I.; Castro-Hartmann, P.; Divitini, G.; Sader, K.; Hunter, C. N. Cryo-EM Structure of the *Rhodobacter sphaeroides* Light-Harvesting 2 Complex at 2.1 Å. *Biochemistry* **2021**, *60* (44), 3302-3314.
(6) Hestand, N. J.; Spano, F. C. Expanded Theory of H- and J-Molecular Aggregates: The Effects of Vibronic Coupling and Intermolecular Charge Transfer. *Chemical Reviews* **2018**, *118* (15), 7069-7163.
(7) van Amerongen, H.; van Grondelle, R.; Valkunas, L. *Photosynthetic Excitons*; World Scientific, 2000. DOI: doi:10.1142/3609.
(8) Gellings, E.; Cogdell, R. J.; van Hulst, N. F. Room-Temperature Excitation–Emission Spectra of Single LH2 Complexes Show Remarkably Little Variation. *The Journal of Physical Chemistry Letters* **2020**, *11* (7), 2430-2435.
(9) Book, L. D.; Ostafin, A. E.; Ponomarenko, N.; Norris, J. R.; Scherer, N. F. Exciton Delocalization and Initial Dephasing Dynamics of Purple Bacterial LH2. *The Journal of Physical Chemistry B* **2000**, *104* (34), 8295-8307.
(10) Irgen-Gioro, S.; Gururangan, K.; Spencer, A. P.; Harel, E. Non-Uniform Excited State Electronic-Vibrational Coupling of Pigment–Protein Complexes. *The Journal of Physical Chemistry Letters* **2020**, *11* (24), 10388-10395.
(11) Cheng, Y. C.; Silbey, R. J. Coherence in the B800 Ring of Purple Bacteria LH2. *Physical Review Letters* **2006**, *96* (2), 028103.
(12) Novoderezhkin, V. I. Excitation dynamics in photosynthetic light-harvesting complex B850: exact solution versus Redfield and Förster limits. *Physical Chemistry Chemical Physics* **2023**, *25* (20), 14219-14231. 10.1039/D3CP00671A
(13) Papiz, M. Z.; Prince, S. M.; Howard, T.; Cogdell, R. J.; Isaacs, N. W. The Structure and Thermal Motion of the B800–850 LH2 Complex from *Rps.acidophila* at 2.0 Å Resolution and 100 K: New Structural Features and Functionally Relevant Motions. *Journal of Molecular Biology* **2003**, *326* (5), 1523-1538.
(14) Koolhaas, M. H. C.; Frese, R. N.; Fowler, G. J. S.; Bibby, T. S.; Georgakopoulou, S.; van der Zwan, G.; Hunter, C. N.; van Grondelle, R. Identification of the Upper Exciton Component of the B850 Bacteriochlorophylls of the LH2 Antenna Complex, Using a B800-Free Mutant of *Rhodobacter sphaeroides*. *Biochemistry* **1998**, *37* (14), 4693-4698.
(15) Sohail, S. H.; Dahlberg, P. D.; Allodi, M. A.; Massey, S. C.; Ting, P.-C.; Martin, E. C.; Hunter, C. N.; Engel, G. S. Communication: Broad manifold of excitonic states in light-harvesting complex 1 promotes efficient unidirectional energy transfer in vivo. *The Journal of Chemical Physics* **2017**, *147* (13).

(16) Strümpfer, J.; Schulten, K. Light harvesting complex II B850 excitation dynamics. *The Journal of Chemical Physics* **2009**, *131* (22).
(17) Fidler, A. F.; Singh, V. P.; Long, P. D.; Dahlberg, P. D.; Engel, G. S. Probing Energy Transfer Events in the Light Harvesting Complex 2 (LH2) of *Rhodobacter sphaeroides* with Two-dimensional Spectroscopy. *The Journal of Chemical Physics* **2013**, *139* (15).
(18) Massey, S. C.; Ting, P.-C.; Yeh, S.-H.; Dahlberg, P. D.; Sohail, S. H.; Allodi, M. A.; Martin, E. C.; Kais, S.; Hunter, C. N.; Engel, G. S. Orientational Dynamics of Transition Dipoles and Exciton Relaxation in LH2 from Ultrafast Two-Dimensional Anisotropy. *The Journal of Physical Chemistry Letters* **2019**, *10* (2), 270-277.
(19) Scholes, G. D.; Fleming, G. R. On the Mechanism of Light Harvesting in Photosynthetic Purple Bacteria: B800 to B850 Energy Transfer. *The Journal of Physical Chemistry B* **2000**, *104* (8), 1854-1868.
(20) Fidler, A. F.; Singh, V. P.; Long, P. D.; Dahlberg, P. D.; Engel, G. S. Dynamic localization of electronic excitation in photosynthetic complexes revealed with chiral two-dimensional spectroscopy. *Nature Communications* **2014**, *5* (1), 3286.
(21) Zanni, M. T.; Ge, N.-H.; Kim, Y. S.; Hochstrasser, R. M. Two-dimensional IR Spectroscopy can be Designed to Eliminate the Diagonal peaks and Expose only the Crosspeaks Needed for Structure Determination. *Proceedings of the National Academy of Sciences* **2001**, *98* (20), 11265-11270.
(22) Tokmakoff, A. Orientational correlation functions and polarization selectivity for nonlinear spectroscopy of isotropic media. I. Third order. *The Journal of Chemical Physics* **1996**, *105* (1), 1-12.
(23) Dreyer, J.; Moran, A. M.; Mukamel, S. Tensor Components in Three Pulse Vibrational Echoes of a Rigid Dipeptide. *Bulletin-Korean Chemical Society* **2003**, *24* (8), 1091-1096.
(24) Tang, Y.; Cohen, A. E. Optical Chirality and Its Interaction with Matter. *Physical Review Letters* **2010**, *104* (16), 163901.
(25) Basini, M.; Pancaldi, M.; Wehinger, B.; Udina, M.; Unikandanunni, V.; Tadano, T.; Hoffmann, M. C.; Balatsky, A. V.; Bonetti, S. Terahertz electric-field-driven dynamical multiferroicity in SrTiO3. *Nature* **2024**.
(26) Govorov, A. O.; Fan, Z.; Hernandez, P.; Slocik, J. M.; Naik, R. R. Theory of Circular Dichroism of Nanomaterials Comprising Chiral Molecules and Nanocrystals: Plasmon Enhancement, Dipole Interactions, and Dielectric Effects. *Nano Letters* **2010**, *10* (4), 1374-1382.
(27) Lloyd, L. T.; Wood, R. E.; Mujid, F.; Sohoni, S.; Ji, K. L.; Ting, P.-C.; Higgins, J. S.; Park, J.; Engel, G. S. Sub-10 fs Intervalley Exciton Coupling in Monolayer MoS2 Revealed by Helicity-Resolved Two-Dimensional Electronic Spectroscopy. *ACS Nano* **2021**, *15* (6), 10253-10263.
(28) Salam, A. The role of chirality in the origin of life. *Journal of Molecular Evolution* **1991**, *33* (2), 105-113.
(29) Lloyd, L. T. Resolving Exciton Dynamics and Couplings in Atomically Thin Semiconductors with Multidimensional Spectroscopy. Ph.D., The University of Chicago, United States -- Illinois, 2022.

Chapter 6

Future Directions

1. Further explorations in chiral exciton dynamics in LH2

The experiments presented in Ch. 5 demonstrate evidence of chirality-controlled exciton transfer in LH2. To understand the mechanism of this phenomenon in depth, further experiments can be performed with different pulse sequences and mutants. For example, in the presented experiments, the RYYY and LYYY pulse sequences are used. In these pulse sequences, the second light-matter interaction occurs with linearly polarized light to create both |R><R| and |R><L| populations in the RXXX pulse sequence, for example. We chose this combination of complementary pulse sequences for the first experiments because earlier work from the group[1] showed the first signatures of chiral dynamics in LH2 with the YXXX pulse sequence. This pulse sequence directly probes the difference between RXXX and LXXX sequences. Moreover, in an achiral basis, RRYY and LLYY experiments directly probe the difference between YYYY and XXYY sequences and are said to not reveal chiral information[2, 3]. However, in a chiral basis, the RRYY and LLYY sequences could directly report on left- and right-handed chiral populations to observe potential differences in their dynamics. Doing experiments in the RRYY and LLYY configuration would also allow us to perform pump-probe measurements with RY and LY pulse configurations for pump and probe respectively. These measurements will yield phased chirality-sensitive data and allow us to track the dynamics of all chiral Feynman pathways. These experiments can easily be performed in the current setup in Redfield lab.[4] Another interesting pulse

sequence that can be explored is the LRYY pulse sequence, that could report on chiral coherences in LH2. These experiments can also be performed at 77 K to observe differences with narrower lineshapes.

To develop a detailed theory of the mechanism of chiral control of exciton dynamics in LH2, further chiral experiments with B800-^{5} and B850-less mutants can be performed. Although the energy transfer from B800 to B850 is under chiral control, the free evolution of the B800 and B850 right- and left-handed states in the absence of the other band's fields can be observed in these experiments.

Finally, circular dichroism in phycobiliproteins is strongly pH dependent and is shown to invert at low pH.[6, 7] These proteins could be used to design pH-controlled chiral exciton dynamics.

2. Unraveling excitonic pathways in Photosystem I

Photosystem I drives the NADPH cycle in oxygenic photosynthesis, and is therefore vital in driving continuous oxygen generation during photosynthesis.[8, 9] Exciton transfer pathways to the photosystem I reaction center remain hidden because of the antenna's non-modular structure. Currently, we have a very broad and detailed understanding of the excitonic pathways of photosystem II's antennas and reaction center because PSII is a modular antenna complex whose components can be separately studied.[10-16] Similarly, other antennas like the phycobilisome also benefit from modularity and spectral separation of pigments in terms of our understanding of its excitonic pathways.[17-24] However, photosystem I is not modular apart from monomers forming trimeric photosystem I. Therefore, we are forced to study ~200 spectrally overlapping pigments in this antenna together.[25-27] All these pigments absorb between 660 and 680 nm, and spectroscopic

studies relying on global analysis fail to provide consistent models for the energy transfer pathways.[25, 26] Sub-diffraction-limited microscopy cannot observe these pathways either because PSI is only 20 nm across. An important fact that confounds us even today is the presence of 'red chlorophylls' in photosystem I. Red chlorophylls are present within 2 ps in FRET time (Sohail, Sohoni, et al manuscript under review) from the reaction center chlorophylls of photosystem I and act as excitation sinks. Their role in the photosystem I antenna is not yet understood because they slow down energy capture in the complex.

I propose coherence-specific[28] and cross-peak-specific[19] 2DES experiments on photosystem I at 77 K[26] to unravel the excitonic couplings and transfer pathways between bulk and red chlorophylls in photosystem I. These experiments would allow us to cut spectral congestion significantly and tease out timescales of energy transfer directly. These experiments would be of physiological importance because they concern photosystem I and would lead to us understanding how the complex maintains a near-unity efficiency of energy transfer to the reaction center in spite of red traps being present very close to the reaction center.

3. Possible routes for increasing the pulse bandwidth in Redfield lab

For compressing 700-900 nm light for LH2 experiments, we used a 1 cm cuvette of water in the beam path, because water has negative third-order velocity dispersion (TVD) at 800 nm.[29] However, water's TVD is highly oscillatory and yields wings in the transient grating (TG) response. *Fig 6.1* shows these wings in the TG response.[30]

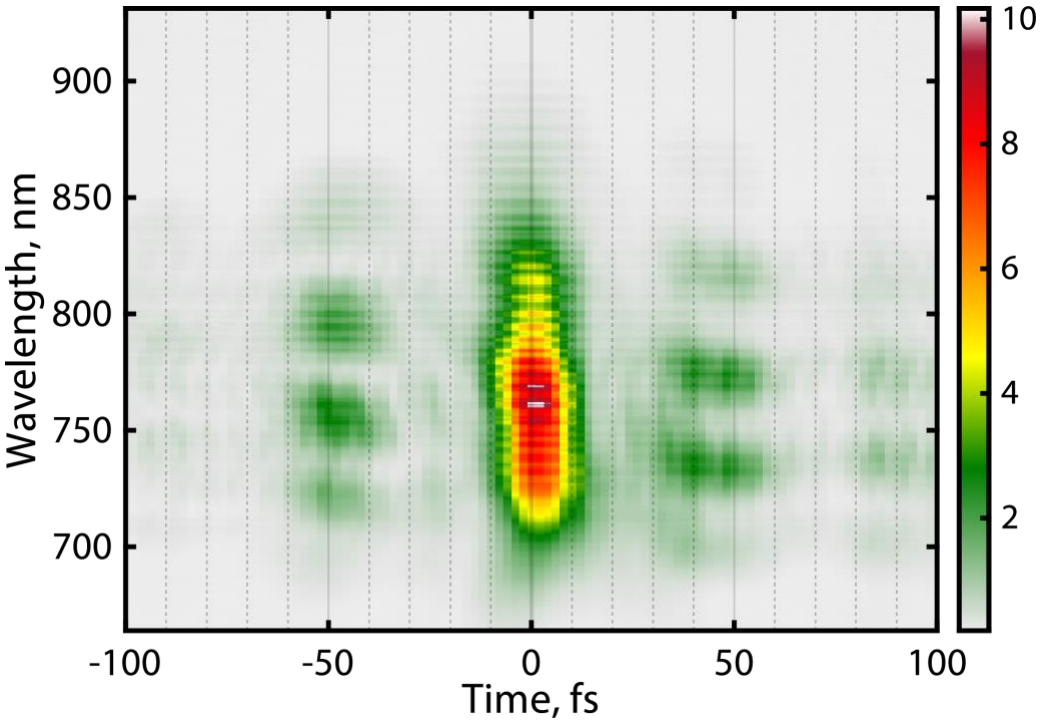

Fig 6.1: Transient-grating response for light between 690 and 860 nm. Wings occur due to the oscillatory TVD of water.

To circumvent this problem, Leone and coworkers suggested the use of an ammonium dihydrogen phosphate (ADP) crystal.[31] This crystal is birefringent and has a higher TVD than group velocity dispersion (GVD). GVD is higher than TVD for most materials. Therefore, ADP can be added to the beam path to remove TVD artefacts from the TG response with additional chirped mirror bounces to compensate for the crystal's GVD.

Currently, light in Redfield lab can be compressed between 500-780 nm and 720-860 nm. We get much higher powers in the 700-860 nm region as compared to the visible region. We shape our visible spectrum with soft shortpass filters from Thorlabs. These soft filters typically do not transmit light red of ~770 nm. To compress light from 500 to 860 nm, we can check with Thorlabs or other manufacturers to design a custom soft filter whose transmission is complementary to our white light spectrum. Using these filters would allow us to have uniform power from 500 nm to

860 nm and a clean Gaussian frequency profile, yielding high quality, sub-4 fs pulses, which would allow observation of all LH2 transitions in a single 2DES frame. Our camera grating can be moved from 600 gr/mm to 300 gr/mm to accommodate the increased bandwidth.

Similarly, we could generate light in the 400-550 nm region to explore dynamics of bismuth perovskite quantum dots, carotenoids, rhodopsins and higher chlorophyll transitions. Recent work by Lienau and coworkers[32] has shown that a gas-filled hollow core fiber setup can be reliably used to produced light spanning from 400 nm to 700 nm with 800 nm fundamental light. This setup can be adapted into the current setup along with soft bandpass filters and chirped mirrors to produced high-quality chirp-free pulses spanning the entire visible spectrum. Similarly, work by Tokmakoff and coworkers[33] has demonstrated that filamentation in air with a laser pulse and its second and third harmonics yields a broadband frequency continuum. To access 400 nm light, part of the 800 nm fundamental can be doubled and then focused into our argon tube with the 800 nm light to generate bluer light. The 400-500 nm region has historically been difficult to access in broadband 2DES, but being able to access it will allow us to observe exciting phenomena in many important systems including blue LEDs, quantum dots, carotenoids etc.

Bibliography

(1) Fidler, A. F.; Singh, V. P.; Long, P. D.; Dahlberg, P. D.; Engel, G. S. Dynamic localization of electronic excitation in photosynthetic complexes revealed with chiral two-dimensional spectroscopy. *Nature Communications* **2014**, *5* (1), 3286.
(2) Zanni, M. T.; Ge, N.-H.; Kim, Y. S.; Hochstrasser, R. M. Two-dimensional IR Spectroscopy can be Designed to Eliminate the Diagonal peaks and Expose only the Crosspeaks Needed for Structure Determination. *Proceedings of the National Academy of Sciences* **2001**, *98* (20), 11265-11270.
(3) Dreyer, J.; Moran, A. M.; Mukamel, S. Tensor Components in Three Pulse Vibrational Echoes of a Rigid Dipeptide. *Bulletin-Korean Chemical Society* **2003**, *24* (8), 1091-1096.
(4) Lloyd, L. T.; Wood, R. E.; Mujid, F.; Sohoni, S.; Ji, K. L.; Ting, P.-C.; Higgins, J. S.; Park, J.; Engel, G. S. Sub-10 fs Intervalley Exciton Coupling in Monolayer MoS2 Revealed by Helicity-Resolved Two-Dimensional Electronic Spectroscopy. *ACS Nano* **2021**, *15* (6), 10253-10263.
(5) Koolhaas, M. H. C.; Frese, R. N.; Fowler, G. J. S.; Bibby, T. S.; Georgakopoulou, S.; van der Zwan, G.; Hunter, C. N.; van Grondelle, R. Identification of the Upper Exciton Component of the B850 Bacteriochlorophylls of the LH2 Antenna Complex, Using a B800-Free Mutant of *Rhodobacter sphaeroides*. *Biochemistry* **1998**, *37* (14), 4693-4698.
(6) Schamagl, C.; Köst-Reyes, E.; Schneider, S.; Köst, H.-P.; Scheer, H. Circular Dichroism of Chromopeptides from Phycocyanin. *Zeitschrift für Naturforschung C* **1983**, *38* (11-12), 951-959.
(7) Maksimov, E. G.; Schmitt, F. J.; Hätti, P.; Klementiev, K. E.; Paschenko, V. Z.; Renger, G.; Rubin, A. B. Anomalous temperature dependence of the fluorescence lifetime of phycobiliproteins. *Laser Physics Letters* **2013**, *10* (5), 055602.
(8) *Light-Harvesting Antennas in Photosynthesis*; Springer, 2003.
(9) Blankenship, R. E. Antenna Complexes and Energy Transfer Processes. In *Molecular Mechanisms of Photosynthesis*, Wiley, 2002; pp 61-94.
(10) Do, T. N.; Nguyen, H. L.; Akhtar, P.; Zhong, K.; Jansen, T. L. C.; Knoester, J.; Caffarri, S.; Lambrev, P. H.; Tan, H.-S. Ultrafast Excitation Energy Transfer Dynamics in the LHCII–CP29–CP24 Subdomain of Plant Photosystem II. *The Journal of Physical Chemistry Letters* **2022**, *13* (19), 4263-4271.
(11) Schlau-Cohen, G. S.; Calhoun, T. R.; Ginsberg, N. S.; Read, E. L.; Ballottari, M.; Bassi, R.; van Grondelle, R.; Fleming, G. R. Pathways of Energy Flow in LHCII from Two-Dimensional Electronic Spectroscopy. *The Journal of Physical Chemistry B* **2009**, *113* (46), 15352-15363.
(12) Yang, S.-J.; Arsenault, E. A.; Orcutt, K.; Iwai, M.; Yoneda, Y.; Fleming, G. R. From Antenna to Reaction Center: Pathways of Ultrafast Energy and Charge Transfer in Photosystem II. *Proceedings of the National Academy of Sciences* **2022**, *119* (42), e2208033119.
(13) Ginsberg, N. S.; Davis, J. A.; Ballottari, M.; Cheng, Y.-C.; Bassi, R.; Fleming, G. R. Solving structure in the CP29 light harvesting complex with polarization-phased 2D electronic spectroscopy. *Proceedings of the National Academy of Sciences* **2011**, *108* (10), 3848-3853.
(14) Nguyen, H. H.; Song, Y.; Maret, E. L.; Silori, Y.; Willow, R.; Yocum, C. F.; Ogilvie, J. P. Charge Separation in the Photosystem II Reaction Center Resolved by Multispectral Two-dimensional Electronic Spectroscopy. *Science Advances* **2023**, *9* (18), eade7190.

(15) Arsenault, E. A.; Yoneda, Y.; Iwai, M.; Niyogi, K. K.; Fleming, G. R. Vibronic mixing enables ultrafast energy flow in light-harvesting complex II. *Nature Communications* **2020**, *11* (1), 1460.
(16) Bhowmick, A.; Hussein, R.; Bogacz, I.; Simon, P. S.; Ibrahim, M.; Chatterjee, R.; Doyle, M. D.; Cheah, M. H.; Fransson, T.; Chernev, P.; et al. Structural evidence for intermediates during O2 formation in photosystem II. *Nature* **2023**, *617* (7961), 629-636.
(17) Womick, J. M.; Moran, A. M. Exciton Coherence and Energy Transport in the Light-Harvesting Dimers of Allophycocyanin. *The Journal of Physical Chemistry B* **2009**, *113* (48), 15747-15759.
(18) Womick, J. M.; Moran, A. M. Nature of Excited States and Relaxation Mechanisms in C-Phycocyanin. *The Journal of Physical Chemistry B* **2009**, *113* (48), 15771-15782.
(19) Sohoni, S.; Lloyd, L. T.; Hitchcock, A.; MacGregor-Chatwin, C.; Iwanicki, A.; Ghosh, I.; Shen, Q.; Hunter, C. N.; Engel, G. S. Phycobilisome's Exciton Transfer Efficiency Relies on an Energetic Funnel Driven by Chromophore–Linker Protein Interactions. *Journal of the American Chemical Society* **2023**, *145* (21), 11659-11668.
(20) Domínguez-Martín, M. A.; Sauer, P. V.; Kirst, H.; Sutter, M.; Bína, D.; Greber, B. J.; Nogales, E.; Polívka, T.; Kerfeld, C. A. Structures of a Phycobilisome in Light-harvesting and Photoprotected States. *Nature* **2022**, *609* (7928), 835-845.
(21) Sil, S.; Tilluck, R. W.; Mohan T. M, N.; Leslie, C. H.; Rose, J. B.; Domínguez-Martín, M. A.; Lou, W.; Kerfeld, C. A.; Beck, W. F. Excitation Energy Transfer and Vibronic Coherence in Intact Phycobilisomes. *Nature Chemistry* **2022**, *14* (11), 1286-1294.
(22) Tian, L.; Gwizdala, M.; van Stokkum, Ivo H. M.; Koehorst, Rob B. M.; Kirilovsky, D.; van Amerongen, H. Picosecond Kinetics of Light Harvesting and Photoprotective Quenching in Wild-Type and Mutant Phycobilisomes Isolated from the Cyanobacterium *Synechocystis* PCC 6803. *Biophysical Journal* **2012**, *102* (7), 1692-1700.
(23) Tian, L.; van Stokkum, I. H. M.; Koehorst, R. B. M.; Jongerius, A.; Kirilovsky, D.; van Amerongen, H. Site, Rate, and Mechanism of Photoprotective Quenching in Cyanobacteria. *Journal of the American Chemical Society* **2011**, *133* (45), 18304-18311.
(24) van Stokkum, I. H. M.; Gwizdala, M.; Tian, L.; Snellenburg, J. J.; van Grondelle, R.; van Amerongen, H.; Berera, R. A Functional Compartmental Model of the *Synechocystis* PCC 6803 Phycobilisome. *Photosynthesis Research* **2018**, *135* (1), 87-102.
(25) Lee, Y.; Gorka, M.; Golbeck, J. H.; Anna, J. M. Ultrafast Energy Transfer Involving the Red Chlorophylls of Cyanobacterial Photosystem I Probed through Two-Dimensional Electronic Spectroscopy. *Journal of the American Chemical Society* **2018**, *140* (37), 11631-11638.
(26) Akhtar, P.; Caspy, I.; Nowakowski, P. J.; Malavath, T.; Nelson, N.; Tan, H.-S.; Lambrev, P. H. Two-Dimensional Electronic Spectroscopy of a Minimal Photosystem I Complex Reveals the Rate of Primary Charge Separation. *Journal of the American Chemical Society* **2021**, *143* (36), 14601-14612.
(27) Anna, J. M.; Ostroumov, E. E.; Maghlaoui, K.; Barber, J.; Scholes, G. D. Two-Dimensional Electronic Spectroscopy Reveals Ultrafast Downhill Energy Transfer in Photosystem I Trimers of the Cyanobacterium *Thermosynechococcus elongatus*. *The Journal of Physical Chemistry Letters* **2012**, *3* (24), 3677-3684.
(28) Schlau-Cohen, G. S.; Ishizaki, A.; Calhoun, T. R.; Ginsberg, N. S.; Ballottari, M.; Bassi, R.; Fleming, G. R. Elucidation of the timescales and origins of quantum electronic coherence in LHCII. *Nature Chemistry* **2012**, *4* (5), 389-395.

(29) Coello, Y.; Xu, B.; Miller, T. L.; Lozovoy, V. V.; Dantus, M. Group-velocity dispersion measurements of water, seawater, and ocular components using multiphoton intrapulse interference phase scan. *Appl. Opt.* **2007**, *46* (35), 8394-8401.
(30) Van Engen, A. G.; Diddams, S. A.; Clement, T. S. Dispersion measurements of water with white-light interferometry. *Appl. Opt.* **1998**, *37* (24), 5679-5686.
(31) Timmers, H.; Kobayashi, Y.; Chang, K. F.; Reduzzi, M.; Neumark, D. M.; Leone, S. R. Generating high-contrast, near single-cycle waveforms with third-order dispersion compensation. *Opt. Lett.* **2017**, *42* (4), 811-814.
(32) Timmer, D.; Lünemann, D. C.; Riese, S.; Sio, A. D.; Lienau, C. Full visible range two-dimensional electronic spectroscopy with high time resolution. *Opt. Express* **2024**, *32* (1), 835-847.
(33) Petersen, P. B.; Tokmakoff, A. Source for ultrafast continuum infrared and terahertz radiation. *Opt. Lett.* **2010**, *35* (12), 1962-1964.

Chapter 7

Conclusions

In this thesis, I have described a few phenomena in photosynthesis which we uncovered using Monte-Carlo simulations, pump-probe spectroscopy, and two-dimensional electronic spectroscopy. Chapters 2, 3, and 4 demonstrate effective engineering of the bath by biology to drive the near-unity quantum efficiency of energy capture. Oxygenic photosynthetic reaction centers operate at fixed 'voltages': the PSI reaction center at 700 nm, and the PSII reaction at 680 nm. However, light across much of the visible spectrum is absorbed by light-harvesting pigments in photosynthetic antennas. If a 570 nm photon is absorbed by an outer phycobilisome rod in cyanobacteria, photosynthesis uses the excess energy to ensure that the created exciton reaches the reaction center with near-unity efficiency. In other words, the light-harvesting process itself requires energy to operate effectively. This energy requirement stems from breaking symmetry between identical pigments in an open quantum system, so that dissipation favors directional movement towards the lower-energy direction.

Proteins tune physical and chemical properties of cofactors by controlling the bath around them to drive biological function. In photosynthetic light-harvesting, multiple cofactors function as antenna pigments, or sunlight absorbers. Antenna pigments are required in photosynthesis because sunlight is a dilute energy source, so associating energy utilization machinery with every light-harvesting pigment is unfeasible. Energy could be absorbed by a pigment up to 50 nm away from the reaction center of the photosynthetic protein supercomplex. Absorbed energy quanta are

transduced for utilization to the reaction center with near-unity efficiency through the protein super-assembly in photosynthesis.

Biosynthesis of pigment cofactors is limited and allows photosynthetic organisms to use chlorophyll, carotenoid, and phycocyanobilin molecule derivatives for light absorption. Therefore, bath interactions must control photophysical properties to a much larger extent in photosynthesis as opposed to in photovoltaics. The high efficiency of absorption-to-charge separation is achieved partly through lossy bath interactions that create a downhill spatial energy funnel towards the reaction center. The protein bath around light-harvesting antenna pigments has to rapidly accept the released heat to drive unidirectional flow of energy.

In Chapter 2, I have described how the clustering of reaction centers on the purple bacterial photosynthetic membrane may be optimized for maximum efficiency in different light-fluences across species. The main claim made in this chapter is as follows: when light absorption by the photosynthetic membrane is faster than the rate at which excitons can be converted to charges at reaction centers, reaction-center clustering allows excitons to explore multiple reaction centers in proximity to get quenched, thus enhancing the efficiency of light harvesting. This strategy would imply a quaternary-level mechanism to make the most of incident sunlight in different photosynthetic niches.

In Chapter 3, I have explored energy transfer in the cyanobacterial light harvesting antenna, phycobilisome. We observe a rapid energy capture process by the lowest-energy pigments of the phycobilisome antenna in this work. We find that the observed rate of energy capture by the antenna cannot be explained by previous Forster-hopping models. We invoke interactions between the antenna pigments and non-pigment proteins to explain the formation of a conduit in the exciton transfer pathway. This conduit acts as a sink for excitons from higher-energy chromophores, and

as an exciton source for lowest-energy chromophores, effectively creating a one-way energy funnel.

In Chapter 4, I have continued to describe our exploration of energy capture mechanism in the phycobilisome antenna. We observe that low-frequency vibrations around the electronic excited state are different for different pigment pairs within the antenna, and seem to be tuned to promote fast downhill energy capture. We also observe Raman signatures of the excited states of the phycobilisome pigments selectively. We find that the excited state nuclear potential of the chromophores remains in a local minimum held together by hydrogen-bonding interactions with nearby amino-acid residues. These findings explain how the biological bath arrests floppy motion of chromophores so that nuclear relaxation and exciton trapping is prevented.

In Chapter 5, I deviate from focusing on effective energy-capture mechanisms. I describe our observation of chirality-controlled excited-state dynamics in the highly chiral LH2 antenna of purple bacteria. We observe that right-handed exciton states of the B800 ring of the LH2 antenna transfer faster to the B850 ring in comparison to the left-handed states. I hypothesize a non-resonant magnetic effect to partly describe our observations. In these experiments too, different bath interactions with left- and right-handed energy quanta are observed and are hypothesized to drive chiral asymmetry of energy transfer.

In Chapters 3, 4 and 5, I have exploited the ability of our BOXCARS 2DES setup for experiments, and of coherent Redfield modeling for theory, to use transition dipole moments' geometries to selectively observe the energy transfer process of interest. In all cases, we observe that fitting isotropically obtained data obscures the details of the quantum-mechanical coupling between specifically-oriented light harvesters, and that control of polarization in experiments reveals otherwise hidden mechanisms of energy transfer.